Author:
Sapountzi, Kallia

Title:
The development of non-collinear non destructive evaluation of aircraft materials

The development of non-collinear non destructive evaluation of aircraft materials

Kalliroi Sapountzi

A dissertation submitted to the University of Bristol in accordance with the requirements for award of the degree of Master of Science by Research in the Faculty of Engineering

Department of Mechanical Engineering
March 2019

c. 23 000 words

Abstract

This dissertation considers the usage of non-linear non-collinear mixing as a non destructive evaluation tool of aircraft materials, i.e aluminium alloys and carbon fibre reinforced plastic composite materials. Non-collinear mixing is a non conventional ultrasonic evaluation method which is under the non-linear methods. Non-linear ultrasonic techniques exhibit higher sensitivity to defects smaller than a wavelength, that they are currently undetectable with the conventional ultrasonic methods. It occurs when two intersecting elastic waves interact in an homogenous material. When the resonance conditions are met, a third wave is generated with frequency equal to the sum of the two input frequencies. For this reason, the non-collinear mixing was selected to investigate sensitivity over kissing bonds, a type of defect of great interest in the aerospace industry mainly due to the luck of conventional procedures that can detect them. Initially, a set-up of two partially closed interfaces was designed to simulate a kissing bond; an adhesive-metallic and a metallic-metallic interface. It was shown that the kissing bond in adhesive joints was highly non-linear with inconclusive results whereas the metallic-metallic interface showed higher sensitivity. In order to investigate this further, the use of phased arrays was selected. Subsequently, basic modelling of the linear field of the phased arrays was computed as well as theoretical calculations of the optimum interaction angles, depths and sub-aperture groups. These results were later used, where experimental application of non-collinear mixing was performed with phased arrays. A successful interaction was performed along with a research of the effect of dependant variables, i.e signal gain, elapsed time, coupling and alignment. Finally, the sensitivity of non-collinear mixing was tested in carbon fibre reinforced plastic contaminated bonds with different fracture toughness values, with the signal amplitudes showing expected trends but overall limited sensitivity.

Acknowledgements

The research was supported by the "Extended Non-Destructive Testing of Composite Bonds - ENCOMB", part of the European Union's 7th Research and Technological Development Framework Program. I am indebted to my supervisors Professor Anthony Croxford and Professor Simon Neild for their enormous support over these years. I would also like to thank the members of the Ultrasonics and Non Destructive Testing group, and especially Dr Jack Potter and Dr Steve Best for their technical and scientific support and friendship during my research. I owe a great deal of gratitude to Ms Carrie White for her support during my recovery.

Finally, I would like to thank my partner Graeme for supporting me through difficult times.

Kalliroi Sapountzi
March 2019

Author's declaration

I declare that the work in this dissertation was carried out in accordance with the requirements of the University's *Regulations and Code of Practice for Research Degree Programmes* and that it has not been submitted for any other academic award. Except where indicated by specific reference in the text, the work is the candidate's own work. Work done in collaboration with, or with the assistance of, others, is indicated as such. Any views expressed in the dissertation are those of the author.

Signed: Date:

Table of Contents

List of Tables

List of Figures

Nomenclature

Abbreviations

FFT	Fast Fourier Transform.
IFFT	Inverse Fast Fourier Transform.
NDT	Non Destructive Testing.

Latin characters

A_1 Amplitude of fundamental harmonic frequency.
A_2 Amplitude of second harmonic frequency.

C Propagation Velocity.
C_l Longitudinal Propagation Velocity.
C_t Transverse Propagation Velocity.

f Frequency.

r Radial distance.

t Time.

V Volume of interaction.

X_1 Amplitude of first input wave.
X_2 Amplitude of second input wave.
X_3 Amplitude of non-collinear wave.

Greek characters

α Frequency ratio.

β Non-linear acoustic parameter.

λ Constant. It's value depends on the type of non-linear interaction.

ω Frequency.

π Mathematical constant.
ϕ Interaction angle.

ρ Density of material.

θ_c Critical angle.
θ_i Angle of incident.
θ_r Refraction angle.

Chapter 1

Introduction

The failure of a structure can occur when forces exceed the load-carrying capacity of a component or a member within the construction, and it is seldom desirable [1]. Particularly, the fracture failure mode is undesirable as it can cause instant and catastrophic failure with no prior warning. It is common for advanced engineering structures, i.e. aircrafts, bridges and nuclear reactors, to undergo extreme and dynamic environmental or loading conditions during their life cycle, which can cause crack initiation and growth.

Thorough the history there are several catastrophic examples that highlight the consequences of failed structures. One of the most notable accident in history of aviation was the explosion of the Aloha Airlines Flight 243. In 1988 the Boeing 737-297 was subjected to major damage after explosive decompression. It was concluded that the damage was caused by fatigue due to long exposure in extreme environmental conditions, mainly salt and humidity. In 1987, a Eurocopter Super Puma crashed into the Norwegian Sea while en route to an oil platform. After investigation it was revealed that a crack was in the shaft connector resulted in loss of power in the engine.

[1] Some components are designed to fail under specific conditions such as crumple zones in cars during a crash

The defect was generated by fatigue in the components of the connector. More recently in 2015, a routine inspection in Forth Road Bridge in Central Scotland revealed a 20 mm crack in a steel support truss. The bridge had to remain closed for two months and the closure cost for the Scottish economy was estimated fifty million pounds.

In order to safely operate these components an understanding of the behaviour of the cracks and defects is required. Last century saw the development of fracture mechanics, significantly increasing our understanding of the characteristics and the prognosis of the behaviour of a crack. Anderson (2005) stated *"In 1983, the National Bureau of Standards (now the National Institute for Science and Technology) and Battelle Memorial Institute estimated the costs for failure due to fracture to be 119 billion per year in 1982 dollars."* It is clear that the integrity and soundness of engineering structures and components is important, not only because of the high cost that goes along with a possible failure but also because the value of a human life is priceless. It is up to engineers to develop more sensitive methods to identify defects in order to avoid such incidences in the future.

A crack might start from microscopic defects inherent in the material or induced during manufacturing, excessive loading or poor design. If the defect initiates and becomes a crack, it can grow inservice to a critical length, where failure occurs. Industrial engineers are concerned with the prediction of failure, which could be due to plasticity, fatigue, creep and corrosion. The accurate definition of parameters such as minimum wall thickness, crack critical size and crack growth rate are crucial for the safe operation of a component. While postmortem examination of components can reveal much about what led to their failure, non destructive testing (NDT) allows the

engineer to gain insight into the behaviour of the defect without damaging the component, and thus before and through the lifetime of the component.

The financial impact after the failure, as well as strict regulations with regards to safe operation in the Aerospace Industry and Nuclear Power Plants are the main drivers which push the implementation of success NDT regimes. These can be performed either as a continuous health monitoring — an online data acquisition method which analyses parameters such as stress or strain in a structure — or an in situ measurements during the.

In the aerospace industry specifically, there is a range of non destructive testing techniques currently being approved and used for aircraft alloys as well as the composite materials. Eddy currents, magnetic particles and dye penetrants are used for defects close to the surface of the components. For defects inside the bulk material, thermography, X-rays and ultrasonic methods are used. Despite the wide range of available methods, ultrasonic testing maintains a leading role in this industry.

Conventional ultrasonic testing is based in the generation of a waveform which reflects or attenuates linearly due to their interaction with the defect. These methods are only sensitive to defects that are of a size close to or greater than a wavelength. Non-linear ultrasonic methods have been developed as an answer to this demand; they have the ability to detect changes in the microstructure of a metallic material due to fatigue, creep, thermal ageing and radiation damage in a scale less than a wavelength. This defect size is not currently detectable with the conventional linear ultrasonic non destructive methods.

Non-linear techniques are mainly based on the generation of higher harmonics and are quantified with the measurement of the acoustic non-linearity β. However, the main challenges of the non-linear ultrasonic methods lie

in the fact that the higher harmonics cannot be traced easily. Due to their low amplitude it can remain buried under the noise signals, mainly from the apparatus of the test set-up. Additionally, non-linear ultrasonic methods exhibit high levels of non-linearity introduced by cables, amplifiers and coupling agents. For example, a small difference in the amount of coupling material between different measurements may affect the sensitivity of the results. Non-collinear mixing offers a certain advantage where system non-linearities can be measured and eliminated by subtracting them from the initial signal.

The aims of the work presented in this dissertation are:

- To develop a non-collinear mixing test set-up and investigate the non-linear behaviour of aluminium-adhesive and aluminium-aluminium interfaces;
- To develop a model to assess the possibility of using phased arrays and investigate the steering and focusing capability of non-collinear beams and investigate how certain parameters affect the the testing;
- To design experiments and validate the results in aluminium and carbon fibre reinforced plastic samples.

Chapter 2

Literature review

2.1 Introduction

Non Destructive Testing (NDT) is a wide array of methods that include different techniques used in science and industry to check to assess the integrity of a material without damaging it. Ever since NDT methods started to be used in the late 19th century different methods have been used to detect defects or features in engineering components that directly affect the reliability, such as fatigue, corrosion, stress, pores. The most common NDT methods are:

- Eddy currents
- Magnetic Methods
- Radiography
- Thermography
- Dye penetration
- Ultrasonic testing

Magnetic methods and especially Eddy currents, discovered by Faraday in 1831, had been used in the aerospace industry for detecting cracks by altering the magnetic fields which is generated by an electrically conductive material and coil and is mainly used in the inspection of turbo engines.(reference from book)

Radiography methods go back to the late 19 century when Röntgen created the first X-ray image of human body. Nowadays, it is a common inspection method in welded parts, as well as for sub surface features. It can be more challenging for planar defects or delaminations of Carbon Fibre Composites. The method consists of a radioactive beam which propagates in a material and depending on itscondition, booksit absorbs in different amounts. This difference can be pictured in a film placed opposite the component. Despite the wide usage, the method imposes certain negatives such as expensive equipment, well trained operating staff and high health and safety risks due to the radiation.

Thermography is a method which detects differences in the temperature profile of the radiation the test object emits with an infrared camera. The detection is taking place in the infrared spectrum (2-5.6 mm and 8-14 mm), Avdelidis et al. (2011).

Dye penetration is cost effective. It is used to find cracks, pores, gaps, seams that are located in the surface of materials, usually metals. Glass, polymers and ceramics may be tested too. The main challenges are the defect has to be in the surface and also is time consuming because of the preparation and cleaning of the surfaces before and after the testing, *Non Destructive Testing - A Survey* (1973). With this method, liquid fluorescent penetrants are applied in the surface of the test specimen. After some time

the excess solutions is wiped away and the penetrated fluid goes back to the surface in case of a defect.

Ultrasonic techniques have been widely used for non destructive testing of engineering components, Halmshaw (1991). Common defects that can be detected are pores, cracks corrosion and delaminations in carbon fibre composite materials. Historically it goes back to 1940 when Dr Floyd Firestone used high frequency waves that propagated in a material and subsequently he measured the time of different reflections and he made assumptions upon the quality Despite their efficiency in large scale defects, bigger than the wavelength, such as cracks, porosity and voids they exhibit limited sensitivity in smaller scale defects with size smaller than the wavelength. Given that micro-structural defects might appear at the very early stage of life of a material, it is important to be able to identify this early damage before macroscopic defects, e.g. cracks and voids are formed. And answer to this challenging engineering problem can be the non-linear ultrasonic inspection.

2.2 Non-linear ultrasonics

A wave is a disturbance or a variation that transfers energy within a medium. Sound is a mechanical wave of pressure or displacement that propagate within a medium (e.g. solid, air or water). Ultrasound is sound with a frequency above the limit (20 kHz) that humans are able to hear. Non destructive evaluation using ultrasound is achieved by transmitting and receiving vibrations using a piezoelectric crystal. The ultrasonic waves are caused by the phenomenon of piezoelectricity; a crystal vibrates due to mechanical stress which results in the generation of electric charge. The piezoelectric effect can produce frequencies between 0.1 Hz and 50 MHz.

Conventional ultrasonic testing is based in the classic theory of elasticity. Here, it is assumed that certain phenomena, such as transmission, refraction and superposition behave in a linear manner. Linear propagation of waves is observed only when their amplitudes are small and also the propagation times and distances are small too. Taking into account the propagation of an *infinitesimal wave* (waves with small amplitude), it is considered that all phases of the ultrasonic propagate with the same velocity.

However, in the case of *finite waves* (waves with large amplitudes) the effects of non-linear propagation take place in a form of higher harmonics to the fundamental frequency. The part of the wave that with higher pressure travels faster than the part with lower pressure. This results in a distortion of the the shape of the wave. After Fast Fourier Transformation, the frequency domain shows the higher harmonic components. When solving the propagation equation with the higher terms, the-non linear parameter β can be calculated. It is proved in literature that β is related to the molecular state of the material and its ability to generate higher to the fundamental frequency harmonics.

The non-linear theory thing goes back to Lighthill (1956) who studied the deformation of the amplitude of finite amplitude waves during their propagation in viscose fluids. In order to study the linear behaviour of acoustic waves, we can use the equation of Euler which represent the motion of a disturbance in an ideal medium. Euler in 1766 produced an equation which described the non-linear plane acoustic waves in air. His work was focused in interpreting why Newtons formula for the speed of sound in air was coming with a loss of 16 per cent. The answer was thought to be with infinite amplitude waves and thus took into account the higher terms to find the value of the velocity. Later on, Earnshaw managed to prove that

the nonlinear waves propagate in a different speed than the linear waves. Lagrange (1761) managed to solve the non-linear wave equations which were followed by Poisson (1808), Airy (1849), Earnshaw (1885,1869) and Rieman (1860) progressed developed the theory of non-linear wave in lossless fluid. Even when the amplitudes are still small, there will still be observed non-linear effects due to the long propagation distance and time.

Non linear ultrasonics have been extensively researched in order to measure the non-linear behaviour of a material. Zarembo and Krasil'nikov (1971) showed that the main source of non-linearity is the anharmonicity of the lattice determined by the higher order elastic constants making the stress-strain relationship in an isotropic material non-linear. The harmonic generation technique relies on non-linearities in a material generating multiple integer harmonics of the input frequency. By measuring the amplitudes of the harmonics, the second harmonic amplitude (A_2) can be normalised against the square root of the fundamental harmonic amplitude (${A_1}^2$) since the contributions of lattice anharmonicity and dislocations are proportional to (${A_1}^2$). Buck, Morris and Richardson (1978) studied the harmonic generation in order to detect micro-cracks on the surface of aluminium during fatigue. They identified a non-linear parameter as $\beta \approx \frac{A_2}{{A_1}^2}$ and showed that this normalisation corrects the variations in A_1 and the parameter is sensitive to applied stress and that harmonic amplitude increases smoothly with fatigue. Yost and Cantrell (1992) and Cantrell and Yost (2001) showed that another source of non-linearity are the dislocation dipoles introduced in a material due to fatigue and it can be used as a non destructive tool.

A number of authors Buck, Morris and Richardson (1978), Kim, Lee and Jhang (2016), Yan, Drinkwater and Neild (2009)have further investigated the

possibility of detecting fatigue, cracks and kissing bonds with the harmonic generation technique.

Despite the promising results of the non-linear ultrasonic inspection, there are two main challenges:

- It is difficult to identify the source of nonlinearity in the material
- It is difficulty to separating the non-linearities introduced by the set-up apparatus, for example amplifiers, function generators and coupling materials.

2.3 Non-collinear mixing

A possible solution to this is the non-collinear mixing technique. The approach was first described by Jones and Kobett (1963) and relies on two intersecting elastic waves interacting in and homogeneous material. In the linear theory the equations of motion are linear and the two waves do not interact, so they propagate without to change in energy. Considering the cubic terms of the elastic energy the equation of displacement becomes non-linear, thus interaction that produces scattering can hold. Jones and Kobett studied three different cases of interaction between two intersecting waves; two shear waves, two longitudinal waves, one longitudinal and one shear. If the resonance conditions are held, two shear waves interact and within the volume of interaction a third longitudinal wave is produced. It has a wavevector equal to the sum of the wavevectors of the primary waves, is formed at an interaction angle ϕ,

$$\cos(\phi) = \frac{{C_t}^2}{{C_l}^2} + \frac{1}{2}\left(\frac{{C_t}^2}{{C_l}^2} - 1\right)\left(\frac{\omega_1}{\omega_2} + \frac{\omega_2}{\omega_1}\right) \tag{2.1}$$

where C_t and C_l are the transverse and shear propagation velocities respectively and ω_1 and ω_2 are the frequencies of the intersecting waves). The amplitude of the non-linear wave, X_3, is given by

$$X_3 = \frac{X_1 X_2 V {\omega_1}^2 a(1+a)\Lambda}{8\pi r \rho C_t C_l} \tag{2.2}$$

where X_1 and X_2 are the amplitudes of the incident waves, V is the volume of interaction, λ is a value depending on the type of interaction which can be found in literature, α is the frequency ratio, r is the radial distance and ρ is the density of the material. Later, Rollins, Taylor and Todd (1964) showed that material non-linearities are responsible for the non-collinear interaction and Rollins experimentally verified the theory introduced by Jones and Kobett.

The main advantages of the non-collinear mixing technique can be summarised as the following:

- The system non-linearities can be measured by subtracting the individual responses of the incident waves after individual excitation from the total response of the system and secondly,
- the technique is much less sensitive to system non-linearities because of frequency selectivity, modal selectivity, spatial selectivity and directional selectivity Croxford et al. (2009).

Although authors have shown promising results in the detection of plasticity and fatigue Croxford et al. (2009) and physical ageing in PVC polymer Demenko, Koissin and Korneev (2014), the technique exhibits significant complexity. Small misalignments and coupling inconsistency can have a crucial impact on the amplitude of the scattered wave.

Chapter 3

Interface non-linearity measurements

3.1 Introduction

An adhesive is a non metallic material used to hold two interfaces together in such a way that the joined materials cannot be broken without the subsequent damage of the bond. Adhesives include glues, epoxies or plastic agents that bond two materials by evaporation of a solvent or by curing an agent with heat, pressure, or time.

The main advantages of adhesive bonding are heat resistance, corrosion resistance, high dynamic strength and the flexibility to join both similar and dissimilar materials, i.e. metal-metal and metal-carbon fibre. Conventional physical and mechanical joining techniques, such as welds and bolts, introduce extra weight to a structure and possible residual stresses that may affect its performance.

The use of adhesive materials as a joining method of metallic materials has become more popular, especially in the aerospace industry. Adhesives

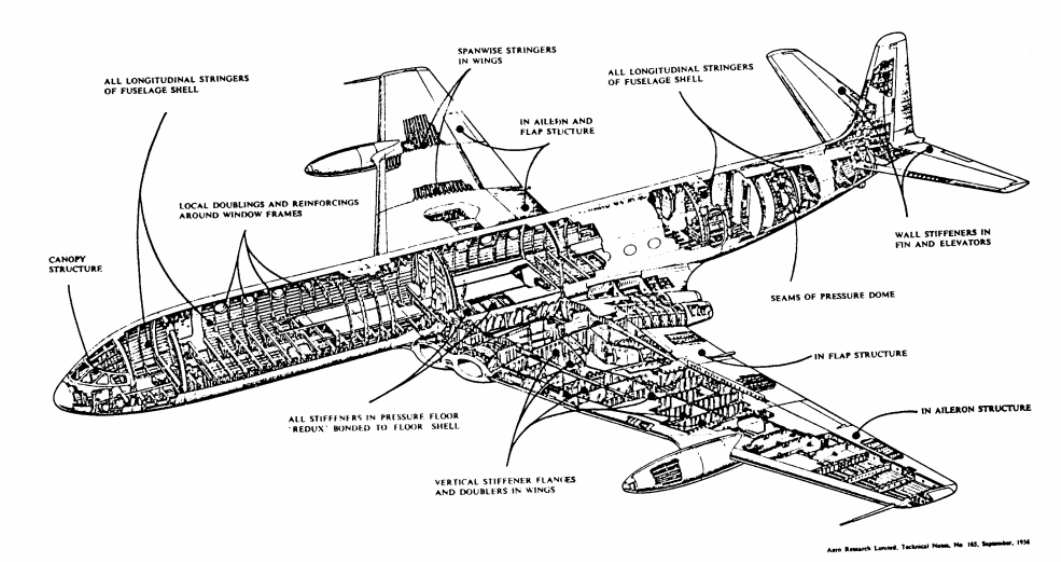

Figure 3.1: Adhesive used in the Comet aircraft, Beevers (1995)

started to be used in the aircraft industry after the Second World War where synthetic adhesives substituted the natural glues. One of the first adhesives used in the automotive industry and later on in the aerospace industry was the Redux adhesive, produced by Aero Research Limited at Duxford. Mainly it was used to fix stringers and doublers to wings and fuselage. De Havilland and Fokker started to use adhesives in their aircrafts, i.e. Hornet, Comet (Figure 3.1), Dove and F27 respectively, Driver (1995).

In the 1990s Boeing started to use adhesives with the main applications being F-15 belly skin and B-12 fuselage components (aluminium–aluminium), F-18 and F22 (titanium–titanium)and Apache AH-64 rotor blades (stainless steel), compliant (1999). More recently, Airbus reduced the weight of the A380 by 40% by extending the usage of adhesive bonded structures. Some examples are shown in Figure 3.2.

Despite the advantages of great flexibility and low weight of structural adhesives, one of the main aspect that needs further consideration is that adhesively bonded components exhibit sensitivity in fatigue, corrosion, high

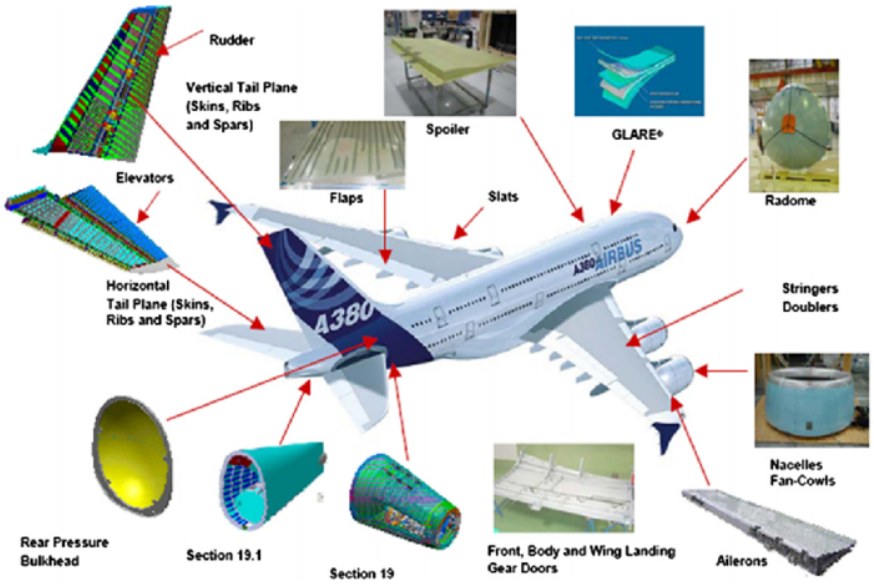

Figure 3.2: Examples of bonded structures in the Airbus A380 aircraft, Katsiropoulos et al. (2012).

loads. These might result in crack, debonding, and potentially failure of the component. In the Airbus A320 turbofan, Figure 3.3, the intake acoustic panels and the titanium attachment rig are bonded together with a layer of Hysol EA 934 adhesive. The difference in the temperature the parts are exposed to during the flying cycles, from -50 to 50 Celsius, affect the corrosion resistance of the adhesive which subsequently affects the mechanical performance of the bond. This might lead to failure, thermal stresses lead to cracks, Anes et al. (2016).

This chapter focuses in the investigation and detection of non-linear behaviour in kissing bonds with the non-collinear mixing technique. Previous researchers (Section 3.2) have shown that adhesive bonds exhibit sensitivity to non-linear ultrasonic methods. The initial idea was to use the Yan et al approach and set-up in order to perform the measurements. It is set-up that provides an interface which is already investigated, it is good quality epoxy, an interface already used by the industry. The first section focuses

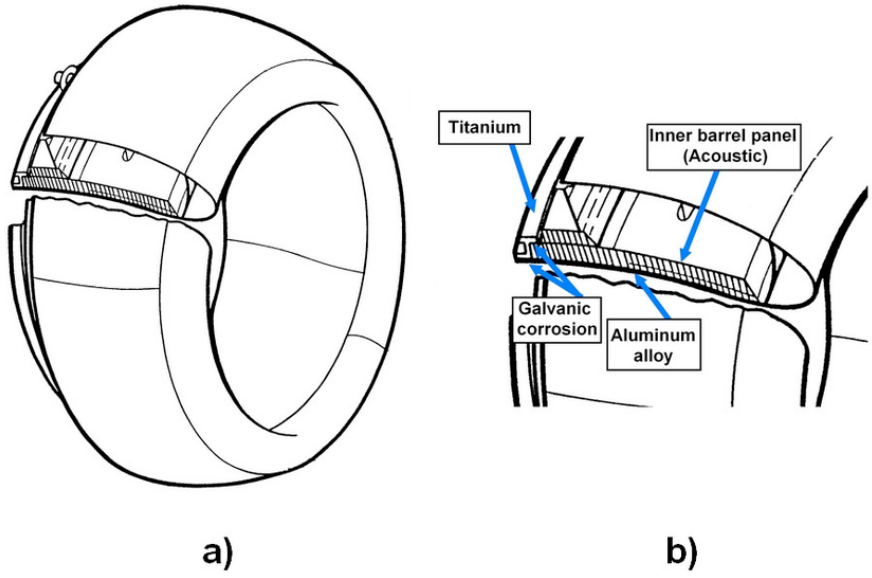

Figure 3.3: A320 intake barrel panel geometry and corrosion area (left) and inner panel (right), Anes et al. (2016)

on the work already done in the field of interfaces and explains why a new approach is necessary. The second section describes the set-up used in the experiments.

3.2 Measures of non-linearity at interfaces

Several authors have investigated the effect of temperature , moist, radiation and fatigue in the mechanical properties of adhesive bonds. Bhowmik et al. (2006) investigated the effect of radiation. adhesives have been used in aerospace applications due to lightweight features which decreases the weight thus the cost. They concluded that the main challenge is to maintain a uniform distribution of stresses during loading to prevent failure. They also studied titanium adhesive in different climate conditions and found that

when adhesives are exposed to radiation and corrosion environments, the adhesive joints are prone to failure.

A kissing bond can be simulated by a partially closed interface. Solodov (1998) showed that if a signal propagates trough a partially closed interface, it will get distorted, consequently if different loads are applied, different levels of non-linearity can be theoretically expected.

Kendall and Tabor (1971) studied the area of contact between stationary and sliding surfaces. An ultrasonic wave was generated in a body and the intensity of the wave transmitted through the interface was measured and related to the interfacial stiffness.

The acoustic technique was successfully used in studying the static contact between different types of materials. However, the interfacial stiffness did not seem to depend uniquely to the true area of contact. Krolikowski applied hydrostatic pressure and created the contact interface by applying hydrostatic pressure in the samples creating spherical voids and the reflection coefficient was calculated, taking results that related pressure and the reflection coefficient, Krolikowski, Szczepek and Witczak (1986).

Later, he used theoretical models to calculate the surface parameters but significant discrepancies were observed Krolikowski and Szczepek (1991). Buck, Thompson and Rehbein studied the harmonic generation in order to detect micro cracks on the surface of aluminium during fatigue. Results showed that the harmonic amplitude increases smoothly with fatigue, Buck, Morris and Richardson (1978).

Partially closed interfaces are of significant importance because the reduced probability of their detection. Significant progress was made in the interpretation of acoustic signals in determining the sizing and density of asperities along with fracture surfaces by the same authors Buck, Thompson

and Rehbein (1984). Drinkwater et al. used a numerical elastic contact model and a simple spring model in order to predict the reflection coefficients from a rubber-solid interface under load and results showed reasonably quantitative agreement between experimental and theoretical results for contact at 80%-100% Drinkwater, Dwyer-Joyce and Cawley (1994). Solodov suggested that a potential source of non-linearity in solid contact interfaces is the 'clapping' mechanism; the local opening and closure of a contact by the acoustic wave and the contribution of the clapping mechanism to the acoustic non-linearity in a material is an indication of a defect developing at the interface Solodov (1998). Kim at. al performed low frequency ultrasonic measurements at cyclically loaded aluminium plates. They showed that non-linear modulation of reflected pulses depend upon the crack length and closing conditions; being weak when a crack is closed or completely open. Additionally big second harmonic generation which is observed when the reflected wave is applied at loads that kept the crack fully open or completely closed and it comes with good agreement with the proposed low frequency scattering model Kim, Yakovlev and Rokhlin (2004). Several authors used the spring model to explain the propagation of ultrasound waves across rough interfaces Delsanto et al. (2002), Kim, Yakovlev and Rokhlin (2004), Baltazar, Rokhlin and Pecorari (2002), Drinkwater, Dwyer-Joyce and Cawley (1996). Drinkwater et.al used a spring model to determine the interfacial stiffness of two aluminium plates under pressure and found good agreement with the experimentally determined values. The predicted stiffness was within an order of magnitude of the measured value Drinkwater, Dwyer-Joyce and Cawley (1996). Baltazar et al. used a spring model to describe the micromechanics of rough surfaces under loads. Results showed that the model were able to predict the dependant of interfacial stiffness constants of the pressure

as well as an estimation of their ratio Baltazar, Rokhlin and Pecorari (2002). Kim et.al showed that an elastoplastic model which was used to describe the hysteresis of cyclically loaded aluminium surfaces showed consistent value of the surface parameters Kim, Yakovlev and Rokhlin (2004). Delsanto et.al used the LISA spring model (Local Interaction Simulation Approach) along with a tensorial parameter in 2D dimensions for two aluminium plates in order to investigate the quality of the interface which was in good agreement with the experimental data Delsanto et al. (2002).

A number of authors categorised the defects in three categories: in the first category gross defects are included, in the second category defects found in the adhesive layer are included and in the last, defects found at the interface of adhesive-adherent are included Adams and Drinkwater (1997) Guyott, Cawley and Adams (1986). Nagy describes as a kissing bond the result of plastic contract between smooth and rough surfaces; a bond that produces little or no strength Nagy (1991). Jiao et al. described the kissing bond as a bond which had perfect contact between two solid media but with no shear stress. Kissing bonds do not exist in real structures but they are used as a guideline model in order to investigate real bonding weakness Jiao and Rose (1991). Achenbach et.al used a spring model and a spring-mass model in order to describe the non-linear ultrasonic interaction with an adhesive bond. They showed that the adhesive layer can be modelled as a non-linear spring that tends towards a thin interface Achenbach and Parikh (1991). Rotherfusser et al. studied the effect of second harmonic generation in an aluminium-epoxy-aluminium adhesive joint. He showed that the second harmonic generated from the adhesive layer itself depends upon the thickness and the sound velocity of the adhesive. Additionally, the theoretical results after Finite Element analysis were of good agreement with

the experimental data Rothenfusser, Mayr and Baumann (2000). Yan et al. measured the degree of non-linearity in perfectly and imperfectly bonded interfaces in aluminium-aluminium and aluminium-adhesive specimens and developed a time domain model in order to simulate the wave propagation through the adhesive as well as to understand the effect of the adhesive layer in the extracted non-linear parameters Yan, Drinkwater and Neild (2009) Yan, Neild and Drinkwater (2012). Bortherhood et.al studied the effect of compression loading on the ultrasonic detectability of dry contacted and liquid layer kissing bonds. He also developed a spring model to predict the reflection coefficient of dry contact kissing bond under load and a numerical model to predict the interfacial stiffness. The models showed good qualitative and quantitative agreement with the experiments Brotherhood, Drinkwater and Guild (2002) Brotherhood, Drinkwater and Freemantle (2003). 'Experimental Adhesive Failure Criteria for Analysis of Aerospace Structures' (2015) and Antunes, Infante and Reis (2016)

3.3 Experimental arrangements

3.3.1 Equipment

In order to investigate the non-linear behaviour of kissing bonds developed in adhesive joints, a test rig that consisted of an aluminium-adhesive interface was designed. The experimental rig was partially designed by Yan (2010) for the PhD project in the *Detectability of kissing bonds in adhesive joints using non-linear ultrasonic techniques*. Yan, studied the non-linear ultrasonic behaviour of kissing bonds with a series of different defects. The manufactured bonded joints were the following:

- Liquid layers specimens where the aluminium adherent was contaminated by lubrication oil;
- Electrically release specimens where electrically released sandwich specimens were cured in different times in order to produce defects in the adhesive layers, i.e. bubbles;
- Compressively bonded specimens; where a number of cylindrical specimens with a different quality of interfaces were used.

For the current project, one of the cylindrical compressively bonded specimens, with 20 mm diameter was used as seen in Figure 3.4.The cylinder had a perfectly bonded 2 mm thick 3M EC3448 structural aerospace epoxy layer from one side. In order to achieve the optimum bonding conditions, the surface of the cylinder underwent specific treatment. That involved the interfaces to be cleaned with acetone, etched in sulphuric acid at 60° for 30 minutes and then rinsed with water to remove remains of the acid and finally dried. Afterwards, the epoxy adhesive was compressed on the free side of the cylinder, Figure 3.4, left.

In order to create a test sample big enough to accommodate both transmitting probes, an aluminium plate with dimensions 260 mm $\times$ 80 mm $\times$ 45 mm was designed to be positioned on top of the cylinder. The plate had enough width to host the ultrasonic transducers along with their wedges as well as another cylindrical metallic mass which was fixed in the aluminium plate for structural purposes. This part was acting as mechanism that transmitted the load from the loading machine to the test rig, Figure 3.5.

Additionally, within this cylinder there was enough room for a small 15 mm dimeter piezoelectric transducer to be bonded on top of the aluminium plate. A 2 mm hole on the side of the cylinder gave enough room for

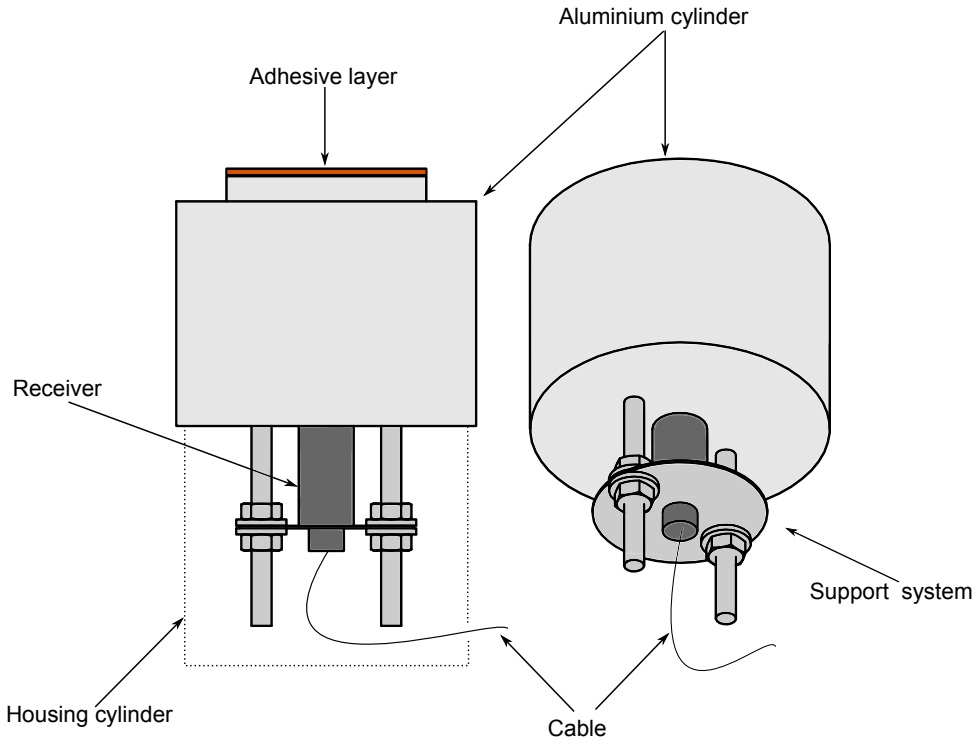

Figure 3.4: Cylinder with a layer of adhesive, to be placed under the aluminium plate. The 10 MHz receiver was held with a system of nuts and bolts.

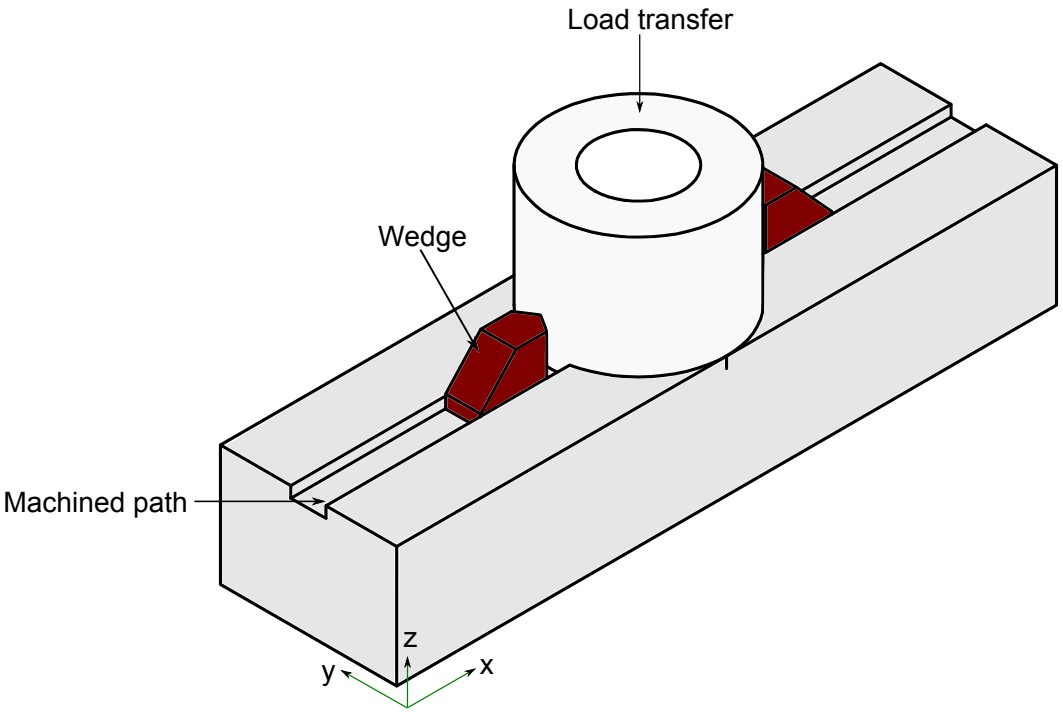

Figure 3.5: Aluminium plate positioned at the top of the cylindrical specimen.

the piezoelectric cables to connect with the apparatus. The receiving probe was held by a fixture of nuts, bolts and a spring, Figure 3.4.

In order to secure a robust fixture for the wedges (where the ultrasonic transducers were mounted on), the top of the aluminium plate was machined all the way along the length of the specimen. Material was removed in 2 mm depth and 1 cm width creating a ”track” where the perspex wedges could slide. This secured a fixed position, leaving the wedges with only one degree of freedom of movement, Figure 3.5. After applying coupling gel, the wedges were secured in the preferred position with G clamps. The screwed clamps would provide enough force to prevent the wedges from moving as well as to push the wedges down, so as to keep them in good contact with the plate. The applied force would remove air bubbles from the coupling gel and thus could secure better coupling conditions, Figure 3.6.

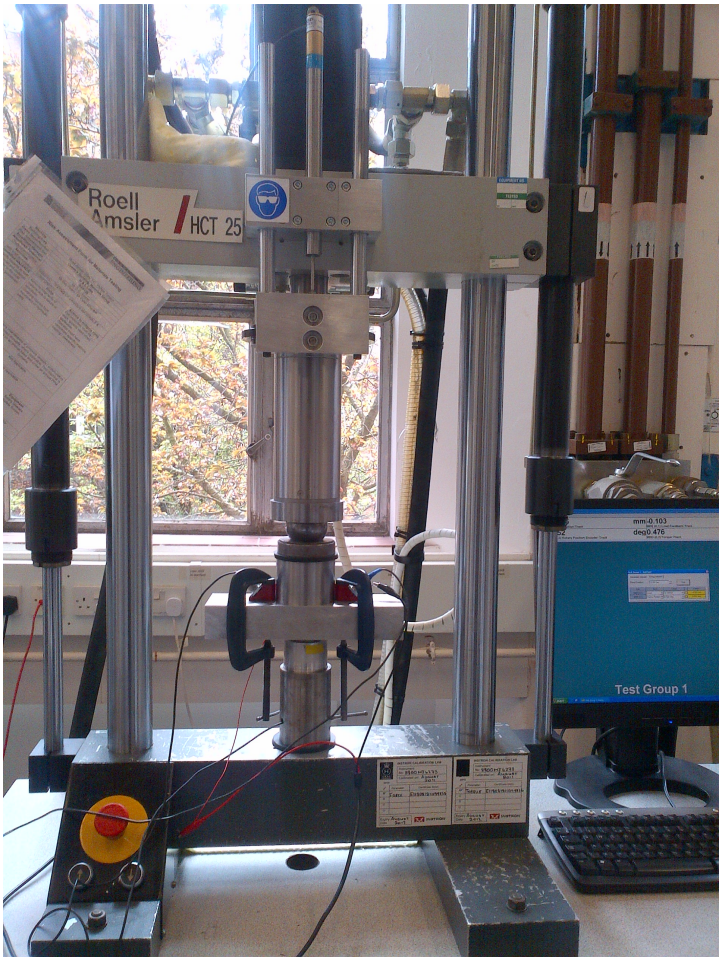

Figure 3.6: Experimental apparatus in loading machine.

In order to simulate a kissing bond, the plates were subjected to cyclic loading. This was performed with an Instron Schenck hydraulic loading machine which was used to subject the specimens to compression in a range of loads up to 14 kN which resulted in a nominal stress of up to 4 MPa. It can also be seen in Figure 3.6.

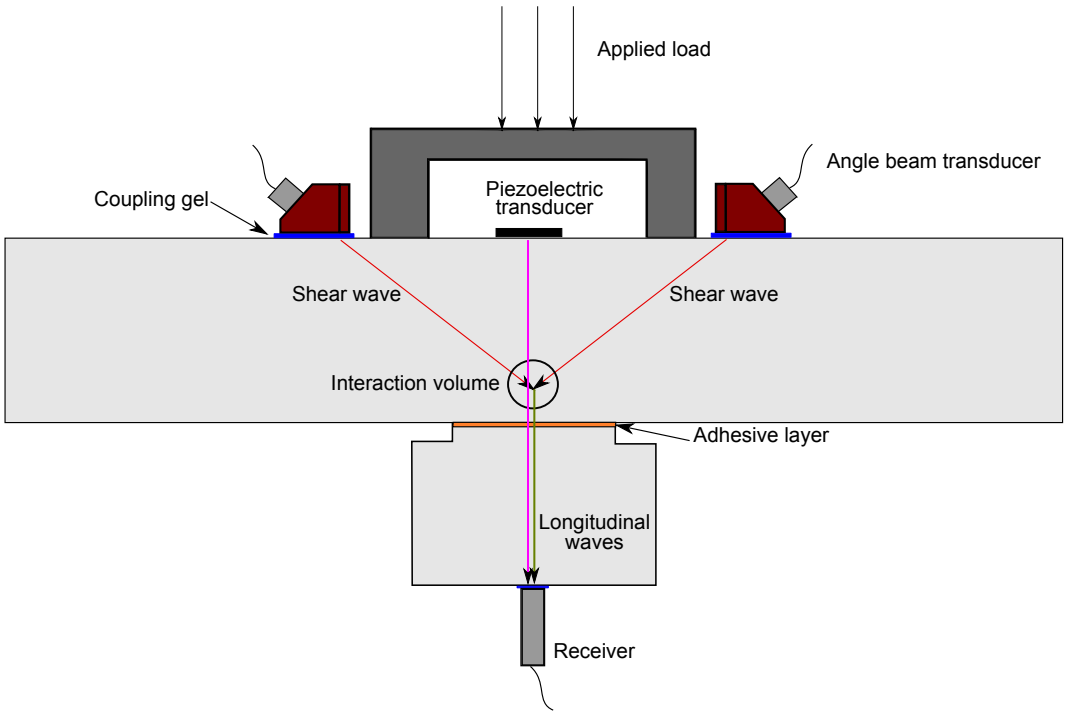

Figure 3.7: Harmonic generation and non-collinear mixing test set-up for the aluminium-adhesive interface.

3.3.2 Excitation and signal capture

Figure 3.6 shows the geometry and the basic components of the test rig as described in Section 3.3.1. For this project, two Olympus angle beam transducers of 5 MHz centre frequency were selected. This frequency is commonly used for the inspection structural components of aluminium and could also provide enough penetration in the test material Darmon et al. (2015). Additionally, this type of angle beam transducers can produce

standard refracted angles in aluminium, generating refracted shear waves or longitudinal waves into the test specimen which are useful for the non-collinear mixing.

As described in Chapter 1, the technique is based on two shear ultrasonic waves interacting with the interaction angle satisfying the resonant conditions, (Jones and Kobett 1962). The minimum angle that results in the generation of a resonant wave for the same driving frequency and for frequency ratio f_1/f_2 equal to one, is 120°. In order to obtain this angle, a refraction angle of 60° from the incident waves was essential. Consequently, by selecting a wedge configuration of 60° and according to Snell's law and mode conversion, inside the material a shear wave in the aforementioned angle would be generated and propagated, whereas the longitudinal wave would not be detectable as it would subject to total internal refraction at the surface of the specimen.

Jason and Kobett showed that for the case of interaction of two shear waves with the same driving frequency, the scattered wave will have the frequency and direction equal to the sum of the driving frequencies and wave vectors respectively. For this reason, an Olympus wideband transducer with 10 MHz centre frequency was selected to detect and capture the non-collinear wave. From the geometry of propagating signals, this wave was expected to propagate in direction perpendicular to the interface of the specimen, thus the receiving transducer was positioned at the opposite side of the set-up.

Along with the non-collinear mixing method, non-linear second harmonic measurements were carried out using a high frequency undamped piezoelectric transducer (Ferroperm, Piezoceramics) of 15 mm diameter and 2 mm thickness. The disc was bonded on the aluminium plate, inside the pressure cylinder as seen in Figure 3.7. The harmonic generation technique is based in

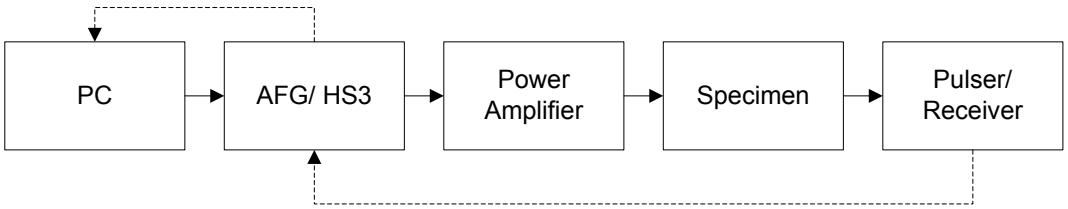

(a) Through transmission

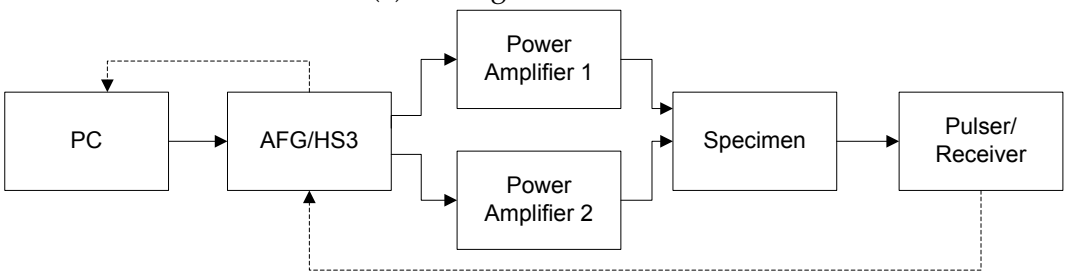

(b) Non-collinear

Figure 3.8: Schematic diagrams of the two different experimental set-ups.

the detection of higher frequency vibrations that are generated in a material, therefore the same Olympus 10 MHz wideband receiver was adequate to receive the higher harmonic frequencies.

The test rig and measuring system arrangements can be seen in Figure 3.8a. An HS3 Tie Pie handyscope worked initially as an arbitrary waveform generator, creating two 15 cycle tone bursts, and was connected to a standard PC with en external power cable.

The signals were amplified by an 75A250 Amplifier Research power amplifier which increased the peak-to-peak voltage of the input signal. The signals were transmitted from the probes, propagated through the specimen and the scattered signal was detected by the 10 MHz wideband transducer. Then it was pre-amplified by a Pulser/Receiver at 2.5 dB. The amplification process was essential as the non-linear signals are several orders of magnitude smaller than the linear signals and thus difficult to detect. The

non-collinear signal was received by the same handyscope and was finally digitised by a MatLab software for further processing.

3.3.3 Signal processing technique

In the non-linear ultrasonic measurements the main point of interest is the detection and the interpretation of higher harmonics. The higher harmonics are several orders of magnitude smaller than the first harmonics. Consequently the non-linear reflections can be either masked within the linear echoes or buried under the noise. Additionally, the apparatus, such as the transducers, power amplifiers, pulser, receiver, cables and coupling gel all contribute to the system's non-linearity. As the signal moves through the path, it goes through further distortion and generation of unwanted features. Consequently, an effective filtering technique is essential in order to remove these features and unmask the non-linear signal.

Figure 3.9a shows the basic steps carried out in both non-collinear mixing and harmonic generation technique. A Hanning band pass window was selected and applied at the full length of the received signal and a Fast Fourier Transformation (FFT) algorithm helped in frequency analysis and revealed the frequency domain. And Inverse Fast Fourier transformation (IFFT) was applied at the part of the spectrum where the second harmonic frequency was. The interference of other frequencies or unwanted features were removed and thus a filtered signal, clean from the unwanted features, was achieved.

Several authors, Croxford et al. (2009), Demcenko et al. (2012), Demenko, Koissin and Korneev (2014), have stressed the benefits of the non-collinear mixing with the main benefit being the ability to remove easier and more

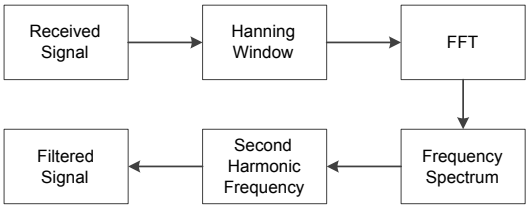

(a) Harmonic generation

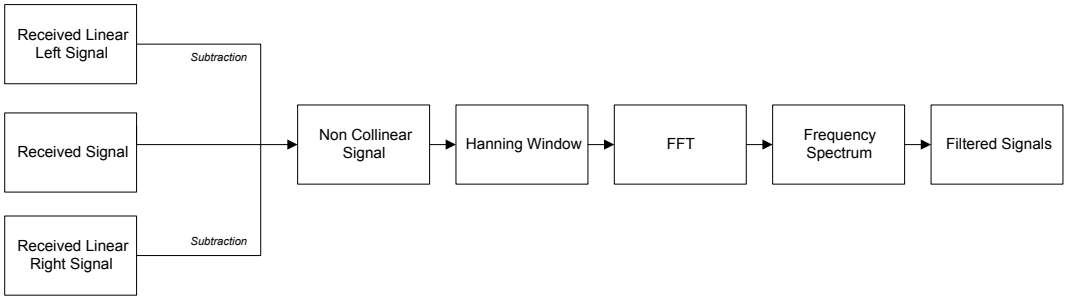

(b) Non-collinear mixing

Figure 3.9: Basic signal processing steps for each method

effectively these non-linearities. This is generally easier to achieve when the following steps are followed:

1. A single excitation of the Left hand transducer (S_L) only.
2. A single excitation of the Right hand transducer (S_R) only.
3. An excitation with both transducers firing simultaneously($S_L + R$)
4. A subtraction of the individual signals (S_L) and (S_R) from the

A Hanning band pass window was applied to the subtracted signal for the revelation of the frequency spectrum and finally the non-collinear signal was received after the IFFT.Figure 3.9 shows the described processing steps.

This was primarily investigated in an aluminium plate with a simple double sided non-collinear set-up. Using the geometry on the test specimen and the sound velocity of the aluminium, the theoretical time arrival of the linear and non-linear reflections could be calculated. In this case, the thickness of the plate was 62 mm, the separation of the probes was 10 cm

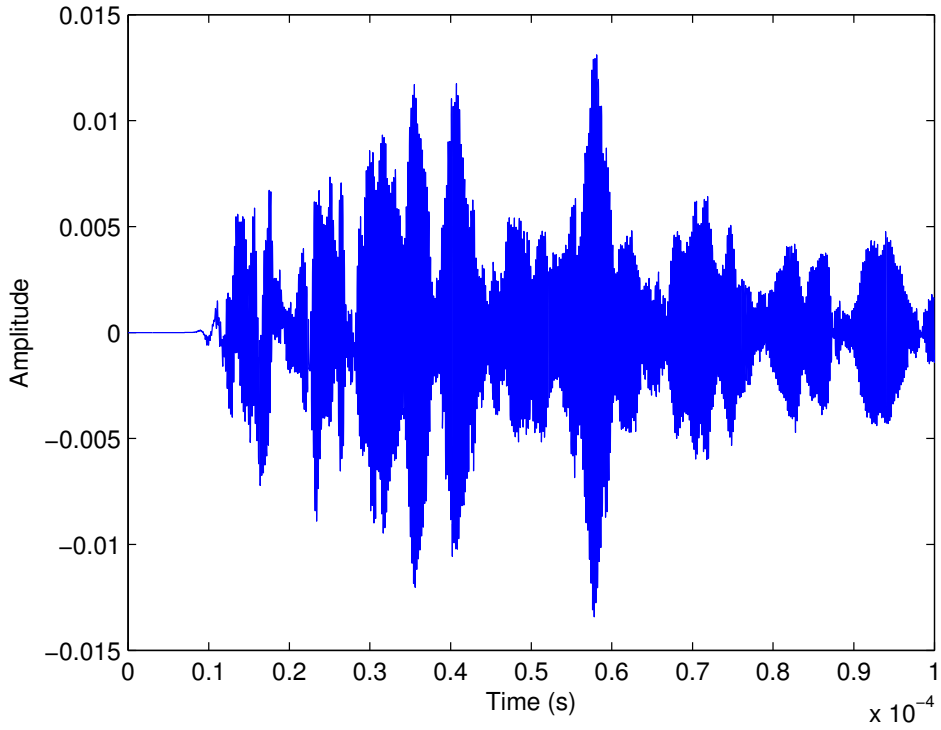

(a) Received signal.

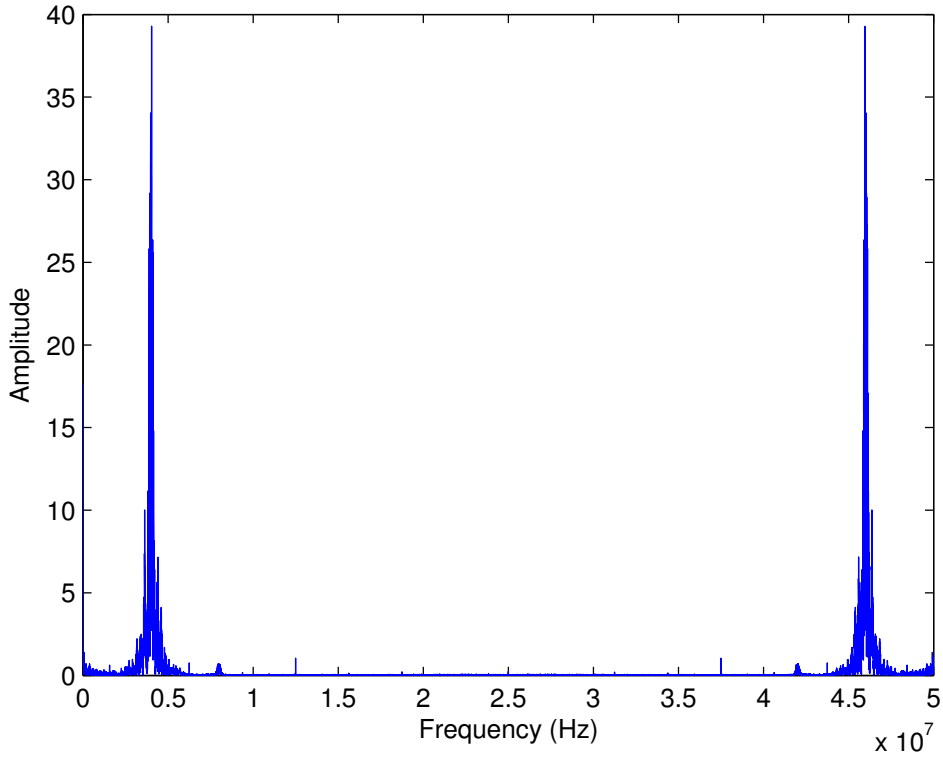

(b) Frequency Spectrum

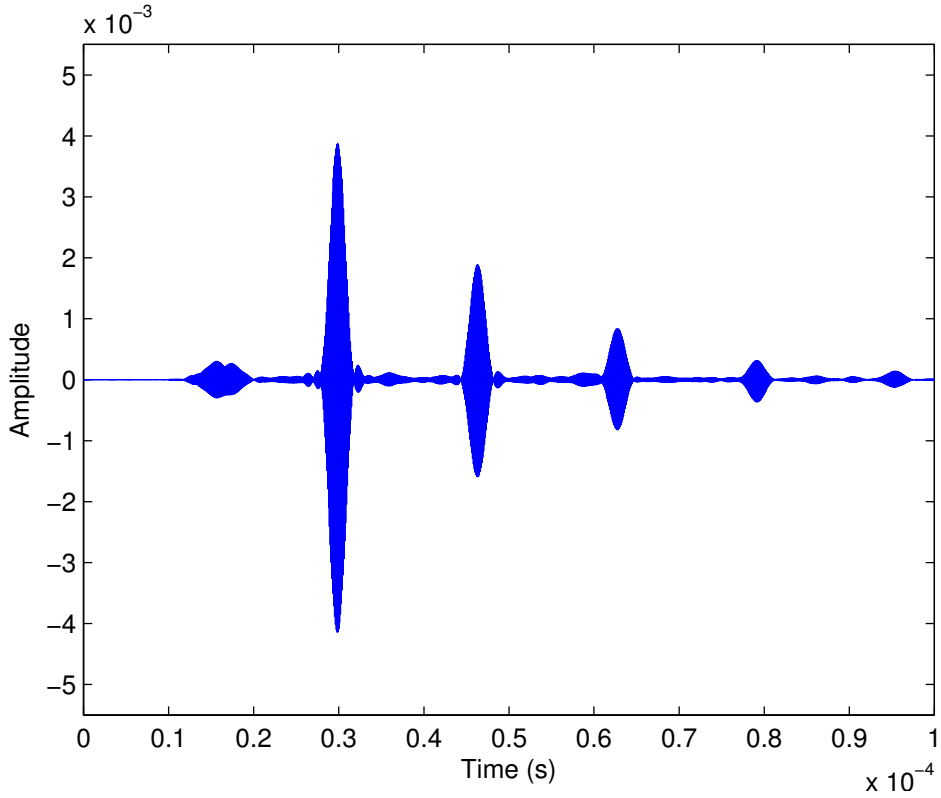

(c) Fitered signal

Figure 3.10: Processing steps for a simple non-collinear mixing test

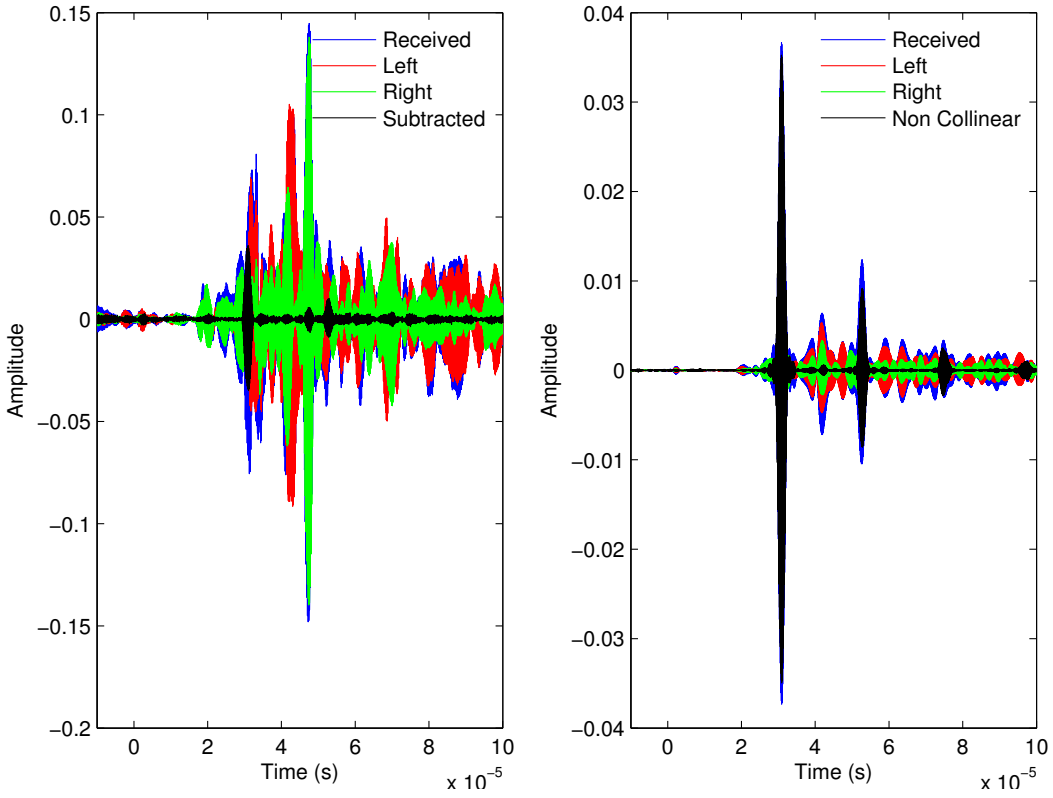

Figure 3.11: Subtraction concept in the non-collinear mixing technique after following the steps described in Figure 3.10. On the left, the black waves represent the result of subtraction of the responses of the transducers fired separately from the actual received signal a.

thus the time arrival of the non-collinear reflections was calculated as shown in Table 3.1. By comparing the theoretical calculations and the results from Figure 3.11 the successful filtering process can be verified.

3.4 Experimental Tests

3.4.1 Aluminium-Adhesive non-linearity

In order to evaluate the non-linear behaviour of the aluminium-adhesive interface with the non-collinear mixing method and for better understanding and interpretation of it, the harmonic generation technique was used as

Table 3.1: Expected time arrival of non-collinear reflections in a 62 mm aluminium plate and 10 cm separation of input transducers during a double sided arrangement testing.

Reflections	1^{st}	2^{nd}	3^{rd}
Time arrival (s)	2.9×10^{-5}	4.8×10^{-5}	8.8×10^{-5}

a reference method. The experimental arrangement for the detection and evaluation of higher harmonics was similar to the one developed by Yan et al. Yan studied the non-linear behaviour of a contact type kissing bond. His kissing bond consisted of two cylindrical specimens with an aluminium-epoxy adhesive interface. In one of the cylinders there was a perfectly bonded epoxy adhesive layer (3M EC3448) with 2 mm thickness. In order to produce a partially closed interface he subjected his specimen in loading cycles. During the loading procedure, he emitted large amplitude ultrasonic waves by a piezoelectric disk boned at the one side of the cylinder. The ultrasonic wave propagated through the kissing bond interface and detected by a probe fixed at the bottom of the cylinder.

In order to achieve high amplitudes for the higher harmonic vibrations, the full power of the transducers had to be used. But for the harmonic generation case, the selection of the proper driving frequency can be associated with the *natural filtering method*. Yan (2010) showed that if the transfer functions of the transmitting element is known, Figure 3.12, the harmonic impurities deriving from the amplifiers and the arbitrary waveform generator can be eliminated simply by selecting driving frequencies that correspond to the resonant peak of transfer function. In practice this means that the ideal transmitting frequency lies in the maximum of the transfer function while at the same time, the harmonic of the input signal should correspond

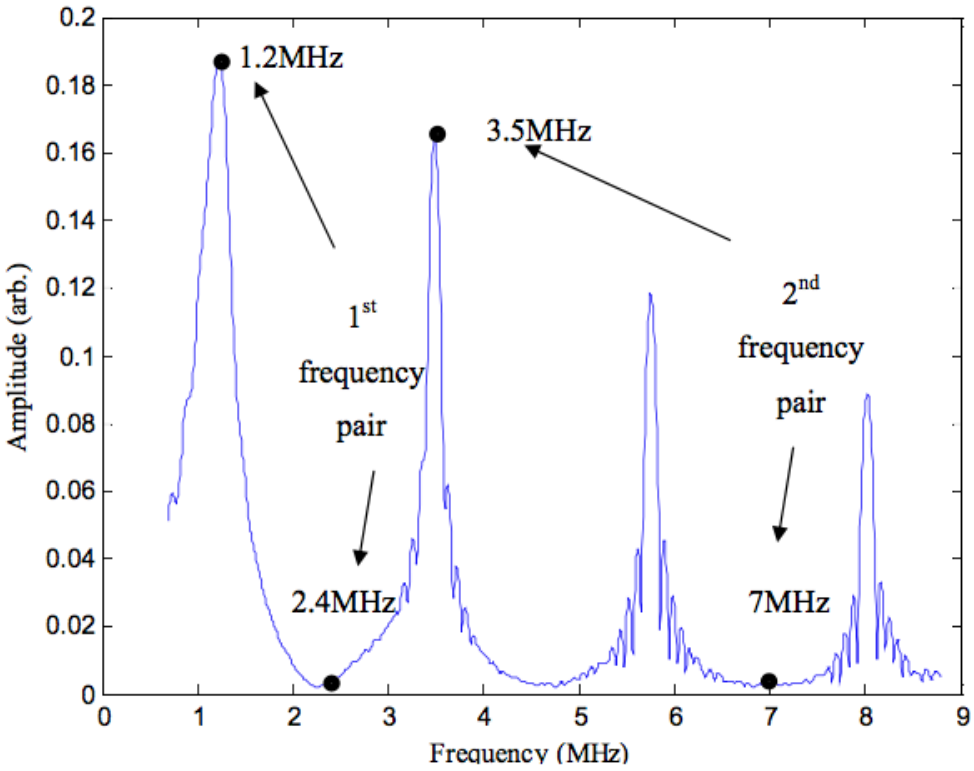

Figure 3.12: Transfer function of undamped piezoelectric disc.

to a minimum. This way, we can have a natural filter simply because the harmonics from the apparatus can be minimised. This was 1.2 MHz, hence the second harmonic was expected at 2.4 MHz.

Figure 3.7 illustrates the transmitters-receivers arrangement in the current set-up. An undamped piezoelectric disc of 155 mm diameter and 2 mm thickness (Pz26, Ferroprem Piezoceramics) was bonded on the top of the plate (Cyanoacrylate, Hencel Loctite). A 15 cycle toneburst with 1.2 MHz centre frequency was generated by an HS3 Handyscope and after amplification by an AR2 power amplifier with 155 V output voltage, was sent to the disc. The signal propagated through the aluminium-adhesive interface and was received by a wideband ultrasonic transducer of 10 MHz centre frequency

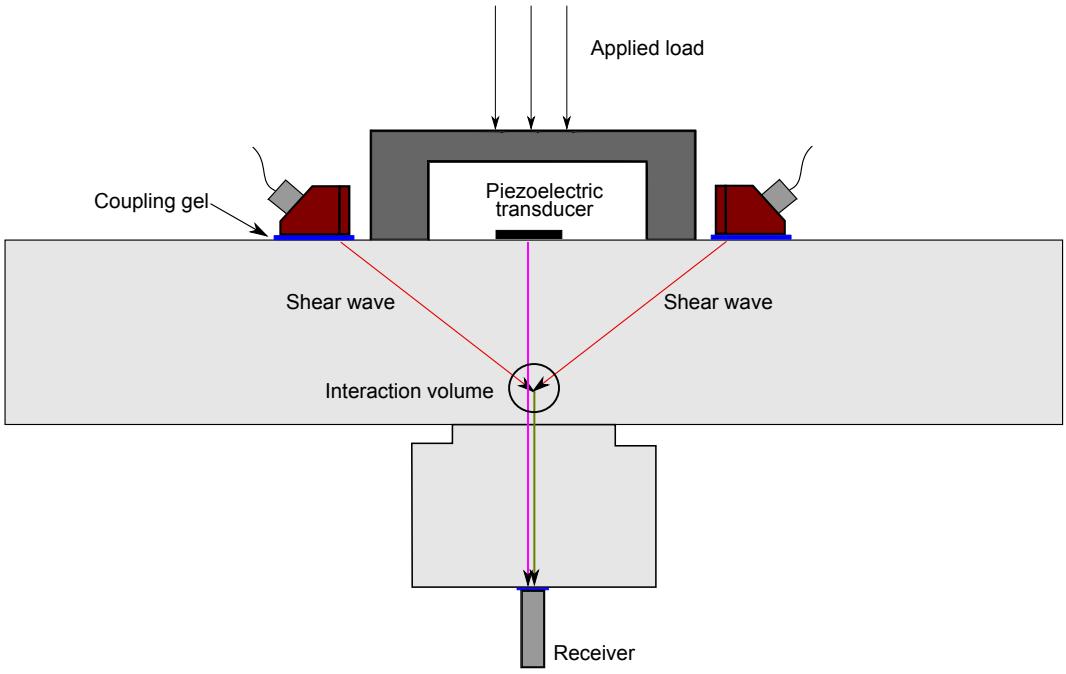

Figure 3.13: Harmonic generation and non-collinear mixing test set-up for the aluminium-aluminium interface.

(Olympus), fixed at the bottom of the cylinder. The received signal was averaged 250 times and was digitised by the HS3 handyscope.

The aluminium-adhesive specimen was subjected to a range of compression loading cycles within the elastic limit (from brotherhood)in an Instron Schenk Compression Loading machine. The applied pressure was chosen from 0 to 4 MPa. This was repeated three consecutive times without removing the fixture of the transducers and the same parameters and coupling conditions were maintained. The signal was received, windowed and filtered at the fundamental and the second harmonic frequency. The first reflection of the linear signal was windowed and filtered to the frequency domain after a Fast Fourier transformation. By filtering the fundamental harmonic frequency the amplitude of the reflections of the linear wave can be calculated. Similarly, by filtering in the second harmonic frequency, the amplitude of the non-linear waves can be determined. The correct time window was selected

and applied to the first reflections and the maximum value was calculated after a Hilbert window function. These processing steps were followed for the signals captured for all the compressive loads for the three consecutive tests.

Figure 3.14 shows the trend of the amplitude of the fundamental frequency over the three loading-unloading conditions. As load increases the asperities of the interfac e have better contact and as higher loads are approached, almost perfectly closed interface was achieved. In lower loads, where the interfaces are not in good contact, more of the incident wave is reflected, thus the amplitude of the transmitted wave has lower values. As load is increased, the transmitted wave propagates through the interface and the amplitude takes higher values. It can be observed, that the response of the transmitted non-collinear wave is higher for the second unloading cycle. This can be attributed to the fact that during the first loading cycle small plastic deformation of the imperfect interface occurs. Asperities, voids or small defects acquire better contact as the load increases. In higher loads, the surface flattened and better contact is achieved. During the loading and unloading, the defects are flattened enough, the interface becomes stiffer and the amount of transmitted wave is higher.

Drinkwater, Dwyer-Joyce and Cawley (1996) showed that there is an elastic contact between the asperities and Kim, Baltazar and Rokhlin (2004) and Kim, Yakovlev and Rokhlin (2004) tried to qualitatively interpret the ultrasonic stiffness. They suggested that this is an essential step in order to minimise the effect of plastic deformation of the interface.

After achieving a flat interface second test was carried out with the same parameters. The signal was windowed and filtered both at the fundamental and at the second harmonic frequency. Figure 3.15 shows the trend of the

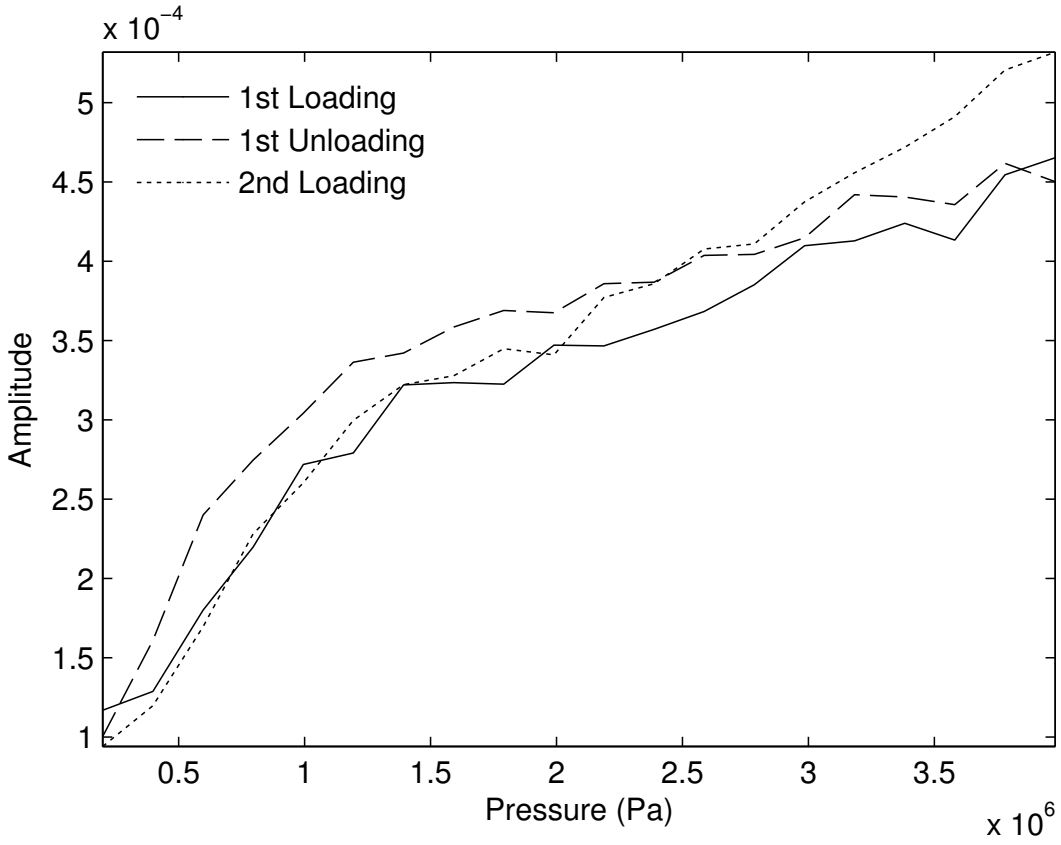

Figure 3.14: Amplitude of the fundamental frequency over pressure for three different loading-unloading conditions.

first harmonic and second harmonic as well as the non-linear parameter. The amplitude of the transmitted input and non-linear waves shows an increasing trend, which can be explained by the theory of the closing interfaces/CAN. The non-linear parameter was plotted towards the applied load, Figure 3.9a.

The next stage of the experimental procedure was to evaluate the performance of the non-collinear mixing technique in the Aluminium-Adhesive interface. Two oblique incidence longitudinal probes with 5 MHz centre frequency were mounted in 60° perspex wedges. The wedges were especially designed so that the interaction angle of the incident waves were 120°. The signals were received by the same wideband longitudinal transducer fixed at the bottom of the cylinder. The signal was generated by the an HS3 handyscope and was split in two ARF power amplifiers. Each one was connected to one of the probes. Three individual measurements were taken: two where the probes were fired individually and one where the probes were fired simultaneously. That was a basic step for the filtering process. The received signals were windowed and after a Fast Fourier Transformation, were filtered at the second harmonic frequency. The final version of the filtered signal was achieved after subtracting the filtered individuals from the main filtered signal. The signal followed the path shown in Figure 3.8b.

This process was followed for a series of loading steps, from 0 to 4 MPa. Taking into account the geometry of the set-up and after working out the refraction angles of the incident beams, a preferred separation of the wedges (thus a preferred interaction point) can be achieved. An interaction at the interface was selected in order to examine its non-linear behaviour. Figure 3.16 shows the received signal, the frequency spectrum of the received signal and the filtered at the second harmonic frequency signal. The size of the second harmonic frequency indicates the difficulty in the detection of the non-

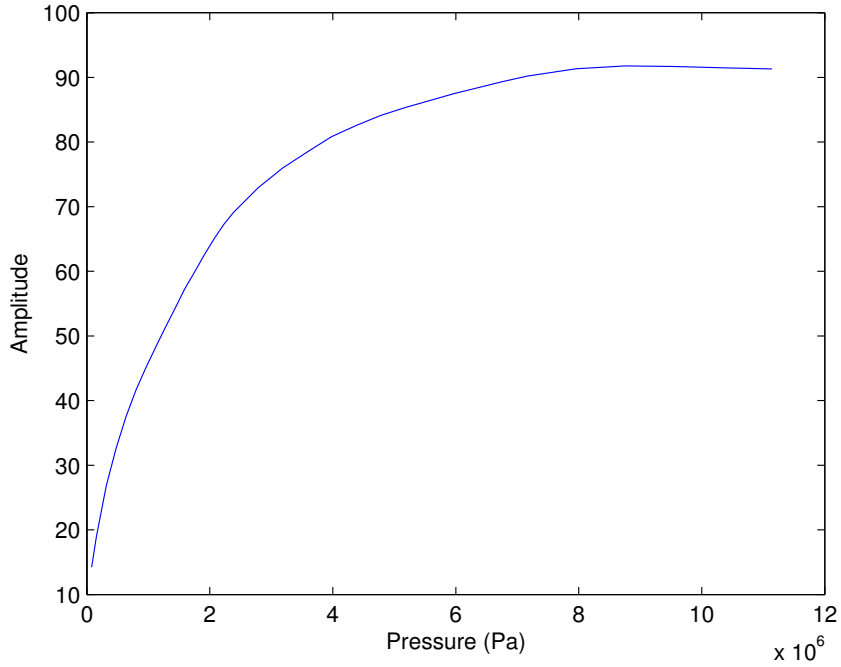

(a) Amplitude of first harmonic.

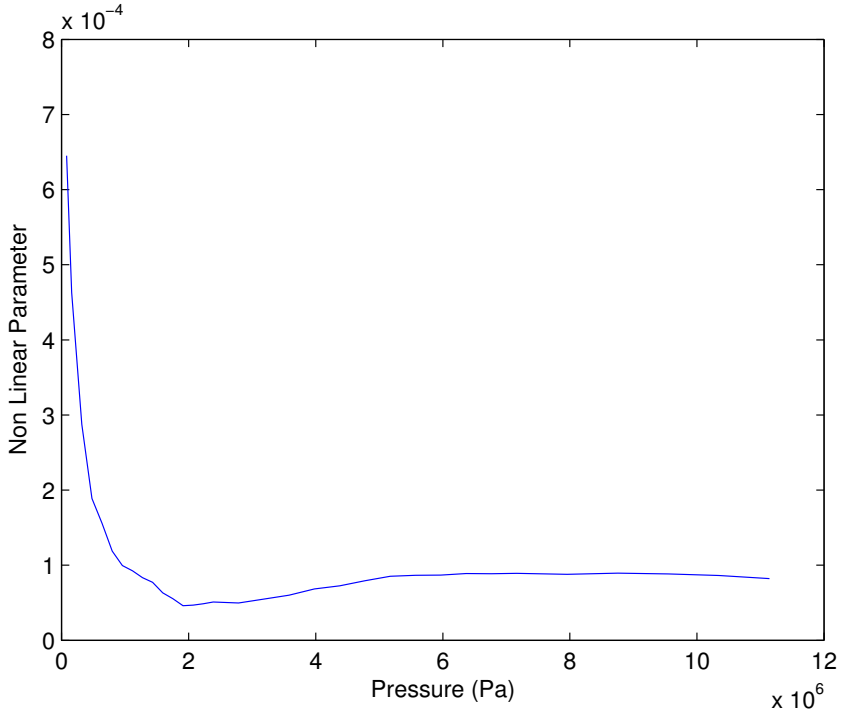

(b) non-linear parameter.

Figure 3.15: Ultrasonic Response of the Aluminium-Adhesive-Aluminium set-up under compression loading. Input frequency 1.2 MHz.

Table 3.2: Expected time arrival of non-collinear reflections of the experimental set-up.

Reflections	1^{st}	2^{nd}	3^{rd}
Time arrival (s)	4.589×10^{-5}	6.172×10^{-5}	7.754×10^{-5}

collinear signal. From the filtered version the red vertical lines correspond to the expected time arrival of the non-collinear signal, Figure 3.16c. It is case the reflections are in the time domain. Buried under the paths.After analysing all possible paths of the reflected signal it was found that the set-up promoted specific reflections and refractions that messed up the final received signal.

3.4.2 Geometry challenges

Several non-collinear tests were performed where good good coupling conditions, good alignments of the probes, enough pressure of the probes and the receiver were secured and careful signal processing; correct size of the Hanning window and careful application of Fast Fourier and Inverse Fast Fourier Transformation. From the geometry and the physical properties of the materials in the test set-up, i.e. sound velocity, the time arrival of the non-collinear wave and its reverberations can be calculated, they are shown in Table 3.2.

Figure 3.15b shows a typical filtered at the second harmonic frequency received signal. It can be observed that it is difficult to clearly identify the mixing wave from the unwanted features. From this figure, we can see that the useful non-linear components are buried under a series of unwanted reflections. In order to investigate the matter further it was imperative to

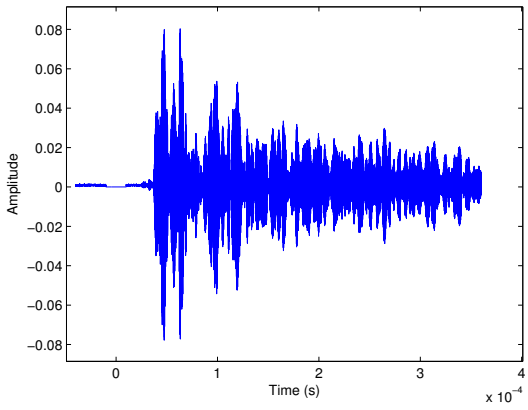

(a) Received signal.

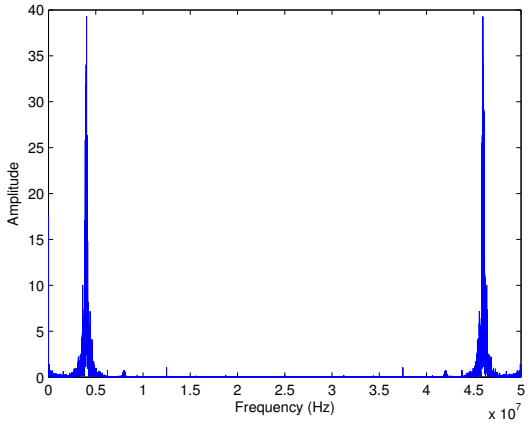

(b) Frequency spectrum.

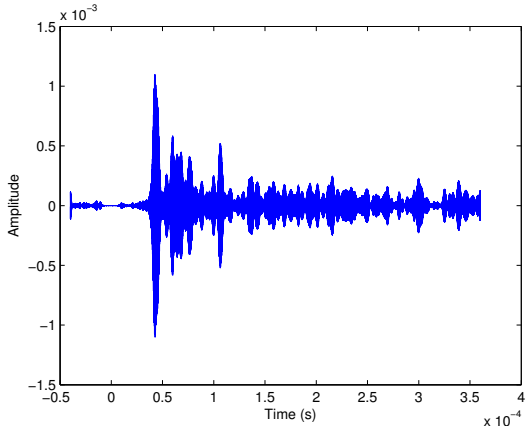

(c) Filtered signal.

Figure 3.16: Received signals from the Aluminium-Adhesive set-up.

Table 3.3: Theoretical expected time arrival of different reflective paths that interfere with the non-linear signal in the cylinder.

Refraction path	Description	Time arrival (s)
1	Reflection from top of plate	6.796×10^{-5}
2	Reflection from interface	5.370×10^{-5}
3	Mode converted propagating straight	5.525×10^{-5}
4	Reflection from side of cylinder	4.003×10^{-5}
5	Longitudinal wave	4.360×10^{-5}

isolate each one of the unwanted features and try to interpret their source. Initially, a series of possible reflection and refractions was mapped in the current set-up and their theoretical time arrival was calculated using the geometry and the propagation velocity within the aluminium. Figure 3.17a shows possible ultrasonic paths that match the theoretical calculation:

1. Reflections from the top of the plate. (1)

2. Reflections from the interface. (2)

3. Mode converted waves propagating straight through the set-up. (3)

4. Reflections from the side of the cylinder. (4)

5. Longitudinal waves propagating straight through the set-up. (5)

Since the theoretical time arrival matched some experimental findings it was verified that the perspex wedges produced longitudinal waves in a range of angles that followed either propagation paths directly through the cylinder or paths that led to reflections from the sides of the cylinder. Additionally, the fact that the thickness of the cylinder was equal to the

thickness of the aluminium plate, both 45 mm, was causing overlapping in the time arrival of the reflections from the interface and from the top of the plate and this didn't help to distinguish the actual source of those features.

Thus, it was important to take those parameters into account and redesign the test rig. Two main parameters had to be taken into account: the size of the interface and the thickness of the specimens. For this reason another aluminium plate was considered to replace the cylinder. Figure 3.17b show the redesigned set-up. Initially, the width of the interface was small enough to obstruct the propagation of the longitudinal waves that were generated from the perspex but wide enough to allow the direct flight of the non-collinear wave. Secondly, the new aluminium plate was wide enough to prevent scattering of the transmitted waves from both sides. Finally, the thickness of both plates was considerably different compared to the previous set-up and this contributed to the different time arrival of the reflected from the interface of from the top of the pates waves. These three factors contributed in the prevention of possible overlaps that could mask the non-collinear signal.

3.4.3 Aluminium - Aluminium non-collinear mixing tests

Following the redesign of the set-up which can be seen in Figure 3.17b a new experimental procedure was carried out. The previous experiments with the aluminium-adhesive interface were inconclusive due to the difficulty in distinguishing the level of contribution of the adhesive material to the non-linear behaviour of the interface. Thus, starting a new series of experiments with a simpler, aluminium-aluminium interface was essential.

The experimental procedure in the redesigned set-up, which was described in Section 3.4.2, followed the same path, showed in Figure 3.8b. Two

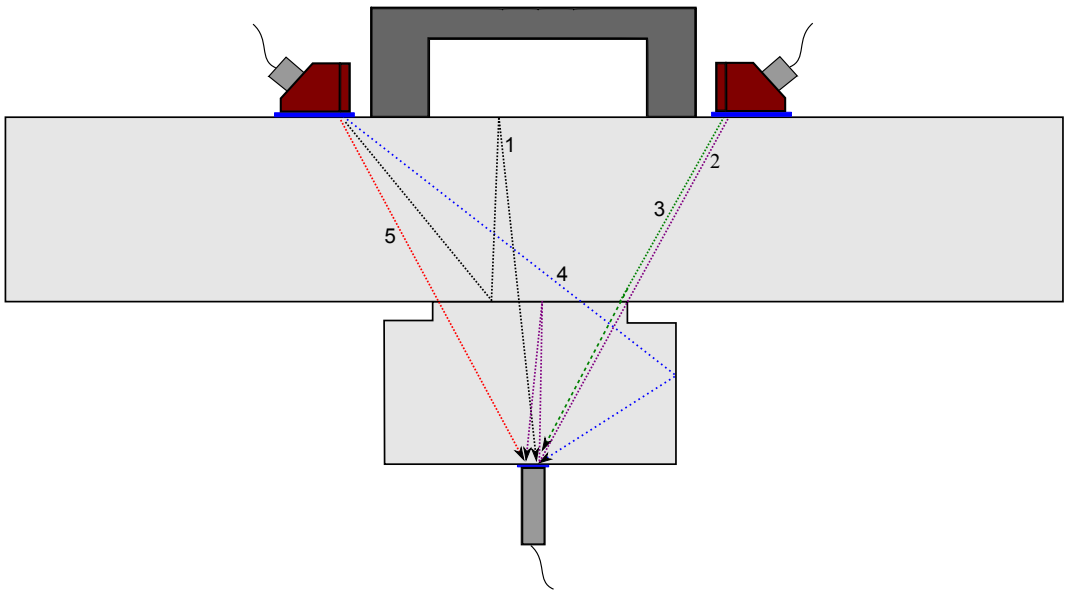

(a) Initial experimental set-up.

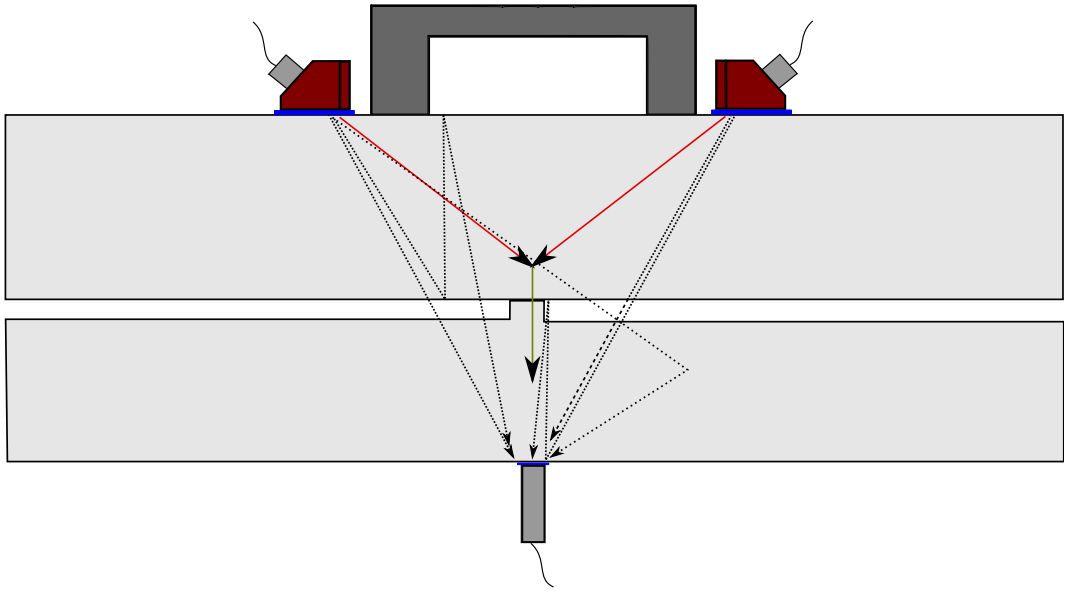

(b) Improved experimental set-up.

Figure 3.17: New geometry of non-collinear set-up which minimises the interference of the drawn refraction paths.

amplifiers were used, each one connected individually to the two oblique incidence longitudinal probes. The main reason for this was to take advantage of the full energy potential of the power amplifiers. Both were giving output voltage of 163 V and 125 V respectively. For each step, three measurements were taken and are the following:

1. The first measurement was with two probes being fired simultaneously so as the two longitudinal waves could propagate and interact within the aluminium.

2. A single excitation of the Left transducer, with the Right transducer and its amplifier manually disconnected.

3. A single excitation of the Right transducer, with the Left transducer and its amplifier manually disconnected.

The processing steps were described in Figure 3.9b. The first step was to perform a single experiment with the current set-up with the maximum pressure applied in order to verify whether the changes in the design along with the filtering process were effective. The maximum pressure of 4 MPa was selected because under this force, a perfectly closed interface can be assumed and most of the energy of the non-collinear signal can theoretically be detected. A random separation of 17 cm ,which was also good enough for the linear left and right signals to propagate, was selected. The expected time arrival of the non-linear wave was at 4.8×10^{-5} s.

Figure 3.18 shows the three measurements and the filtered at the second harmonic frequency signal. Figure 3.18a shows the raw received signals, where both transducers fired, Figures 3.18b and 3.18c show the linear left and right signals respectively, Figure 3.18d shows the subtracted left and

right signals from the raw received. The red perpendicular line represent the expected time arrival of the first reflection of thee on collinear signal. Finally, Figure 3.18e shows the filtered signal along with the expected time arrival of the non-collinear signal and it's reverberations. This test was a good indication of a successful design as well as a motivation for further tests.

The same loading parameters were applied here as well; the Instron hydraulic machine applied a series of loading steps for 0 to 4 MPa. The Harmonic Generation technique was also applied to the aluminium-aluminium interface. For each loading step, a 15 cycle toneburst of 1.2 MHz driving frequency, was amplified with 155 V output voltage, was received by the HS3 handyscope and digitised after 250 averages. Figure 3.19 shows the amplitude of the first harmonic and the non-linear parameter. The ultrasonic response follows the same trend as with the aluminium-adhesive interface.

Subsequently, a series of non-collinear mixing tests were performed. In order to distinguish the level of contribution of the non-linearity due to the interaction, five different areas of interaction were selected within the material. One of the main advantages of the non-collinear mixing technique, is the spatial selectivity, which means that the non-linear interaction is limited to the region where the two incident beams intersect. If the separation between the firing transducers is changed, then interaction point will change. Figure 3.20 shows the concept of the increased interaction depth with the increase in the probes separation. The black dots represent the selected five areas of interaction. The test parameters for each separation are shown in Table 5.1.

For each interaction depth, all measurement were taken without moving the fixture of the transducers and the same coupling conditions were main-

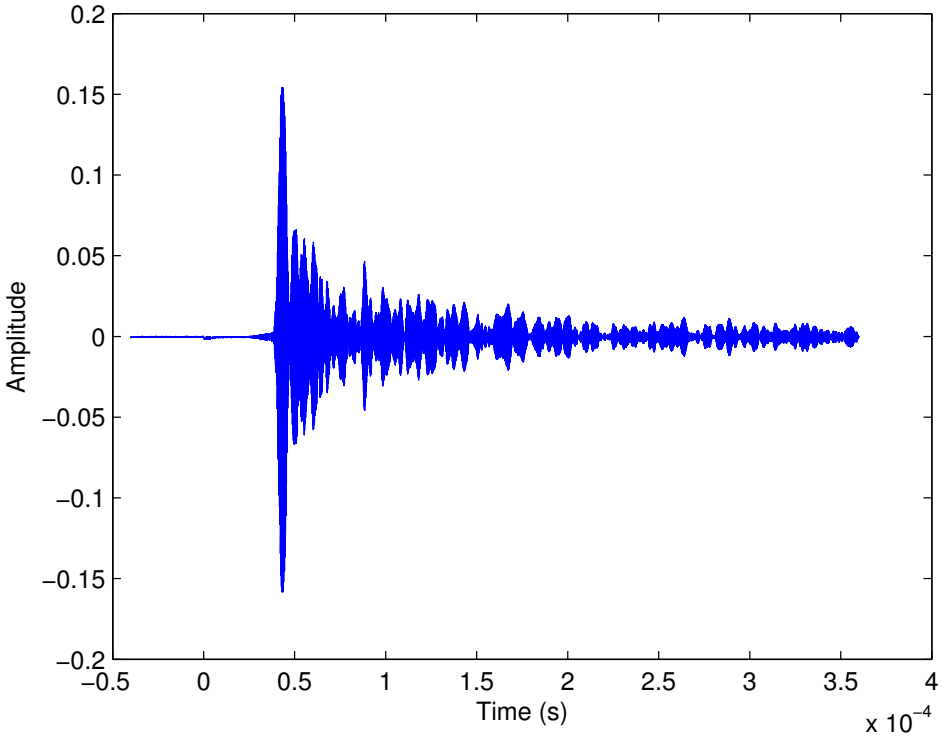

(a) Received Signal after non-collinear mixing.

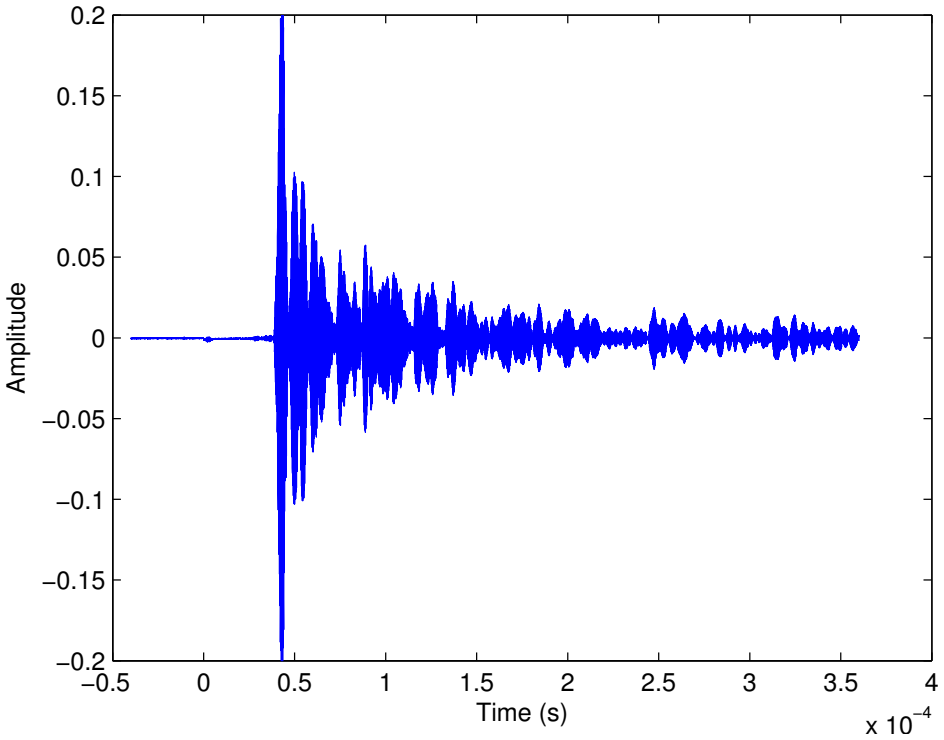

(b) Linear Left Received Signal.

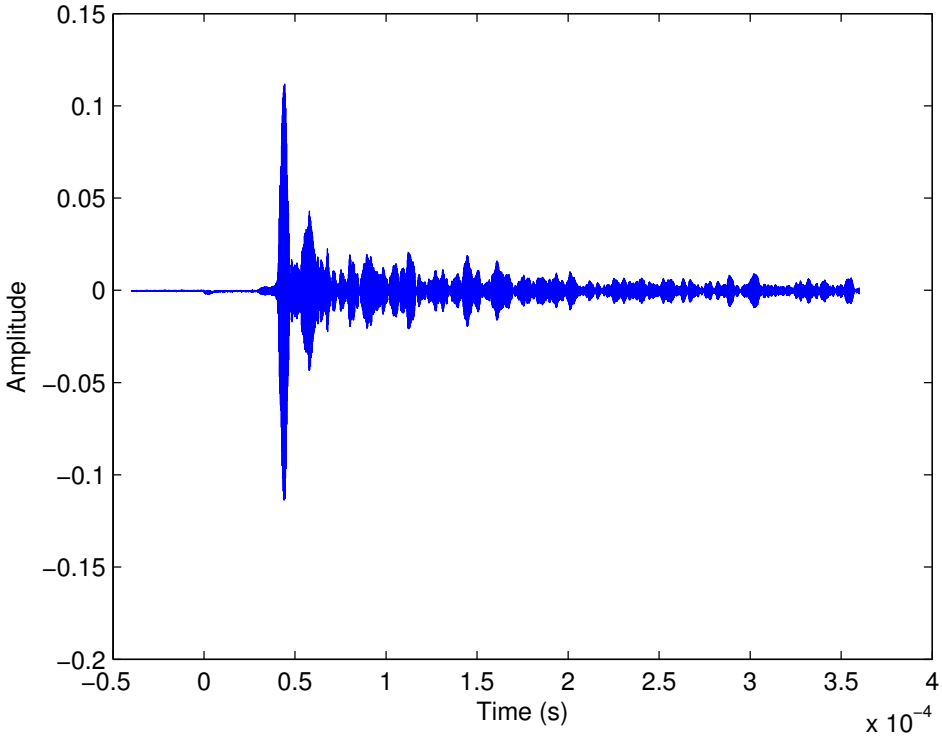

(c) Linear Right Received Signal.

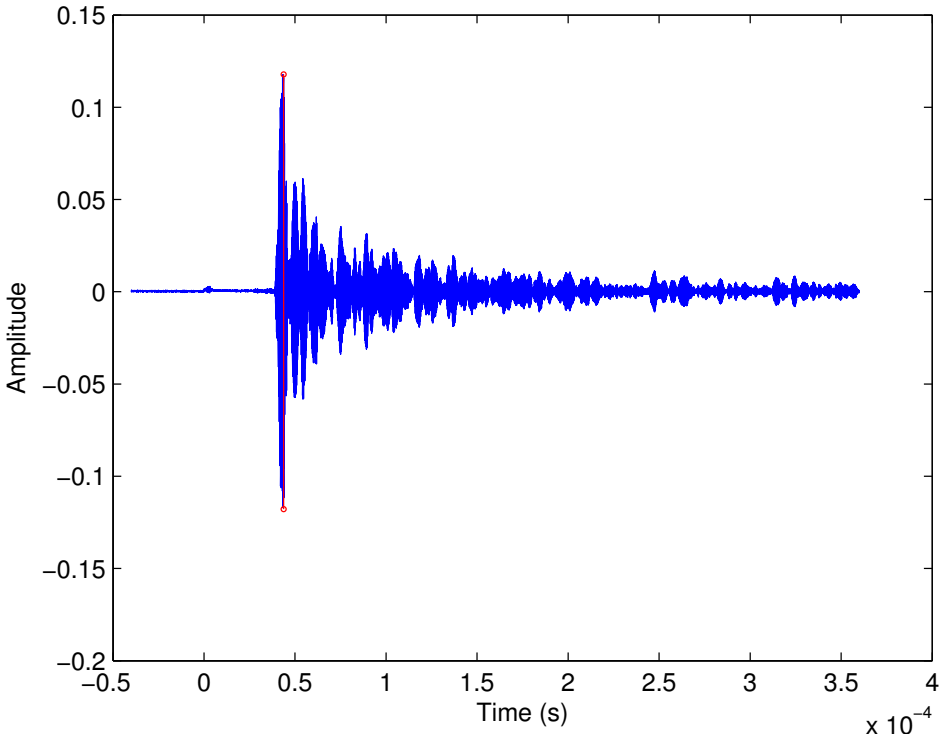

(d) Subtracted non-collinear signal.

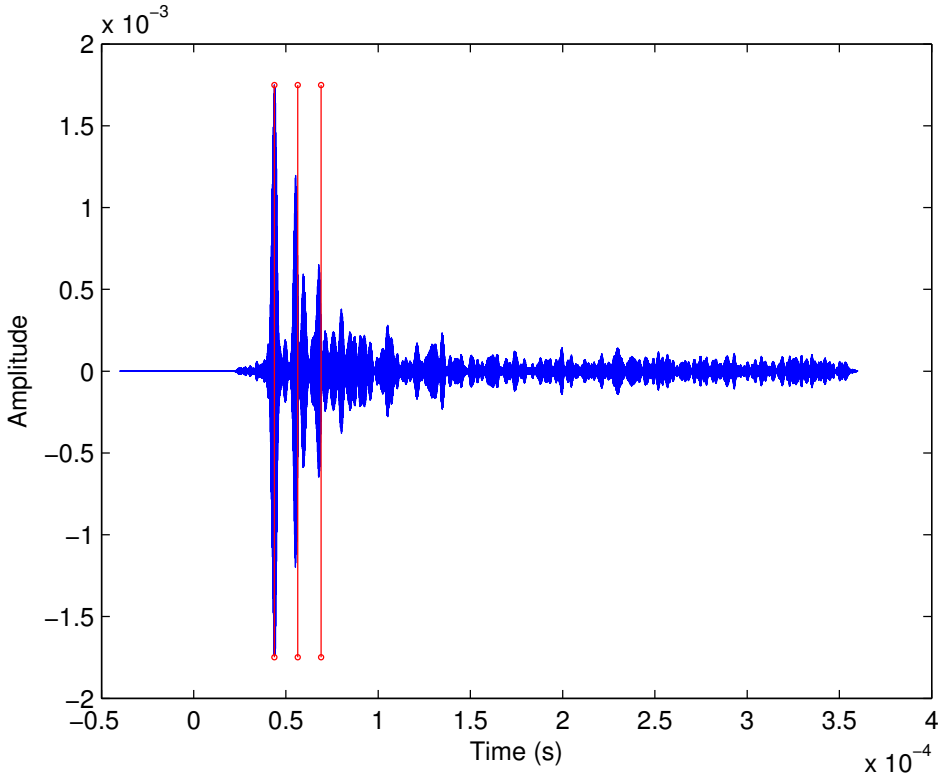

(e) non-collinear signal filtered at the second harmonic frequency.

Figure 3.18: Subtracted and filtered at the second harmonic frequency non-collinear signals. The red lines represent the theoretically estimated time arrival of the mixing wave and its reflections.

Table 3.4: Test parameters of non-collinear mixing tests.

Separation	Volume of interaction	Arrival of 1st echo
12 cm	Above the interface	4.1171×10^{-5} s
14 cm	Above the interface	4.3953×10^{-5} s
15.4 cm	At the interface	4.5900×10^{-5} s
16 cm	Below the interface	4.6735×10^{-5} s
17 cm	Below the interface	4.8126×10^{-5} s

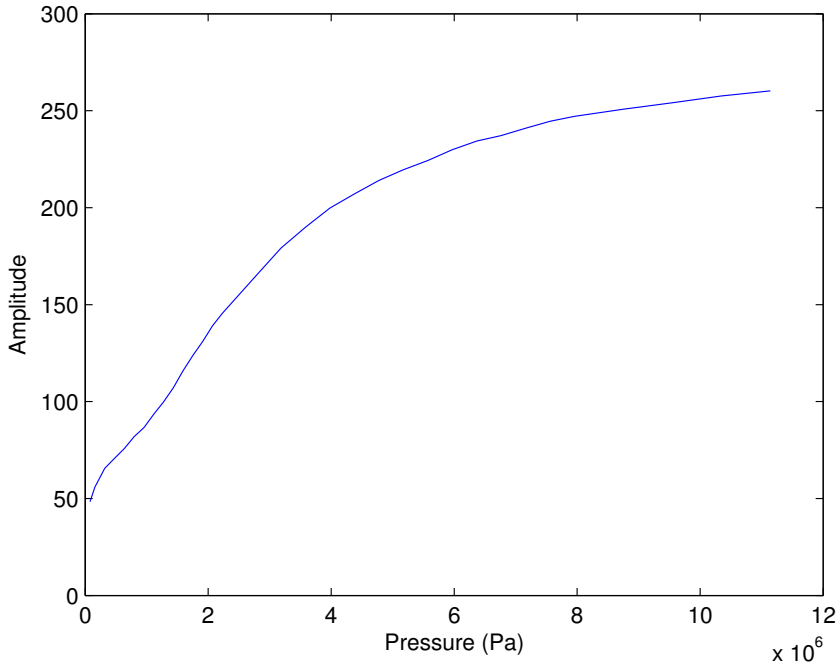

(a) Amplitude of first harmonic.

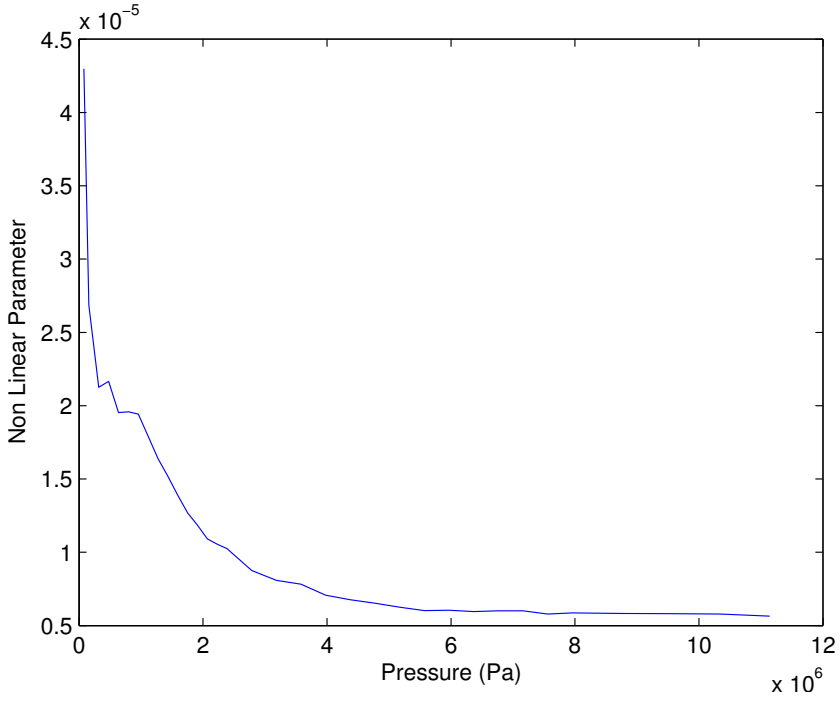

(b) non-linear parameter.

Figure 3.19: Ultrasonic Response of the Aluminium-Aluminium set-up under compression loading. Input frequency 1.2 MHz.

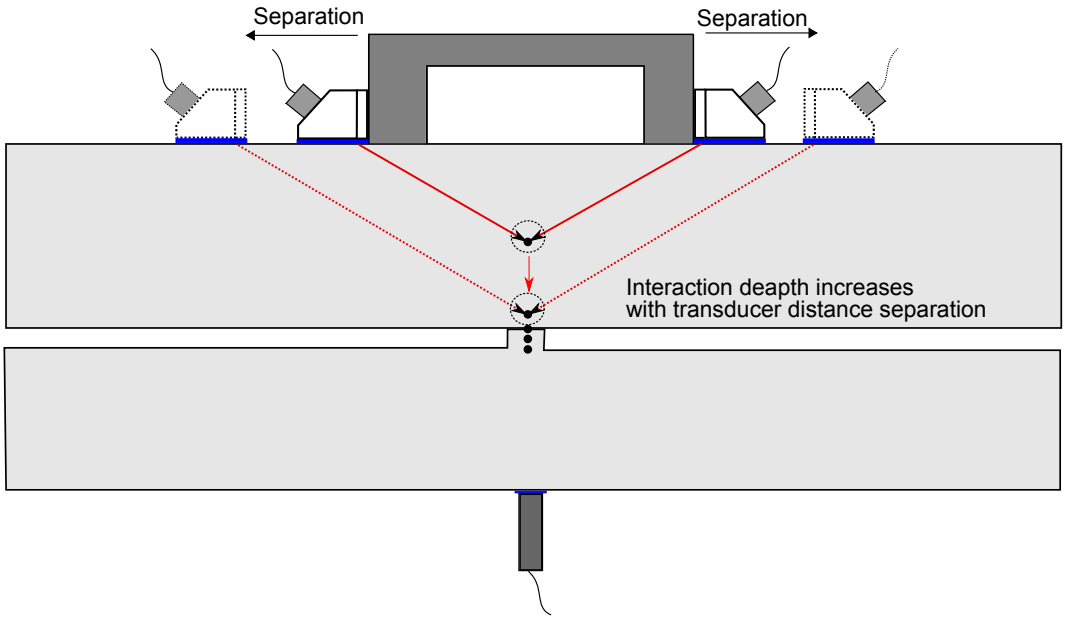

Figure 3.20: Different separation leads to different interaction depths. The black dots show the five interaction points selected for the tests.

tained. Elastic bands with high stiffness were used in order to provide the wedges with adequate contact conditions with the specimen, and the same fixture with bolts and a spring was used for fixing the receiver at the bottom of the set-up. The amplitude of non-collinear signal followed the procedure described in Section 3.3.3.

Figure 3.21 shows the difference it the amplitude of the transmitted waves for each separation. Despite the difference in amplitude, they exhibited the same trend with the results taken with the harmonic generation technique, Figure 3.19a. The interface shows higher non-linearity compared to other cases.

At the non-collinear mixing technique, the possible sources of non-linearity are the bulk non-linearity of the tested materials, the non-linearity of the interface (Contact Acoustic non-linearity) and the non-linearity from the interaction of the two intersecting waves. In order to minimise the non-linearity due to wave interaction, the amplitude of the waves was normalised towards

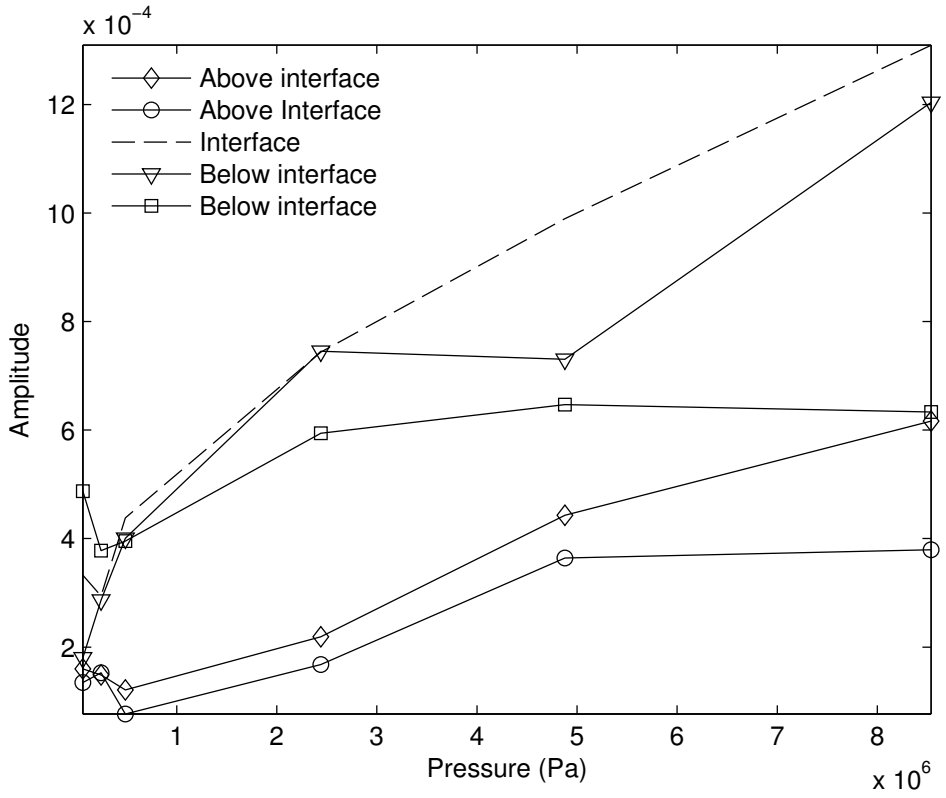

Figure 3.21: Maximum amplitude of non-collinear waves for five different separations.

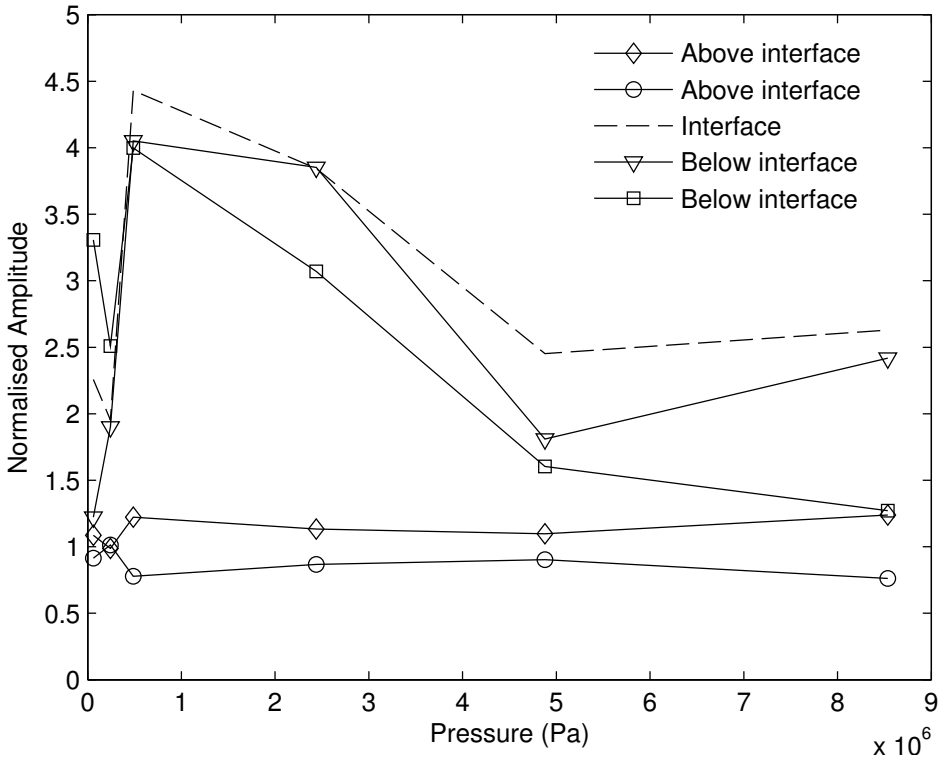

Figure 3.22: Normalised amplitude of non-collinear waves for five different separations.

the average values of those that resulted from the interaction above the interface. Figure 3.22 shows the results of the normalisation process. The amplitudes show a descending trend but it is qualitatively and quantitatively different compared to the trend of non-linear parameters from the Harmonic generation technique. The higher levels if non-linearity in higher loads make it difficult to understand the contribution of contact acoustic non-linearity and the bulk non-linearity to the behaviour of the system.

Finally, another series of tests were conducted in order to investigate the repeatability of the results in Figure 3.21. For this reason, the probes were removed form the set-up, were cleaned and carefully fixed in the preferred position after a thin layer of coupling gel was applied. The test parameters were kept the same but more pressure elements were selected for greater

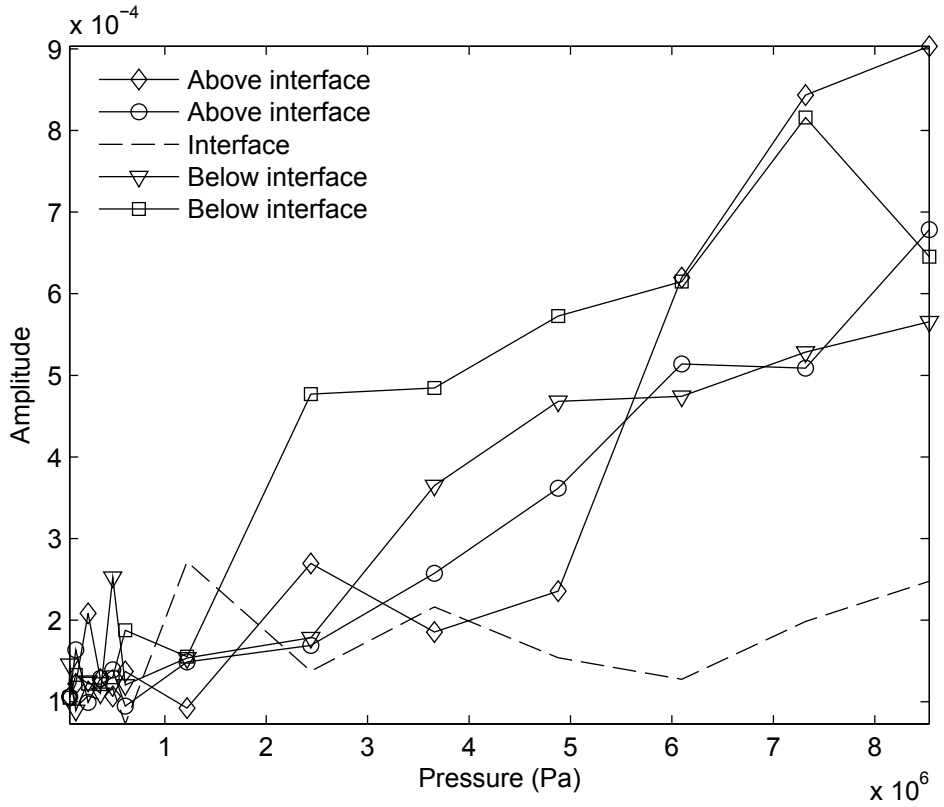

Figure 3.23: Second test. Maximum amplitude of non-collinear waves for five different separations.

resolution. Figure 3.23 shows the maximum amplitudes of non-collinear waves. The trends exhibit higher levels of non-linearity, possibly because of the higher resolution. Although the results are preliminary and it is difficult to make assumptions, the same trend as well as the same order of magnitude verify the feasibility of the method.

3.5 Concluding remarks

In this section, the results from the experimental procedure that was performed in Aluminium–Adhesive and Aluminium–Aluminium interfaces are presented.

- This chapter describes the work done in the investigation of the stiffness of partially closed interfaces. For this reason the non-collinear mixing technique was selected. The interfaces an aluminium-adhesive interface in the form of a plate on top of a cylinder that has bonded a layer of adhesive layer. The main goal was to evaluate the sensitivity of the technique and see how effectively it can evaluate the changes in the stiffness of the adhesive layer. In order to assess the results two different experiments were carried out; a though transmission experiment in addition to the non-collinear mixing tests.

- The selected specimen was an aluminium block of dimensions 260 mm $\times$ 80 mm $\times$ 45 mm positioned on top of a cylinder with a 2 mm thickness structural aerospace epoxy layer, 3M EC3448. The interface was compressive loaded before the yield point. The Harmonic Generation technique, showed high levels of non-linearity at low loads which was expected due to Contact Acoustic non-linearirty.

- The non-collinear mixing experiments showed high levels on non-linearity. The test was inconclusive as the non-collinear wave could no be detected. Possible solution: an aluminium-aluminium interface.

- An aluminium cylinder was placed at the bottom of the plate, Figure 3.13 and a non-collinear test was performed. As explained in Section 3.4.2, the time arrival of the reflected waves as well as the mode converted waves, were matching the expected time arrival of the non-collinear wave. It was clear the the current set-up was not convenient for the carrying out measurements and extracting results.

- The next step was to design an experiment that would restrict the unwanted features so as to identify the non-collinear signal. The re-designed rig is shown in Figure 3.17b.

- For all the compression loading steps,the processing can be summarised in Figure 3.9b. For each measurement the same processing steps were applied. The maximum value of the first reflection of the transmitted waves were plotted towards the applied load.

- Different interaction points were selected against the interface of the two materials; two above the interface, two below the interface and at the interface. Figure 3.21.

- In an attempt to reduce he non-linearity due to the wave interaction, the results were normalised against the average values of those that resulted from the interaction above the interface. Results are shown in Figure 3.22. The amplitudes show a descending trend, like the trend of the non-linear parameter.

- The same non-collinear mixing tests were performed again to investigate the repeatability of the method. The set-up was taken apart, the probes were cleaned and put back together. The parameters were kept the same and more Pressure steps were added. Figure 3.23 shows the maximum amplitude of the non-collinear waves. Higher levels of non-linearity is exhibited possibly due to higher resolution.

Chapter 4

Non-collinear simulation with phased arrays

4.1 Introduction

In the previous chapter the sensitivity of non-linear non-collinear mixed wave was investigated for the assessment of quality of kissing bonds. It was found that there are complex non-linear phenomena taking place at the area round the interface of the bond, making received non-linear signal difficult to correlate with the condition of the bond.

In contrast with single element probes, a phased array consists of multiple elements that can be fired at the same time so that the array can work similarly to a single element transducer, or the elements can be fired with relative delay so that the phased array can be used for more advanced purposes. Figure 4.1 shows the basic inspection mode of a phased array.

The beam steering and the beam focusing are two techniques mainly used to increase the resolution of the image as well as the time required to perform a specific test. Phased arrays have specific advantages over the

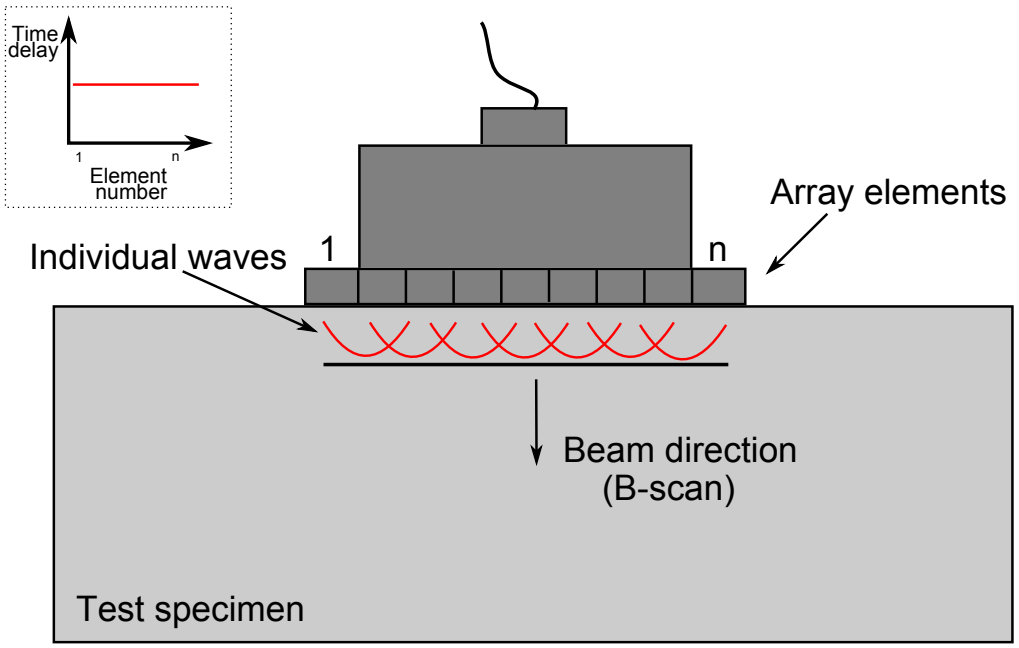

Figure 4.1: Basic operation mode of a phased array.

single element counterparts: by altering the delay laws, the directivity of the beam can be achieved, thus scan a specific area without having to move the probe. That means we can use the arrays to perform multiple scans in different areas of a material from a single firing point which helps in reducing the time needed to perform a single test. Additionally, the fact that the probe is not moved gives higher reliability on the test results. This derives from the fact that without moving the probe, the same coupling conditions can be maintained, thus we get better acoustic measurements.

In order to assess the level of non-linear contribution of the interface, a more reliable experimental procedure was designed by using phased arrays. Prior to the experiment procedure, a model was developed to simulate the linear beams of the input waves in order to predict and assess the feasibility of the interaction. A series of parameters were also investigated, i.e optimum focal depth vs interaction angles vs optimum sub-aperture set.

4.2 Linear beam modelling

At the early stages of development of any inspection methodology certain qualitative tools are required. Achenbach (1992) states *A fundamental approach to NDT must be based on quantitative models of measurement process of the various techniques*.

Modelling is a powerful tool to simulate and represent the behaviour of a system before the actual adoption of a successful methodology. Knowing the behaviour of the model one can understand the several aspects of the test procedure, analyse parameters that might affect the results and thus decide which is the best way to proceed with the non destructive testing investigation.

Additionally, by investigating specific fort this research topic parameters, such as non-linear amplitudes, interaction angles, sensitivity, and scanning depths, the experimental procedure can be calibrated *a priori* by modelling the experimental set-up.

Huygen's Theory

In order to manipulate the beams of the phased arrays, it is essential to calculate and apply the delayed fired times in the different elements of he aperture. This can be achieved by using Fermat's Principle. Fermat's principle is usually referred as *the principle of the least time* and it states that a ray of light, or in our case an ultrasonic wave, will always chose the shortest distance in order to travel between a point A(x1,y2) and point B(x2,y2), Figure 4.2a. Given than the focal point is point B, then the time required for

the beam to reach this point is

$$\mathrm{t} = \frac{\sqrt{(x_2 - x_1)^2 + (y_2 - y_1)^2}}{c_1} + \frac{\sqrt{(x_f - x_2)^2 + (y_f - y_1)^2}}{c_2} \tag{4.1}$$

The application of Fermat's Principle relies on Snell's law. The formula gives the relationship between the angles of incidence and refraction when an ultrasonic travels between two different isotropic materials. Snell's Law is given by

$$\frac{\sin(\theta_1)}{\sin(\theta_2)} = \frac{c_1}{c_2}. \tag{4.2}$$

The time required for travelling between point A and B is given by

$$\mathrm{T} = \frac{\sqrt{x^2 + y^2}}{c_1} + \frac{\sqrt{(L - x)^2 + y_2^2}}{c_2} \tag{4.3}$$

We know from Fermat's Principle that the time it will take to travel between those points will be the minimum, thus:

$$\frac{\mathrm{d}t(x)}{\mathrm{d}x} = 0 \tag{4.4}$$

From the derivative at maximum or minimum, we need

$$\frac{\mathrm{d}T}{\mathrm{d}x} = 0 \tag{4.5}$$

So that

$$\frac{x}{c_1\sqrt{a^2 + x^2}} = \frac{d - x}{c_2\sqrt{b^2 + (d - x)^2}} \tag{4.6}$$

From trigonometry, this leads directly to

$$\frac{\sin \alpha_1}{c_1} = \frac{\sin \alpha_2}{c_2} \tag{4.7}$$

The critical angle is the angle of incidence above which the total internal reflection occurs. The angle of incidence is measured with respect to the normal at the refractive boundary. Figure 4.2b and Figure 4.2c. Assuming that an oblique longitudinal wave propagates within a medium. When the longitudinal wave hits the interface, then a mode will refract back to the same medium and some of the energy will propagate within the second medium with different mode. This is what we call mode conversion: the longitudinal wave will convert to shear. The refraction angles can be easily calculated by Snell's law.The angle of incidence is measured with respect to the normal at the refractive boundary. Consider a longitudinal wave passing from a medium 1 to medium 2. The energy emanating from the interface is bent towards the second medium. When the incident angle is increased sufficiently, the transmitted angle reaches 90 degrees. It is at this point no light is transmitted into second medium. The critical angle θ_c is given by Snell's law

$$n_1 \sin \theta_i = n_2 \sin \theta_t \tag{4.8}$$

Rearranging Snell's Law, we get incidence

$$\sin \theta_i = \frac{n_2}{n_1} \sin \theta_t \tag{4.9}$$

To find the critical angle, we find the value for θ_i when $\theta_t = 90$ and thus $\sin \theta_t = 1$. he resulting value of θ_i is equal to the critical angle θ_c.

Now, we can solve for θ_i, and we get the equation for the critical angle:

$$\theta_c = \theta_i = \arcsin\left(\frac{n_2}{n_1}\right) \tag{4.10}$$

The array beam modelling can be produced by applying the principles of superposition and Huygens. Modelling the ultrasonic beam in this case is important because we can get information about the width of the beam, the focal ability and the length of the near field zone.

The focal law for probes in direct contact with the specimen, has a parabolic shape for depth focusing. It is based it the Huygen's principle which is the superposition of fields from point sources. According to this, more complicated fields can be predicted simply by integrating the simple fields from the point sources.

Figure 4.3 shows the basic geometry of a phased array. Assuming a point A (Focal spot in Figure 4.3) and its distance r in an isotropic media, the field can be described by:

$$P(r) = A\frac{1}{\sqrt{r}}e^{i}(kr - \omega t) \tag{4.11}$$

where A is the complex number representing the size and the phase of the source, So, the sum form all the sources

$$P(x,z) = \sum_{n}^{j=1} \frac{1}{\sqrt{r_j}}e^{(}ikr_j - \omega) \tag{4.12}$$

In polar coordinates the field can be calculated:

$$P(R,\theta_s) = \int_{-\alpha/2}^{\alpha/2} \frac{1}{\sqrt{r}}e^{i}(kr - \omega t) \tag{4.13}$$

where

$$r = \sqrt{R^2 + x^2 - 2R\cos(90 - \theta s)} \tag{4.14}$$

And after integration:

$$P(R,\theta_s) \approx \frac{\alpha}{\sqrt{R}} e^{i}(kR - \omega t)\frac{\sin\frac{1}{2}k\alpha\sin\theta}{\frac{1}{2}k\alpha\sin\theta} \tag{4.15}$$

The pressure varies with angle and this is the *directivity function*:

$$D_f(\theta_s) \approx \frac{\sin\frac{1}{2}k\alpha\sin\theta}{\frac{1}{2}k\alpha\sin\theta} = \sin c\frac{\pi\alpha\sin\theta_s}{\lambda} \tag{4.16}$$

In order to calculate the delays an element with zero delay is picked (usually the central one) and accordingly the delays of other elements are worked out. In the Figure 4.3 we get:

$$t = \frac{t_r - t_R}{c} \tag{4.17}$$

An example is shown in Figure 4.4. Here is shown the delay that needs to be applied to the firing time in each element of the arrays in order to focus on a series of different depths. The horizontal axis shows the element number of the transmitting arrays and the vertical axis is time in seconds. Each colour in the figure corresponds to a different depth in the specimen.

Figure 4.5 shows three different examples of calculated delays for three different focal points. The waves are modelled to propagate in perspex, refract in aluminium and focus close to the interface (a), 15 mm from the interface (b) and 40 mm from the interface (c).

4.3 Parameters investigation

In the previous section the importance of modelling the array fields was addressed. The main advantage lies in the fact that the modelling process

allows to have a visual experience of a test procedure with its results, before actually implementing it in practise. Here, the developed model is used to predict the linear fields generated by the two longitudinal phased arrays. The direction and the amplitude of the linear beams can be vital in the determination of the best possible test procedure.

The non-collinear mixing has two major advantages; spatial and frequency selectivity. The first, implies that the non-linear wave is limited to the area where the two linear waves interact and the latter means that the direction of the non-linear wave is different from the direction of the incident beams. It is clear that those two parameters leave plenty room for investigation. For example, different separation of the arrays lead to a different area of interaction, thus a possible difference in the level of non-linearity.

In this case, the modelling parameters of the phased arrays were 32 active elements and 0.63 mm pitch. The defined material of the wedges was perspex with 50 degrees angle and the defined testing material was aluminium. The longitudinal sound velocity in perspex is C= 2730 m/s and the aluminium sound velocities are C_t = 3130 m/s and C_l =6320 m/s. The perpendicular distance of the first element from the interface was 53 mm. The length of the base of the wedge was 90 mm. The refraction angle of the shear ultrasonic wave was 60 degrees. As the ultrasonic beam was propagating through the perspex-aluminium interface, mode conversion occurred in angle of 120 degrees.The centre of each element is used as a source of the beam.

Figure 4.6 shows the sound field generated by the two phased arrays which results from the two unfocused beams. All 32 elements of the array emit waves that follow a parallel propagation path within the wedge. When they meet the interface they all refract to the aluminium specimen.

Figure 4.7 shows the sound field generated by the two phased arrays when the beams are focused in the a location 2 cm from the interface. There is a clear difference between the two areas of interaction in intensity and size.

More clearly, in the zoomed areas of interaction as shown in Figure 4.8a and Figure 4.8b and given that both images are on the same scale, it is clear that the volume of interaction in the unfocused case is several orders of magnitude larger than the volume in the focused case, whereas the linear amplitude at the point of interaction is much higher in the focused model, in the fraction of 3 orders of magnitude. By calculating the quadratic mean of the amplitudes in the area of interaction in both cases, we can quantify the average value of amplitudes.

One of the main advantages of phased arrays is the ability to perform multiple tests from one location, without moving the array probes. By using the delay laws a scan along the perpendicular axis of the specimen can be achieved. The delay times for a specific focal spot can be calculated from the geometry of the specimen, as described in section 4. Parallel with the calculation of the delay times, the construction of the model for each focusing depth can provide valuable information with regards to the feasibility of the measurement. This is because, the generation of the non-linear wave in the non-collinear mixing can only be achieved when certain parameters are met; in this setup an interaction angle of 120 degrees. After theoretical calculations, a depth of 20 mm from the surface was found to meet the interaction criteria for both the focusing and non focusing tests. A model that shows the interaction for both cases can be useful in order to compare the potential of each method.

4.3.1 Volume effects

Now, by calculating the focal law for a specific focal point, the model of the focused beams can be produced. The focal spot was selected at 20 mm form the surface of the specimen. Figure 4.7 shows the acoustic field from the 32 elements of the array. Figure 4.8b shows a magnified image of the interaction area at 20 mm depth. By comparing the two images, 4.8a and 4.8b, the amplitude at the area of interaction at the focused beam is much smaller, 12 mm width difference and 8 mm depth difference. There is also a considerable difference in the amplitudes at the area of interaction, indicating that the there is higher level of constructive interference of the incident waves when the beam are focused. This is expected as the energy the array transmits is higher when the diameter of the beam is smaller.

4.3.2 Sweeping angle of interaction

The depth scanning is mainly important as it gives the opportunity to perform measurements with the phased arrays fixed in a specific position. The non-collinear mixing technique cannot be performed unless the angle of interaction fulfils the resonance parameters. By taking into account Figure 4.9 we can see that there are focal points that do not meet the interaction angle criteria. The figure shows that the angles that meet the non-linear interaction principle correspond to interaction depths.

Also, by doing this, we can investigate another important parameter in our sets of experiments that will give the opportunity to fully understand the potential of the method. This is the investigation of the change of amplitude with respect to small changes of the interaction angle. It is known that the non-linear amplitude is sensitive to the interaction angle but we also need to

investigate how this can change and to what extent. Having this information can develop better understanding an better calibration of the experimental procedure.

Going back to the first addressed issue, in order to investigate the the possibility of performing measurements in all areas without moving the fixture a new set of experiments was designed. Figure 4.10 shows that we can alter the interaction angle without moving the fixture, simply by choosing a different sub aperture of the transmitting array.

When a phased array that is mounted on an angled wedge is used for focusing, the focal beam refracts in a series of angles. In each case, the refraction angle of the middle active element is used to calculate the angle of the beam. Worth noting that in come cases not all of the angles fulfil the resonance conditions. Taking advantage of the number of active elements, we can use only a sub sets from the active elements aperture. By altering or minimising the number of active elements used for transmitting, we can adjust the refraction angle of the beam and effectively modify the interaction angle.

While keeping the arrays fixed in a specific location can be useful to avoid introduced non-linearities, on the other hand, by moving the probes and also taking advantage of the delay laws we can focus in different locations. This means that by introducing separation, a new range of locations that fulfil the resonance conditions are up for investigation.

Having that in mind the next step was to investigate how the amplitude of the mixed wave changes with the change of interaction angle in a specific focal point. To calibrate this set of experiments two parameters must be taken into account; the introduced separation between the probes and the theoretical interaction angle.

- Separation: Keeping the probes in a specific location gives us a limited range of exploration. Introducing three different separations can give us an idea about examining different range for a specific location.

- Interaction angle: Using the model we can calculate the theoretical interaction angles for each measurement.

Figure 4.10 sums the results from the theoretical calculations. The coloured dashed lines represent the interaction angles from the middle element and their matching vertical lines show the angle of the first and last elements. The black perpendicular dashed line represent the optimum range of angles in order to meet the interaction criteria. It is clear that in order to chose the right interaction parameters we have to make sure we are within the limiting range of ideal interaction angles.

4.4 Conclusions

The main conclusions drawn from this work are:

- Models provide a useful insight to the behaviour of a system, allowing sensitivity studies to be conducted, and the experimental procedure optimised;

- It is important to model the focused beams of the incident waves and compare the generated amplitude with the amplitude of the unfocused beam;

- When all energy is focused in a specific location, the focused beam shows higher amplitude than unfocused beam;

- Investigating the interaction angles is useful in order to determine the area, consequently the depth limitation with respect to the angle the incident beams meet;
- Figures from sub aperture show the variation of the amplitude when small changes in the interaction angle are introduced.
- Different depths can be tested if separation is introduced between the wedges.
- The main drawback is the interaction of focused beams is a few orders of magnitude smaller than that of unfocused beams.
- Therefore, dependent on the type of investigation desired, the focused beam offers more sensitive to small features due to higher resolution, and the unfocused beam provides the possibility of investigating a larger area due to the wider interaction point but with less sensitivity.

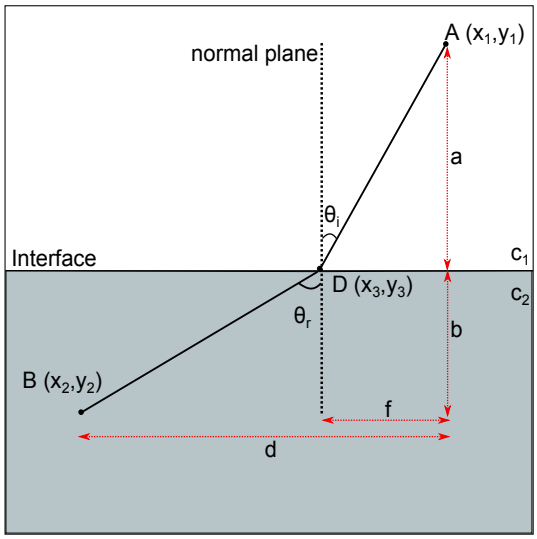

(a)

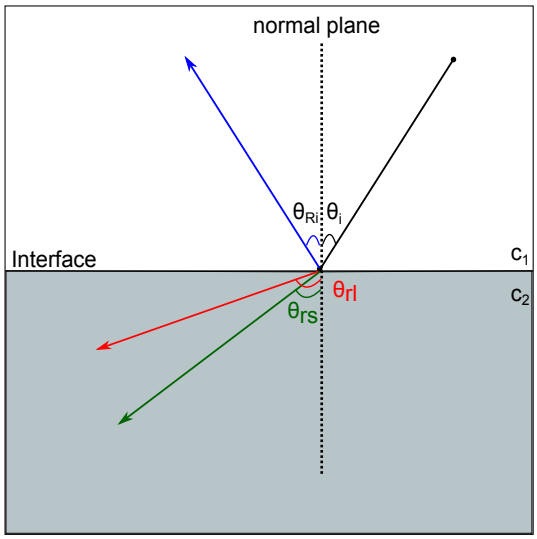

(b)

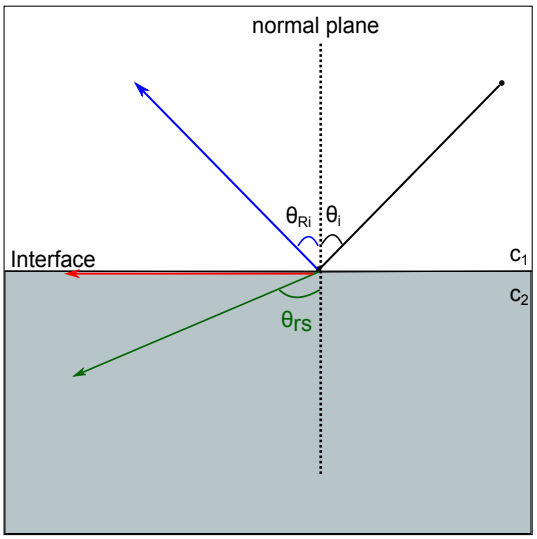

(c)

Figure 4.2: Propagation paths of an ultrasonic wave from medium A to medium B. θ_i is the incident angle, $\theta_r s$ is the angle of refracted shear wave, $\theta_r l$ is the angle of refracted longitudinal wave, $\theta_R i$ is the angle of the reflected wave. The green, red, blue arrows represent the mode converted shear wave, longitudinal wave and reflected

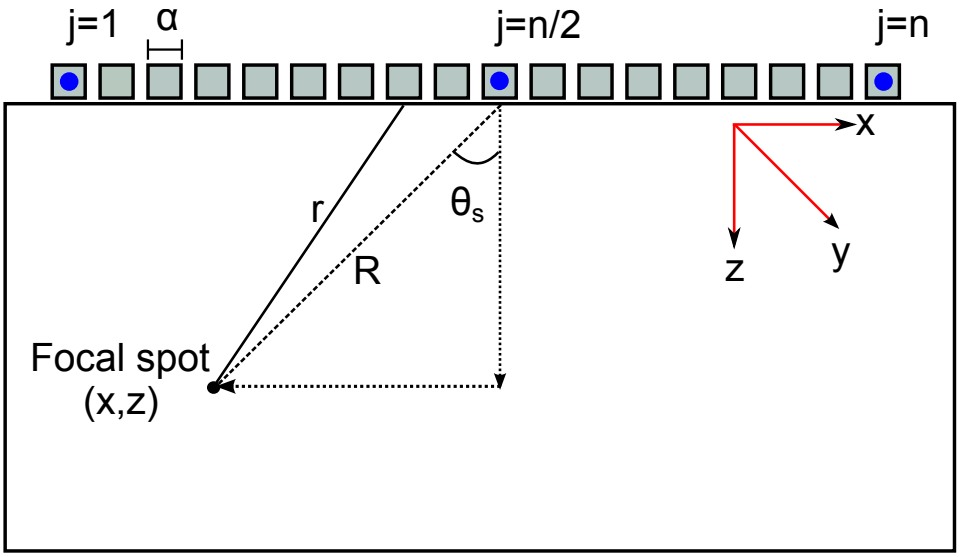

Figure 4.3: Geometry of a phased array.

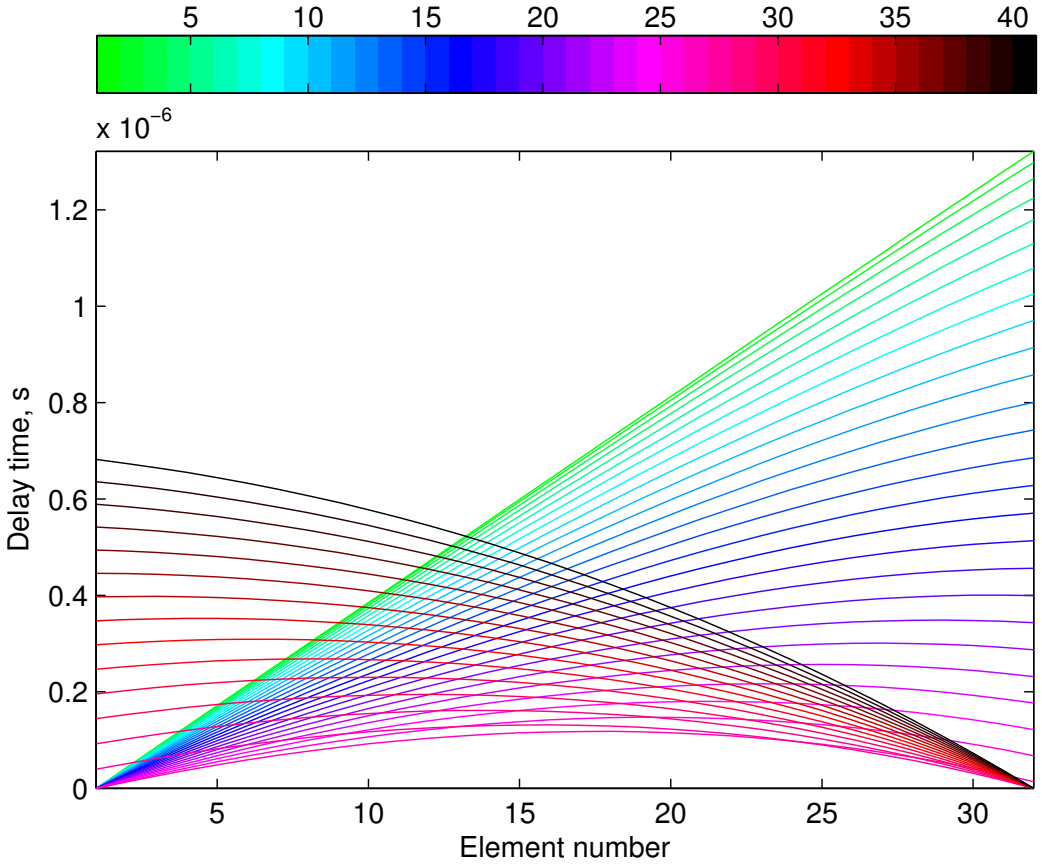

Figure 4.4: Profile of delay laws for each one of the 32 active elements. The colour map represents a series of different depths, from the top of the specimen to 40 mm from the surface.

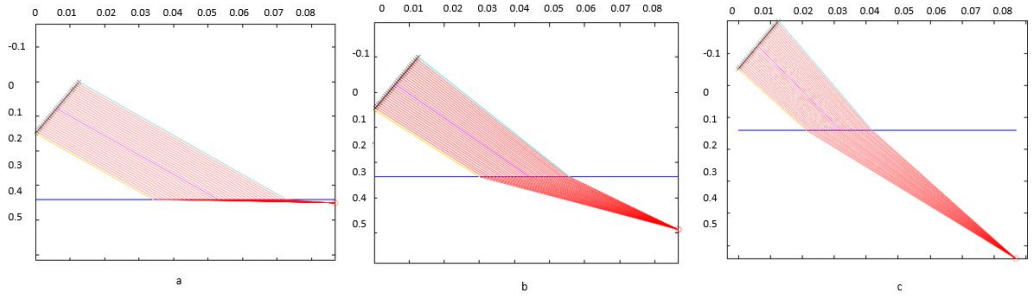

Figure 4.5: Model of delay laws for a series of focal points (a) close to the interface, (b) 15 mm from the interface and (c) 40 mm from the interface. The crosses represent the the active elements, the yellow line the first element, the magenta line the middle element and the green line the last element of the aperture.

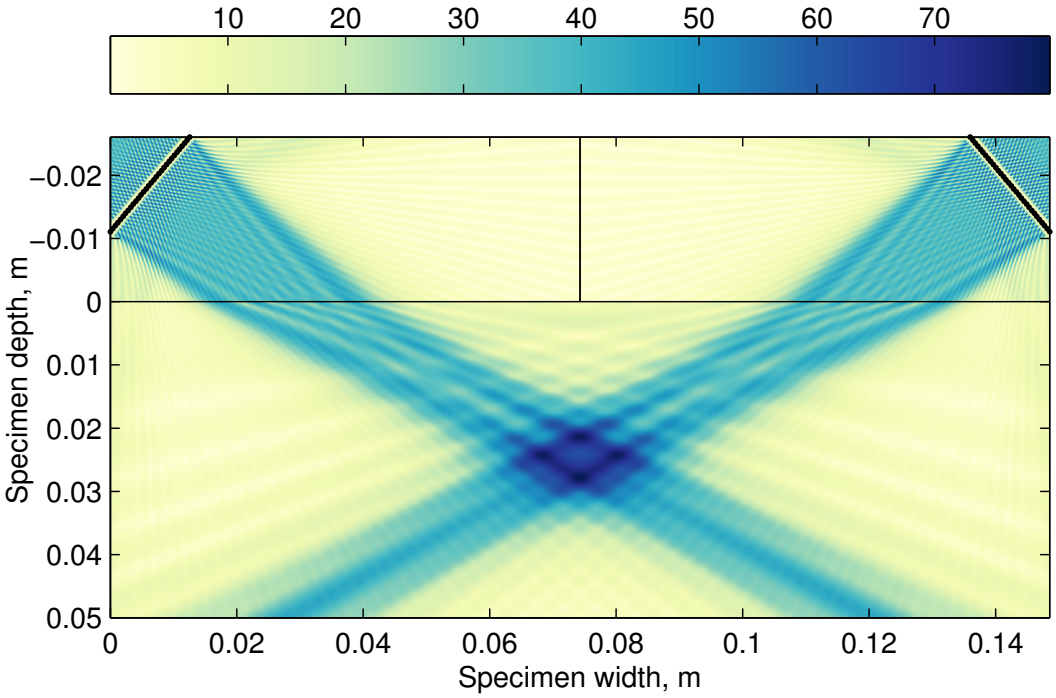

Figure 4.6: Model of linear field of two intersecting unfocused beams.

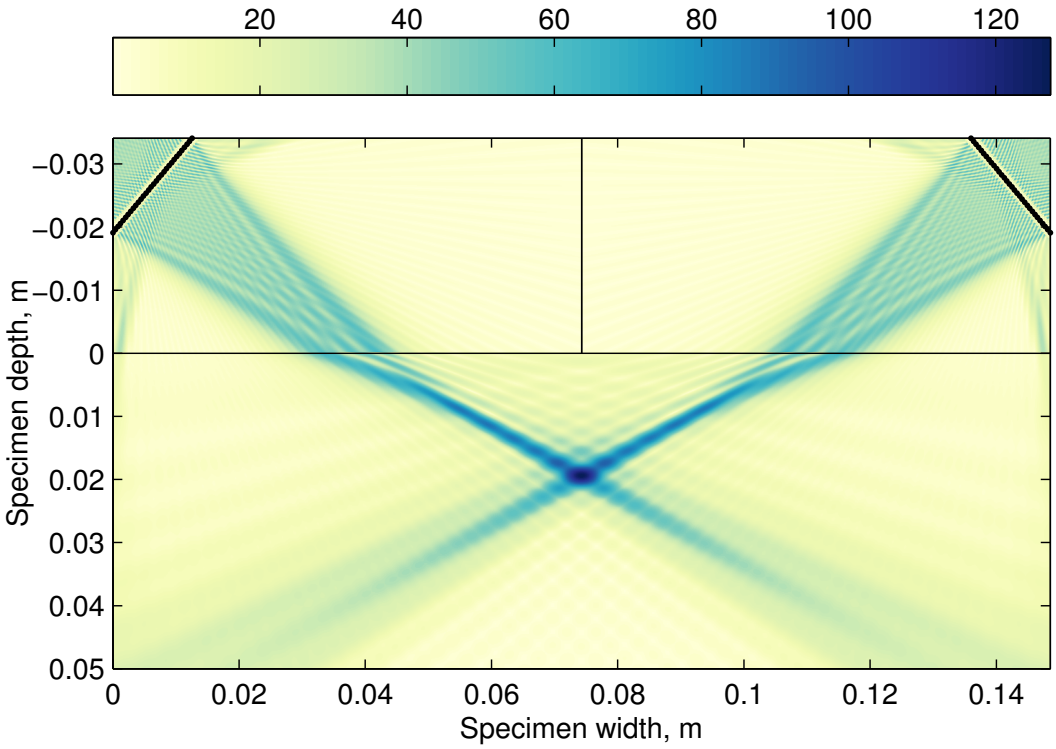

Figure 4.7: Model of linear field two intersected focused beams.

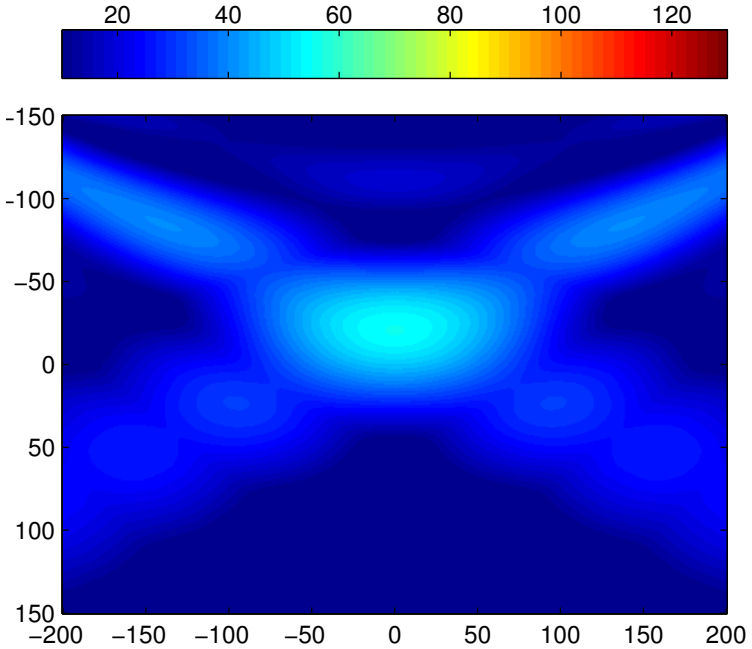

(a)

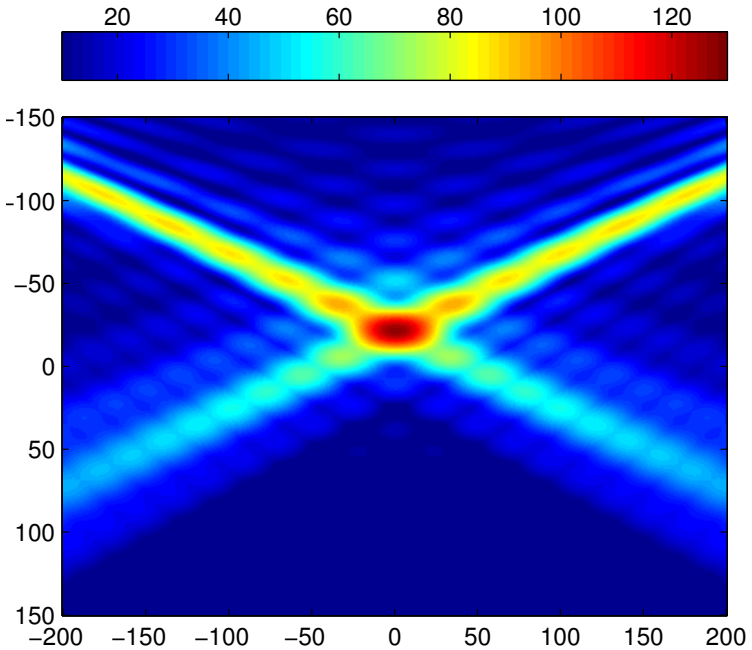

(b)

Figure 4.8: Zoomed images of the area of interaction as shown in Figure4.6 and Figure 4.7, that correspond to (a) and (b) respectively.

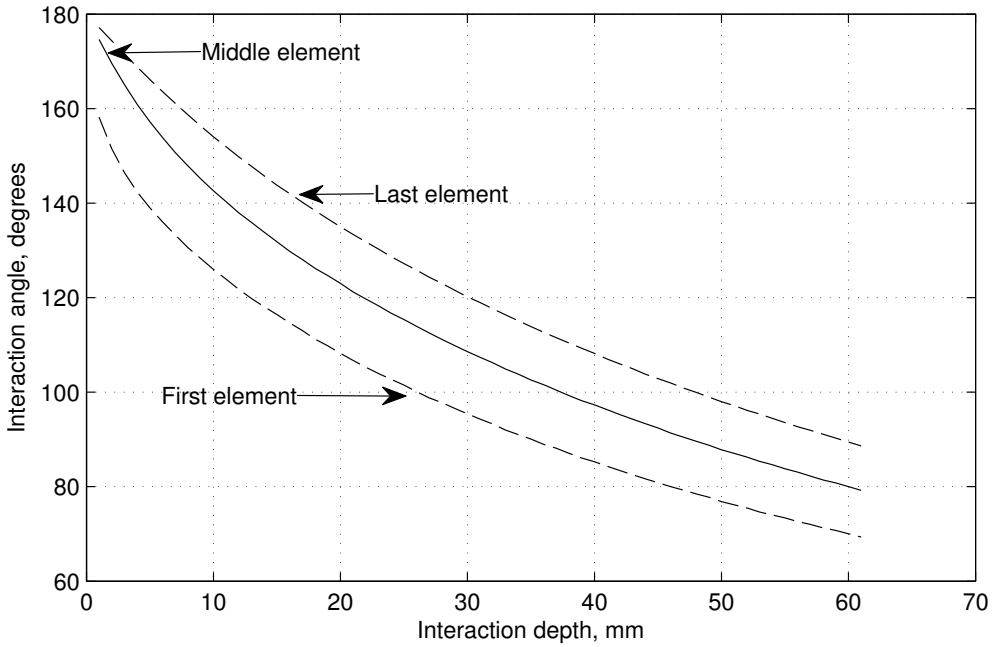

Figure 4.9: Theoretically calculated interaction angles for a series of focal depths.

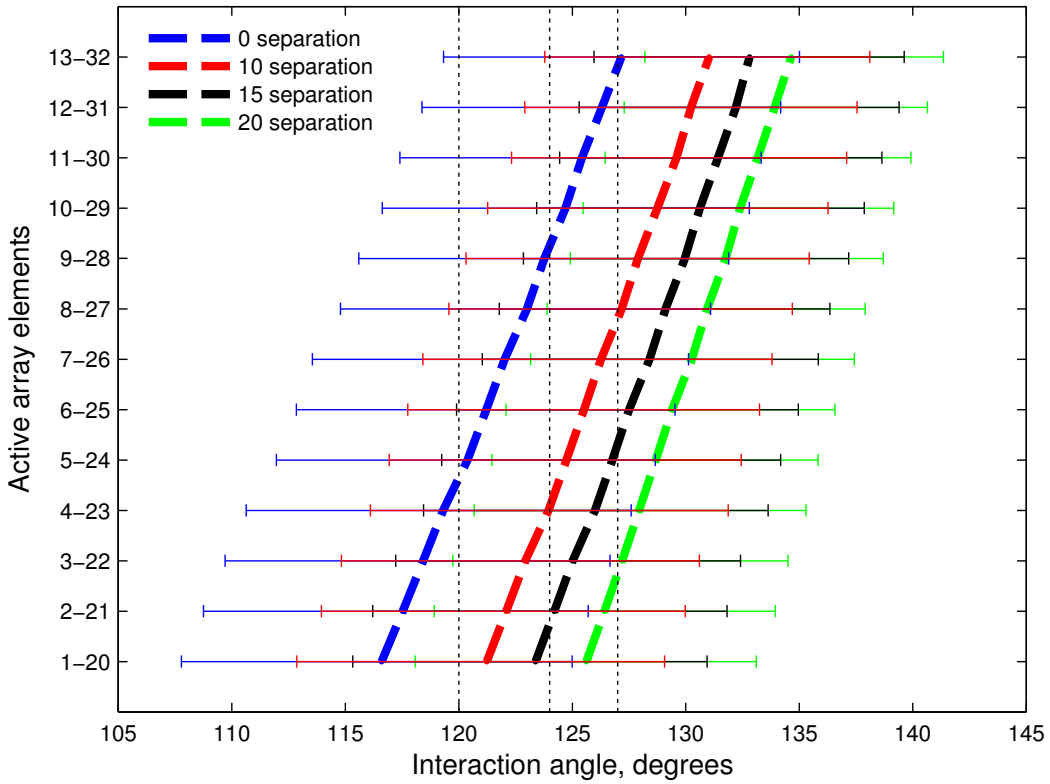

Figure 4.10: The figure shows the sub aperture set for four different separations (0 mm, 10 mm, 15 mm and 20 mm) that shall be selected for a successful non linear interaction. The black vertical dotted lines represent the interaction angle values that should be met for a successful non linear interaction. The first dotted line corresponds to the first sub aperture element, the second dotted line corresponds to the middle element and the third line corresponds to the last element. Each one of the coloured dotted lines represent the interaction angle of the middle element of the respective sub aperture for the four different separations. The small coloured vertical lines, represent the interaction angle of the first and last element of the respective sub aperture.

Chapter 5

Non-collinear tests with phased arrays

5.1 Introduction

This chapter focuses on the application of phased arrays in the non-collinear mixing experimentation. After developing models using the Huygenes principles to investigate the possibility of using the ultrasonic phased arrays for steering and focusing the beams, in this chapters the experimental applications of non-collinear measurements with phased arrays were performed. The effect of test variables, i.e repeatability, elapsed time, signal gain, was measured. Subsequently, experimental focusing of the array beams was performed and measurement of the non-collinear signal. Given that the generation of non-collinear signal depends on the interaction angle of the two incident beams, a set of different sub apertures can be used. The effect of different sub apertures in the amplitude of the non-collinear signal was also investigated.

5.2 Experimental procedure

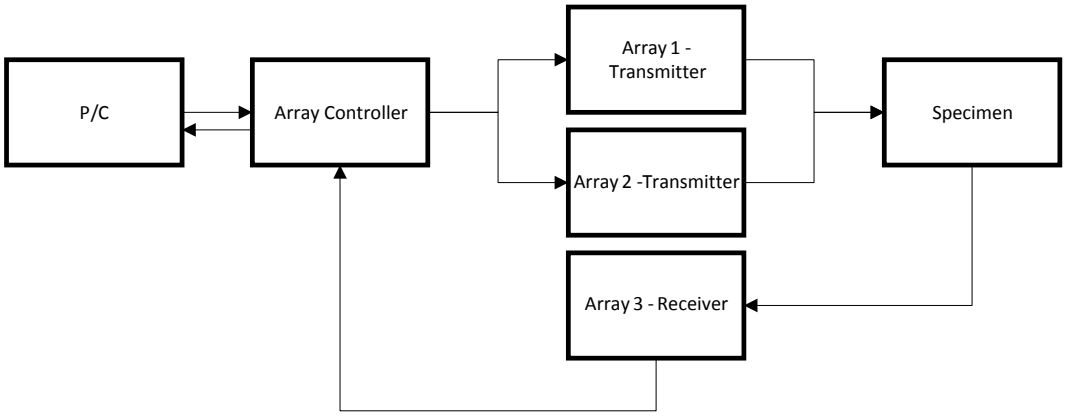

Figure 5.1: Schematic diagram of the experimental configuration.

The experimental configuration that was used all the experiments of this chapter is described in Figure 5.1. Two Imasonic (Besancin,France) phased arrays with 32 active elements, 5 MHz centre frequency and 0.63 mm element pitch were selected. Most of the industrial alloys, i.e Magnesium, Titanium, Steel and Aluminium can be inspected within the frequencies of 1-5 MHz. Thus, for these experiments the chosen frequency is 5 MHz as it is widely used in the industry. The signals were received with a phased array with 10 MHz centre frequency, 64 active elements and 0.3 mm element pitch. An Micropulse Peak NDT array controller (Derby, UK) was used to transmit and collect the signals from the array probes. Subsequently, the received data was captured and furthered processed using algorithms developed in MatLab software.

The standard acquisition test parameters that were applied in the array controller are shown in Table 5.1. It was essential to maintain the values for output voltage and gain hight in order to take advantage of as much transmitted energy as possible but at the same time within a certain limit to avoid saturation. Due to fact that the amplitude the non-collinear signal is

several orders of magnitude smaller from the input signal, a large number of averages was essential on order to smooth the noise in the output signal.

Table 5.1: Standard test parameters for non-collinear mixing tests.

Parameters	Values
Transmitting arrays	5 MHZ, 32 elts, 0.63 mm pitch
Receiving arrays	10 MHz, 64 elts, 0.3 mm pitch
Sampling Rate	50 MHz
Voltage	200 V
Centre Frequency	5 MHz
Gain	40 db
Sampling Bits	16
Number of averages	10000

The specimen that was used in the experimental procedure was a plate of aluminium with dimensions 100 mm $\times$ 50 mm $\times$ 100 mm. Two wedges were designed with preferred refraction angle for an angled linear scan 60° and manufactured by acrylic perspex. Due to the difference in acoustic impedance between perspex and aluminium the longitudinal incident beams are mode converted to shear waves as they propagate through the perspex-aluminium interface. The array probes were secured on the wedges with a pair of bolts. This would allow the fixture to be robust enough, so the transducers can stay in the predefined position avoiding misalignments, yet simple so that would be easy to disassemble for cleaning and coupling purposes.

Due to the difference in acoustic impedance between perspex and aluminium the longitudinal incident beams are mode converted to shear waves

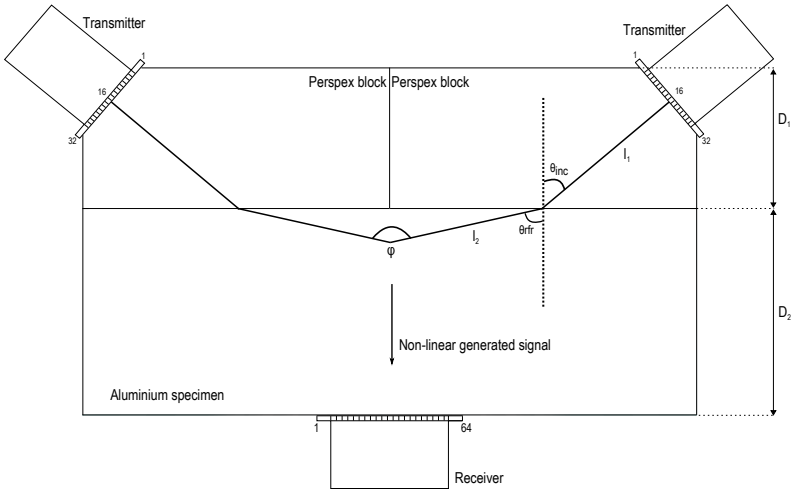

Figure 5.2: Geometry of the test set-up and simulation of the linear acoustic field generated by the two 5 MHz phased arrays. The black arrow indicates the direction of propagation of the wave generated by material non-linearity.

as they propagate through the perspex-aluminium interface. Figure 5.2 illustrates the design of the set-up. Due to the symmetry of the setup, the longitudinal non-collinear wave which is shown with the arrow propagates perpendicular to the surface, thus the receiving probe, 65 element Imasonic 10 MHz array with an element pitch of 0.3 mm (Waltham, USA), was orientated at the opposite side of the specimen and carefully placed symmetrically in such a way so that the middle element of the aperture would be positioned in the area of the expected arrival of the non-collinear wave. The receiving probe was held in place with elastic bands of adequate stiffness.

5.3 Signal Processing Steps

The amplitude of non-collinear interaction signal is several orders of magnitude smaller than the amplitude of the incident beams. In order to remove the frequencies associated with the linear transmissions and to reduce the effect of deleterious sources of non-linearity, such as from the coupling gel or

the array dynamics, a series of signal processing steps were carried out. The steps are summarised in Figure 5.3. The procedure uses three signals, one where both probes are triggered simultaneously and two where one or other probe was fired individually.

To minimise the effect of non-linearities in the system the responses from exciting individual probes, Figure 5.4. Panels (b) and (c) were subtracted from the response in which both probes are excited, panel (a). The amplitude of the harmonic of this subtracted signal, panel (d), is sufficiently clear that it can be detected at the expected time arrival. However to make it clearer a Hanning band pass window of 10 MHz centre frequency and 2 MHz bandwidth was applied at this subtracted signal resulting in a signal such as that in panel (e). The black vertical line indicates the line of symmetry in the setup, with the received signals confirming that the alignment is satisfactory.

To extract an amplitude of response, two time windows are selected, one across the region of the non-linear component and the other when just noise is present. The maximum value of subtracted-filtered signal is identified for both these windows giving a signal and a noise amplitude respectively for each receiver array element. While in many of the subsequent plots these amplitudes are shown as a function of receiver element location, x, where this data has been compressed to a mean amplitude this represents a mean across the receiver elements.

The amplitude of this component could be detected at the expected time arrival. Figure 5.3 shows the post processing steps: at the subtracted signal, a Hanning Band Pass window of 10 MHz centre frequency and 2 MHz bandwidth was applied at this component followed by a Fast Fourier Transformation, the resulting signal was filtered at the second harmonic

frequency. Two equal length time windows were applied one across the region of the non-linear component and the other when just noise is present.

A series of different values were extracted from the selected data sets in order to analyse and present the respective amplitudes. The mean and the maximum value of the the amplitude of each window as a function of the receiving array element numbers were calculated. Means and maximums were taken from these values as a method of characterising the amplitude trend. It was found that taking the maximum values would result in a large variance in the amplitude values, consequently the mean values were used to present the respective amplitudes for each measurement.

5.4 Dependant variables

Phased arrays were selected to perform non-collinear mixing tests order to apply the beam steering feature. By carefully calculating and altering the delay laws a series of measurements which result in different areas and depths of interaction can be performed without moving the fixture. This is particularly interesting since non-linearities from misalignments of the probes or due to the coupling material can be eliminated. Before the performance of depth focusing experiments, three features were investigated in order to determine their effect on the measured data: the applied signal gain, the repeatability over extended time and the coupling and alignment repeatability.

In order to select the most convenient area of interaction of the two focused incident waves it was essential to theoretically calculate the resulting interaction angle in a series of different point along the perpendicular axis of the aluminium specimen. The angle values were calculated by the theoretical

model developed in MatLab software. When we take two focused beams into account, it is difficult to calculate a precise interaction angle because the size of the beams spreads from the first active element of the array till the last active element. Thus, three different angle calculations were performed; from the arrays' first elements, from the middle elements and finally from the last elements. Figure 5.5 shows all the possible interaction angles that can result in the focused experiment and the arrows indicate the element of the transmitting array probes that was used for the calculations.. The results can be useful when it comes to defining the optimum interaction point. For the experiments to investigate the dependant variables, the interaction angle was measured by taking into account the middle elements, thus from Figure 5.5 can be deducted that the focal depth that corresponds to 120° interaction angle was 20 mm from the top of the surface of the specimen.

Before considering the possibility of scanning depth and interaction angle, which mechanically can be achieved by varying the transmitter separation distance and wedge angle or electronically by imposing appropriate delays to the signals sent to the transmitter array elements, the variability in the setup will be considered. The unsteered tests, in which no delay between elements was used, were conducted using the full aperture of the transmitters. The resulting interaction angle is 120° with the centre of the interaction volume at 20mm from the upper surface.

5.4.1 Signal Gain

For all the experimental procedures, it is imperative that we use the maximum power in the output signals so that we can achieve interactions that will result in non-collinear signals with distinctive amplitudes, higher than

the level of the noise. Thus, is important to experimentally verify the conditions in which the optimum gain is achieved.

For this reason, a series of measurements were taken in order to characterise the mean non-collinear amplitude with regards to the excitation signal gain. The tests were carried out at 5 V intervals, over the range 50 V to 200 V, to characterise the amplitude response as a function of input gain. During this test procedure, the set-up remained untouched with the same coupling, alignment and pressure conditions.

Figure 5.6 shows the mean values of the envelopes of the filtered signal with a focal depth at 20 mm at the expected time arrival for the non-collinear wave.

In all the measurements, the level of incoherent noise remained constant throughout the the experimental process and independent of the amplitude of non-collinear signal. The amplitude of the non-linear wave shows an increasing quadratic trend (trend line shown). This is verified by the theory since the amplitude of the scattered wave is dependent on the product of the amplitudes of the two input waves X_1 and X_2, Equation 2.2. Consequently, the operation test limit was above 80 V and the optimum voltage for the subsequent tests was selected at 200 V and the test parameters for the subsequent tests are summarised in Table 5.1.

5.4.2 Test dependancy validation

The second parameter which was important to investigate was the effect of elapsed time on the measured data from the experimental set-up. The coupling gel can be source of non-linearity and its non-linear contribution in the final filtered signal might fluctuate if the properties change. One

possible parameter that should be taken into account is the temperature of the coupling gel. The more time a set-up is coupled, the more temperature of the agent is expected to change. Consequently, it is important to evaluate whether the final amplitude of the non-collinear signal is subjected to changes.

Table 5.2: Effect of time and coupling variability of non-collinear signal and noise amplitude for a set of ten measurements. Amplitudes $\times 10^4$ shown.

Variable	Signal	Mean	Max	Min	St. Dev.
Elapsed Time	non-collinear	7.03	7.31	6.70	0.217
	noise	2.62	2.81	2.46	0.108
Coupling	non-collinear	5.71	6.86	4.16	0.902
	noise	2.27	5.00	1.59	0.980

A series of ten measurements were performed with an interval of 30 minutes between measurements in order to assess the effect of elapsed time on the measured data from the experimental set-up. The measurements were taken after validating good alignment of the arrays; before each test an unfocused linear measurement was taken and the time arrival of the linear waves from the left and right array probes was cross checked with the theoretically estimated values. The received signal was plotted and the left linear signal was compared to its right counterpart. If the left was the mirror image of the right, this suggested the same time arrival of the two was the same, consequently a good alignment. Figure 5.7 shows that the amplitude remains consistent over the 270 minutes of the test showing that possible temperature change of the coupling material due to lapse of time is not a source of non-linearity. This is of practical importance in real

engineering fixtures, the measurements are reliable with a set-up is fixed for a long time. The baseline noise remained low with a constant average amplitude of 0.26×10^{-3}, Table 5.2.

5.4.3 Coupling and alignment test set-up repeatability

The final set of experiments were performed in order to assess the level of variation in the final amplitude of the filtered signals. The non-collinear mixing tests exhibit high sensitivity in certain parameters such as coupling and alignment. It is important to be able to quantify the amount of variation when these parameters are altered. For this reason, a series of tests were conducted in which between each test the transducers were removed from and reapplied to the specimen.

This process involved removing sensors, cleaning the sample, then re-applying coupling gel and repositioning the transducers. The realignment procedure was checked and the probes adjusted by comparing the single excitation received signals for symmetry. Again Table 5.2 gives a summary of the results and it can be seen that reattaching the probes results in a small, but significant when considering the size of the measured signals, variation in amplitude with a standard deviation that is four times that of the elapsed-time tests.

5.5 Focused tests

The key attraction of phased arrays is the ability to electrically steer and focus the transmitted waves. Using the full aperture of the transmitters, this enables us to scan over depth from a single set of transducer locations hence avoiding repositioning and the signal variability this introduces. However

the interpretation of the results is not straightforward as by scanning depth the incident angle at the perspex-aluminium interface (and hence the mode conversion efficiency) and the interaction angle must also alter.

Using a sub-aperture of the transmitting elements and varying the centre element of this sub-aperture offers the potential to scan over a limited range of depths or interaction angles. Additionally the generated waves can be focused to allow a small volume of interaction. The advantage of using the full aperture of the transmitter arrays is that the input power is maximised. Figure 5.9a shows the maximum received signal as a function of receiver element location for a range of depths. It can be seem that the difficulty in interpreting this data is that as well as altering the depth of the interaction volume, the interaction angle has also been altered. Altering this has the effect of changing the behaviour of the interacting waves, which exhibit a resonant-like response across interaction angle.

5.5.1 Angle Investigation

For this test the delay laws were altered in such a way that the interaction point was at 20 mm from the top of the specimen. In order to investigate the interaction angle in a specific location and its relationship with the interaction angle, a sub aperture of 20 active elements were used and moved across the array. For each sub aperture the delay laws were carefully calculated to ensure interaction at the same point.

For each measurement, the window of the firs arrival was averaged and the maximum amplitude was extracted. In Figure 5.10 can be observed the amplitudes of the non-collinear signals with respect to the position of the aperture and thus the interaction angles.

A similar test was performed where a the effect of the interaction angle as a result of different separations was performed. The delay laws had to be recalculated for each separation. Three different separations were selected: 0mm, 10mm, 15mm and 20mm. Due to the difference in the geometry, the delay laws required a different set of elements, nevertheless that can be of importance since with different sub apertures we can generate a wider range of angles. The results are shows in Figure 5.11.

5.6 Discussion

- This chapter describes a series of non-collinear ultrasonic measurements with phased arrays. Although the non-collinear mixing technique shows strong advantages against other non-linear methods, there are a number of disadvantages.

- Coupling inconsistency and small misalignments in the fixture can have a significant impact on the scattered wave. In order to minimise those factors, phased arrays were selected as multiple beam profiles can be generated without moving the probes.

- A series of experiments were performed in order to investigate and identify key parameters in the variability of measurement quality. It was experimentally confirmed that the maximum amplitude was obtained using 200 V, the highest available gain. The technique showed consistent measurements could be taken with an elapsed time of several hours with an unchanged experimental set-up and during repeated, identical, experimental set-ups.

- Several tests were performed with the set-up fixed in a specific location. By choosing a sub aperture and scanning along the length of the array, the volume of interaction effectively moves along the vertical axis of the specimen. The difference in the interaction area is illustrated where the amplitude of the non-collinear wave varies with respect to the sub aperture set. Subsequently, a map was created for focal depth versus time in the time window showing the focal depths of the maximum amplitude of non-collinear signal.

- A similar map of amplitude was created for focal depth versus element number though the specimen showing maximum amplitudes found at focal depths corresponding to interaction angels between 90° to 120°. A fixed focal depth was selected and tests were performed in order to assess the potential of steering and focusing the array beams from a fixed location. By altering the delay laws, the beam was initially steered and then focused to the preferred focal depth. By using a sub aperture of 20 elements of the arrays interaction angle was varied for a fixed focal depth and showed an optimum interaction angle between 120° to 124°.

- Results showed a similar trend for the values of amplitude for both both steered and focused tests. The amplitude of non-collinear signals generated from steered beams was several orders of magnitude bigger than those generated from focused beams. That can be attributed to the fact that not all active elements fulfil the resonance condition during focusing, so the energy of the beam for the interaction is relatively lower. The steering tests provided higher amplitudes because the beam diameter is larger. The steered beam provided good non-collinear

amplitudes for bigger volumes of interaction. Although the focused beams could be eliminated due to resonance conditions, the showed sensitivity over a smaller interaction area.

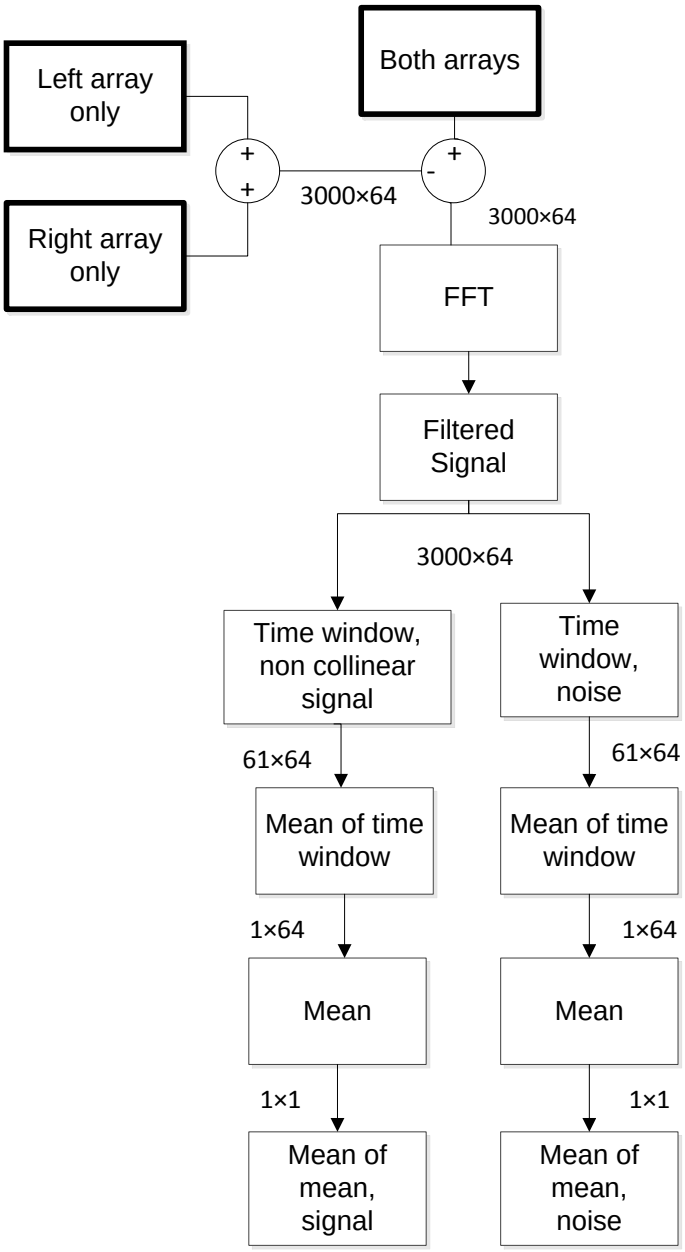

Figure 5.3: Post processing steps with the three measurements, where the left array, the right array and both arrays were used.

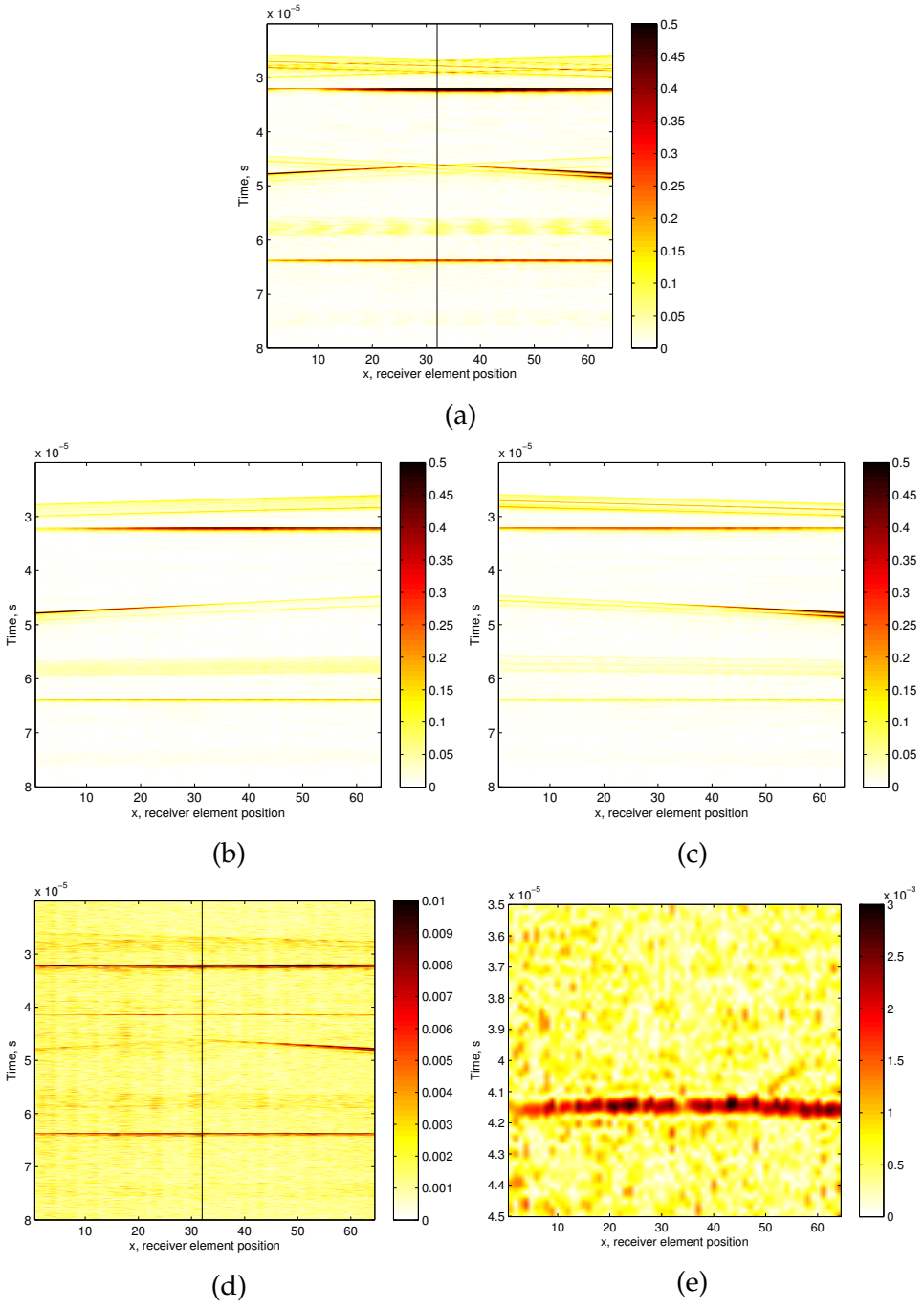

Figure 5.4: Summary of signal processing steps of a non-collinear mixing test. (a) received signal with both arrays, (b) signal received with left array only, (c) signal received with right array only, (d) subtracted signal, (e) filtered signal at the second harmonic frequency. The black perpendicular line indicates the centre of the receiving array and confirms a good alignment of the set-up. The non-collinear signal can be detected at 4.2 s which is the expected time arrival.

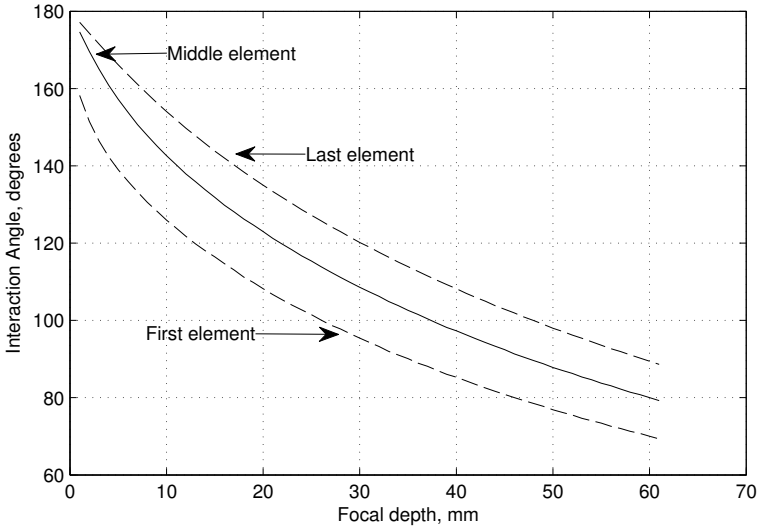

Figure 5.5: Theoretically calculated interaction angles for a series of focal depths.

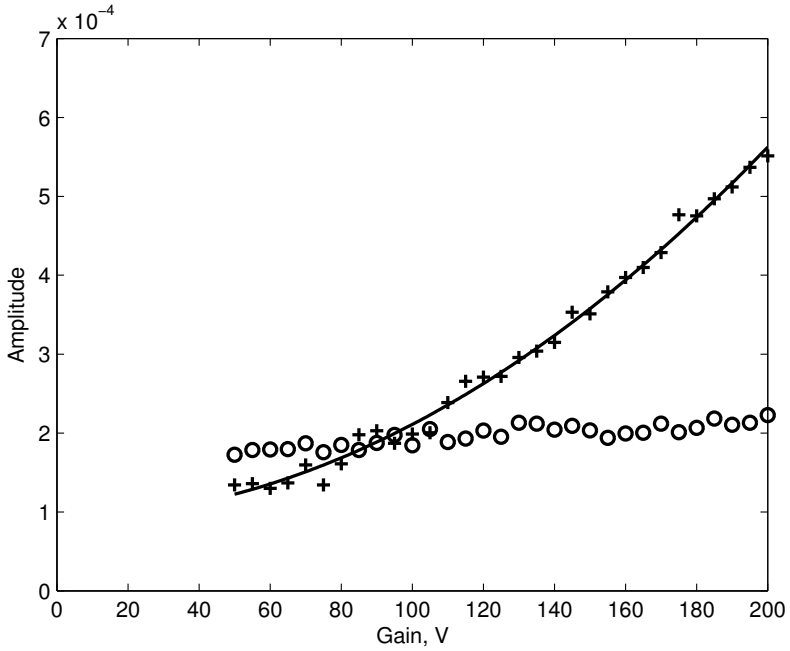

Figure 5.6: Amplitude as a function of gain for the time window covering the non-collinear signal (crosses) and the window of sampling the noise (circles). A quadratic trend line is added for the mean amplitude data points.

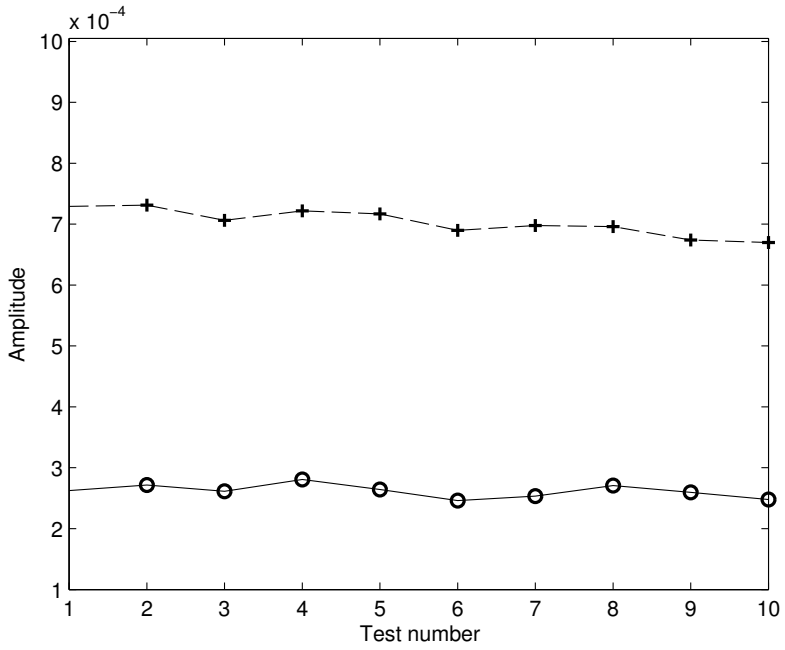

Figure 5.7: Mean amplitude of non-collinear signal (crosses) and noise (circles) as a function of time.

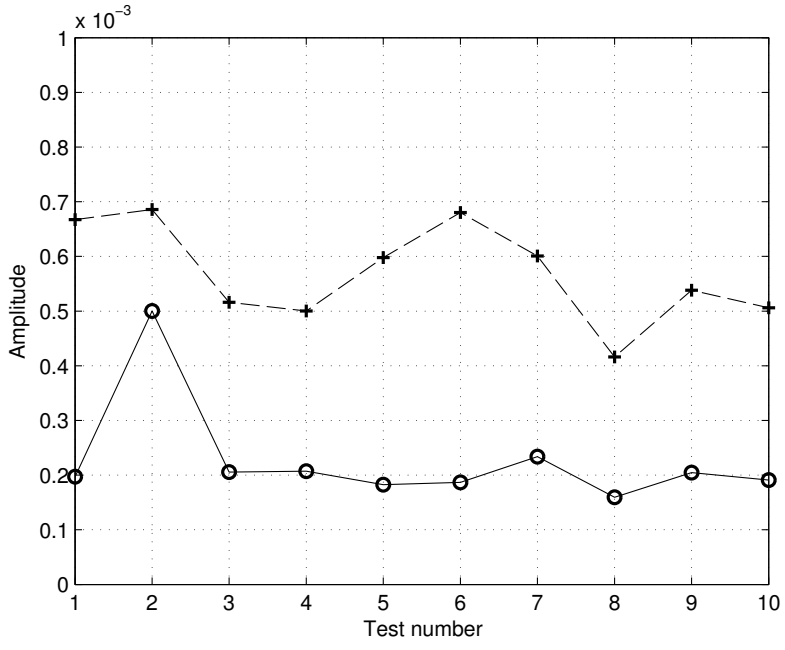

Figure 5.8: Mean amplitude of the non-collinear signal (crosses and noise sample (circles) for each repeatability test.

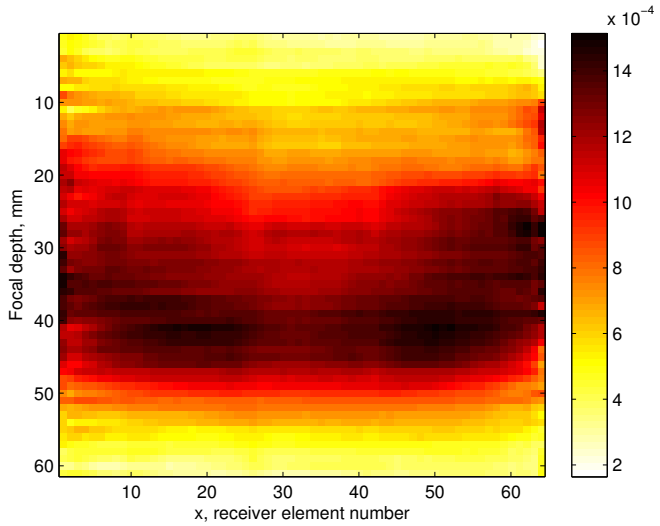

(a)

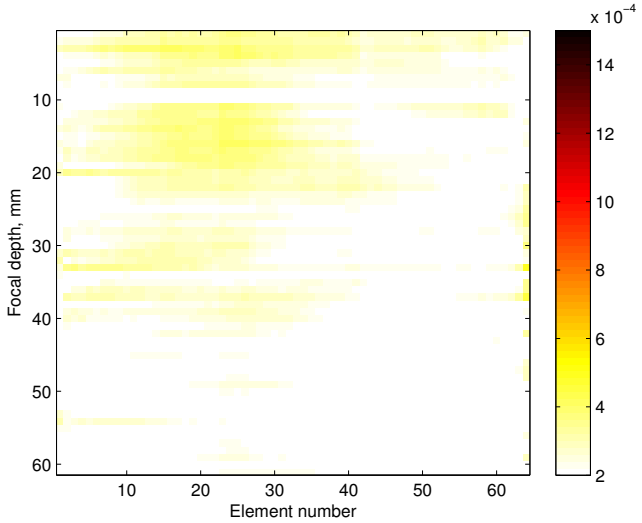

(b)

Figure 5.9: Envelopes of (a) non-collinear signals and (b) noise sample for focusing at different depths at a plane perpendicular to the longitudinal direction of the specimen.

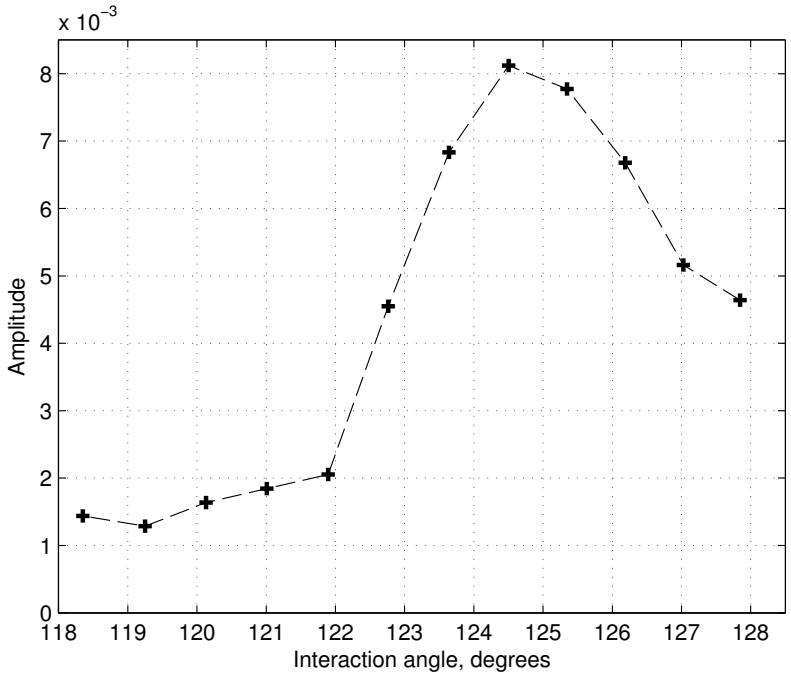

Figure 5.10: Maximum value of amplitude in a range of interaction angles for a fixed depth of 20 mm for the beam steering tests.

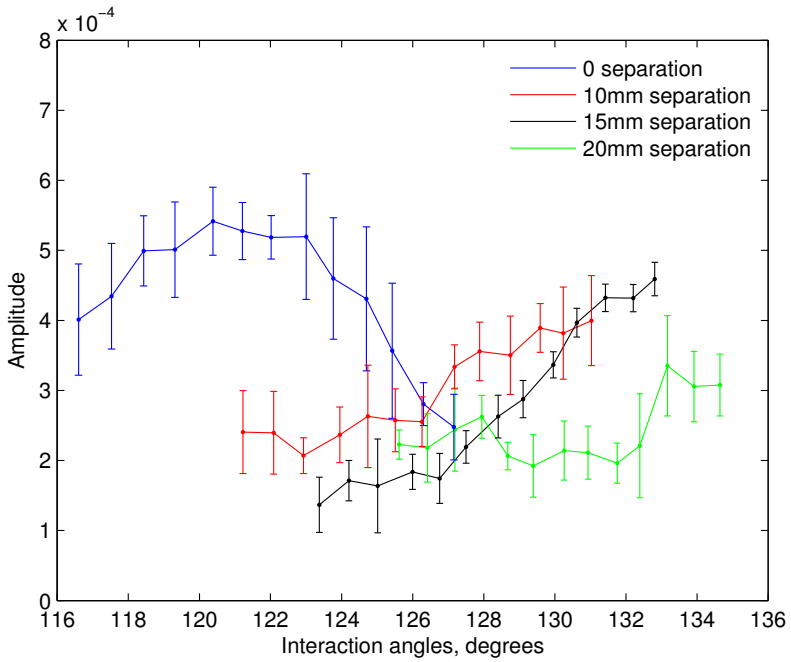

Figure 5.11: Mean value across the elements of the amplitude for a range of interaction angle and for a focal depth of 20 mm for a different array separations.

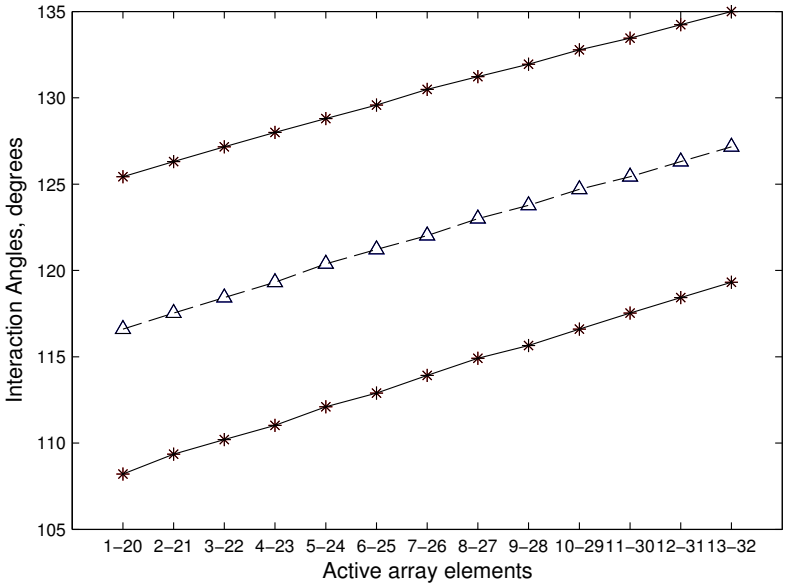

Figure 5.12: Theoretically calculated interaction angles for 20 active elements as they move across the array.

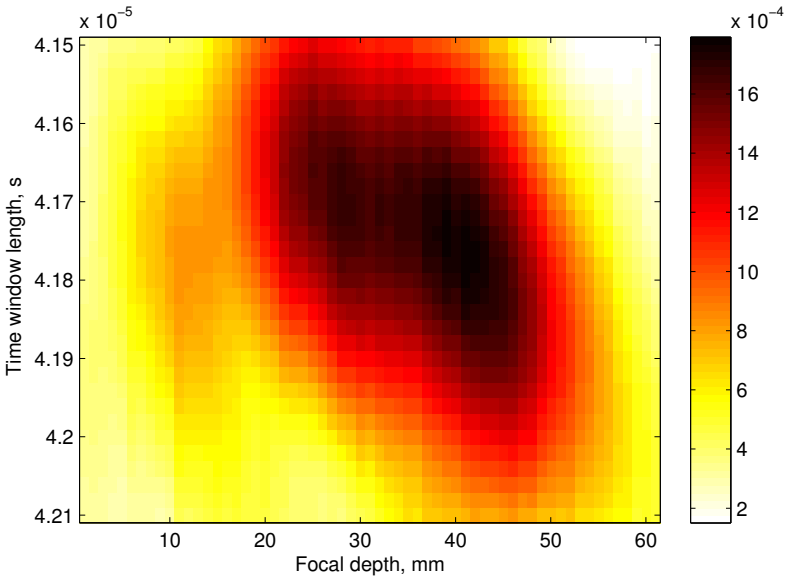

Figure 5.13: Mean value of envelopes of non-collinear signal.

Chapter 6

Non-collinear carbon fibre reinforced plastic testing

6.1 Introduction

Composites are materials which are produced after the combination of two or more materials with different individual properties, giving the final material unique and superior properties, such as higher strength with lower weight. In the case of Carbon Fibre Reinforced Plastics (CFRP), the matrix is of polymer nature and the fibres work as reinforcement. Depending on the dimensions, the orientation and the way the fibres are spread within the matrix, the composite material exhibit different mechanical properties. Carbon Fibre Reinforced Plastics can be five times stronger than AISI 1020 steel (Brinell hardness of 119 235 and tensile strength of 410-790 MPa) while having only one fifth of the weight. Additionally, although aluminium may have similar weight to Carbon Fibre Composites, still the composite can have twice the modulus and up to seven times the strength.

Because they combine unique properties, they are attractive in engineering applications, especially aerospace and automotive industry. For example, the Boeing 787 Dreamliner brakes are manufactured by carbon fibre composites. They exhibit great wear and tear resistance, good energy absorption, particularly important in emergency landing where high stresses are applied in the aircraft, good thermal conductivity and greater overall strength. The reduction in weight is also important resulting in a lighter structure which effectively results in lower carbon monoxide emissions per passenger per kilometre during its operation. Another example is Eurofighter Typhoon with its air frame consisting in 70% carbon fibre composites, 15% metal and 15% other materials. This results on 30% less traditional materials used. These weight savings will have further effects on the size and weight of the engines and from overall weight savings there are significant reductions in fuel consumption thus further reductions the direct operating costs.

Despite the fact that carbon fibre reinforced plastic is a mature material, one of the biggest challenges lies in the detection of defects. Composite materials are now widely used in safety critical components and the integrity of these parts is crucial. Defects can be a result of poor design, i.e. improper spread of reinforcement in the matrix, improper manufacturing, i.e. poorly cured resin, or damage during operation, i.e. debonding, cracks, delaminations. For example, Kim, Lee and Lee (2005) and Fu and Lauke (1996) showed a change in fibre orientation within the matrix may result in two dimensional deformation.

Fitzer and Huttner (1981) stated that although the CFRP have higher mechanical properties compared to conventional carbon materials, care has to be taken with the bonding element as it is always the weakest part. Smith et al. (2009) stated the importance of advanced non destructive testing methods

in carbon fibre composites as aerospace materials especially because their usage has expanded the last decades from military applications to civil aircraft components. Now, the challenge is not only to control the quality of the materials during it's application but also during the manufacturing process. Up till now, there are several conventional non destructive testing techniques being used in order to ensure the quality and safety of CRFP structural components.

- Infrared Thermography: This is a method where thermal energy emitted from a specimen is monitored and afterwards related to defects in the structure. Zalameda et al. (2012) showed that carbon fibre samples that were subjected to cyclic loading and fatigue were tested with thermography showed good sensitivity when used along with X-rays and Ultrasonic inspection but the main drawback is that the results are more qualitative than quantitative. Overall, it is an expensive technique and does not have the sensitivity the ultrasonic methods might provide.

- Shearography: This a relatively good optical method for detecting disbonds and voids in the surface of the composites. The procedure involves applying stress to the test specimen and after image processing algorithms shear images are produced that show the stress field around a defect. Subsequently, images can be compared to the ones taken before the stressing. Although this method shows more practicality, according to W. Steinchen and Mackel (n.d.) is sensitive to environmental conditions; external noise or environmental heat can affect the final results. Although the results can be fast, the main drawback is the need of actual application of stress in the object, making it less practical than other methods.

- Eddy current: They are useful in composites as they exhibit higher sensitivity in certain levels where ultrasound does not but they are limited in the penetration depth. More precisely, according to Cheng et al. (2017), Eddy Current testing advantages lie in the on line inspection during the manufacturing process of the composites, in the raw carbon fibre and the uncured carbon fibre.

- X-rays: X-Ray computer tomography is used in the detection of fibre waviness but according to Halmshaw (1991) (pp. 98–99) is an expensive process with the main limitation being the safety and hazard issues involved with the test procedure. Jandejsek et al. (2014) have investigated the possibility of using X-ray techniques to detect delaminations in composite aircraft materials. Although the results showed some sensitivity, the accuracy of the method is limited and accuracy has yet to be determined.

- Magnetic methods: The problem here is that the test material has to be ferromagnetic severely limiting its applicability .

Littles, Jacobs and Zureick (1998) used laser based contact transducers to investigate fibre reinforced plastic samples and calculated the engineering constants for application to civi engineering. The most common defects in composite materials are porosity and cracks.

Pain and Drinkwater (2013) used ultrasonic phased arrays and developed a scattering matrix extraction method which was later implemented in composite samples. Results showed good sensitivity with regards to the waviness of composites but further work has to be done with respect to quantifying the level of the defects.

Li et al. (2013) used the Total Focusing Method as an imaging tool for relatively small scale drilled holes with 1.5 mm diameter and 6 mm in length were drilled in a carbon fibre composite specimen of 82 plies. Authors showed that with the careful selection of parameters of filtering, definition of angle limit and the right attenuation correction can give good results in the detection of defects. The challenge is that authors assumed that the material behaves as spatially homogenous which is limiting for real applications and also the method cannot be further implemented due to lack of a propagation model in composite materials. Meng-Chou Wu (1991) showed that the non-linear harmonic generation technique exhibits a sensitivity over small scale features produced by fatigue in graphite EPOXY material. The method was proven sensitive for small scale defects and delaminations. The non-linear parameter was increased with fatigue. Gao et al. (2009) tested nanotubes in carbon fibre composites because the nanotubes can act as sensors within the epoxy.

Felice et al. (2014) developed a new post processing method implemented after total focusing method for the detection and quantification of small cracks but the technique is limited to cracks very close to the surface. Brotherhood, Drinkwater and Freemantle (2003) developed an ultrasonic wheel sensor capable of scanning aerospace components 25 times faster than the conventional methods but de to the size of the wheel sensor, the area of scanning was limited.

Cuevas et al. (2013) studied composite samples with different curing rate / contamination level. The test parameters were the attenuation level and the velocity and showed that air coupled ultrasonics can be more sensitive in non cured samples. Smith et al. (2013) investigated the fibre waviness and showed potential in 3 dimensional mapping.

Karabutov and Podymova (2014) showed that the attenuation level in CFRP laminates can be quantitatively correlated to the average porosity level but still there is work to be done with regards to microscopic voids and interply delaminations. Genovés et al. (2015) studied the attenuation curves in Glass Fibre Reinforced Cement (GCR) materials with different porosity as mechanical properties and showed that relationship can be attributed between attenuation and degradation. El-Sabbagh, Steuernagel and Ziegmann (2013) showed that there is correlation to attenuation as well as to the longitudinal sound velocity with regards to the fibre content in Natural Fibre Polymer Composites.

Up until now, the research that has been done in the field of non-collinear mixing of ultrasonic waves is in isotropic materials. Croxford et al. (2009) used the method to study the plasticity and fatigue in Al2014-T4 aluminium alloy specimens.

Demcenko et al. (2012) studied the physical ageing in PVC and were able to identify cracks in water pipe PVC specimens. Demenko, Koissin and Korneev (2014) carried out further research and monitored the ageing in thermoplastics and epoxy cure. Around this time, McGovern, Buttlar and Reis (2014) showed that the technique exhibit sensitivity in the detection of non-linearities of asphalt during the oxidisation process. Although work has been carried out in the field of non destructive testing in composites as seen in Section 6.1 little or no work has been carried out with non-linear methods. For this reason, the four carbon fibre samples were tested with non colinear ultrasonic mixing technique.

Fast method: One setup can be used to scan multiple locations without moving and having to rearrange. Only the scanning algorithm has to change which can be quickly done by changing parameters in the processing file.

Reliable: By maintaining the same setup, we prevent non-linearities to interfere in the signal. After a series of measurements and tests we can end up with results and images that are relative and comparable to each other.

Complex parts: With the progress of carbon fibre composites in the aerospace industry, parts with complex geometries are produced. Producing curved carbon fibre parts is still a challenge due to out of plane ply waviness defects, thus effective ndt methods are imperative. The original equipment manufacturers require specific limits when it comes to wavelength and amplitude of wrinkles is composites. These limits are likely to decrease as technology progresses. The non-collinear method can provide an effective tool to investigate layers of carbon fibre with higher sensitivity due to the focusing ability.

Finally, although, Demcenko et al. (2012) and Demenko, Koissin and Korneev (2014), have used the non-collinear mixing in non metallic materials they have only used a single interaction angle and a specific frequency ratio. Although their results in the detection of the physical ageing of PVC were encouraging, still it is unsure whether another set of parameters could be more effective.

6.2 Manufacturing of samples

The materials used for the experimental procedure were 4 samples produced especially for the Extended Non-Destructive Testing of Composite Bonds (ENCOMB) project, part of the European Union's 7th Research and Technological Development Framework Program. The package which was sent to the University of Bristol consisted of four carbon fibre samples with weakened

bonds, manufactured by the European Aeronautic Defence and Space, now Airbus group S.E.

The four samples were produced with the vacuum bagging lay up method. According to Graham-Jones and Summerscales (2015) this is the manufacturing method usually applied in high performance composites. In this method, wet materials are laid on top of each other and subsequently are put in a sealed bag where the air is removed with a pump. As the air is being removed, the pressure in the bag increases up to 1 bar, helping in the consolidation of the layers. In this case, the first layer was a non perforated release film underneath the CFRP laminate. On top of the laminate was placed a perforated release film and then a second laminate was placed on top of it. Care was taken to avoid air bubbles between the layers. Subsequently, the assembly was placed in a vacuum to cure at 180 °C, following the IPS-01-006-02 cure cycle (Airbus Issue 4, 2008). Figure 6.1 shows the sequence of the layers and the manufacturing method for all the specimens.

The raw materials that were used in order to produce the final samples were Hexcel M21 epoxy resin, Hexcel T700 UD carbon fibre plies and for the bonding of the two parts the film adhesive FM300 K.05 by Cytec, as shown in Figure 6.1. In order to produce different bonding properties, the surface of the specimens was contaminated with the silicon based release agent Frekote 700 NC using different concentrations of it in the solution; 1%, 5%, 10% and 30%. Afterwards the samples were dried for 30 min at room temperature and subsequently heated for 60 min at 80 °C in an air circulating oven. The contaminated surfaces were characterised by Xray Photoelectron Spectroscopy (XPS) analysis where one measurement was made at the top of the sample and another one at the bottom of the sample, Table 6.1. The measured silicon content is used as an indicator for the

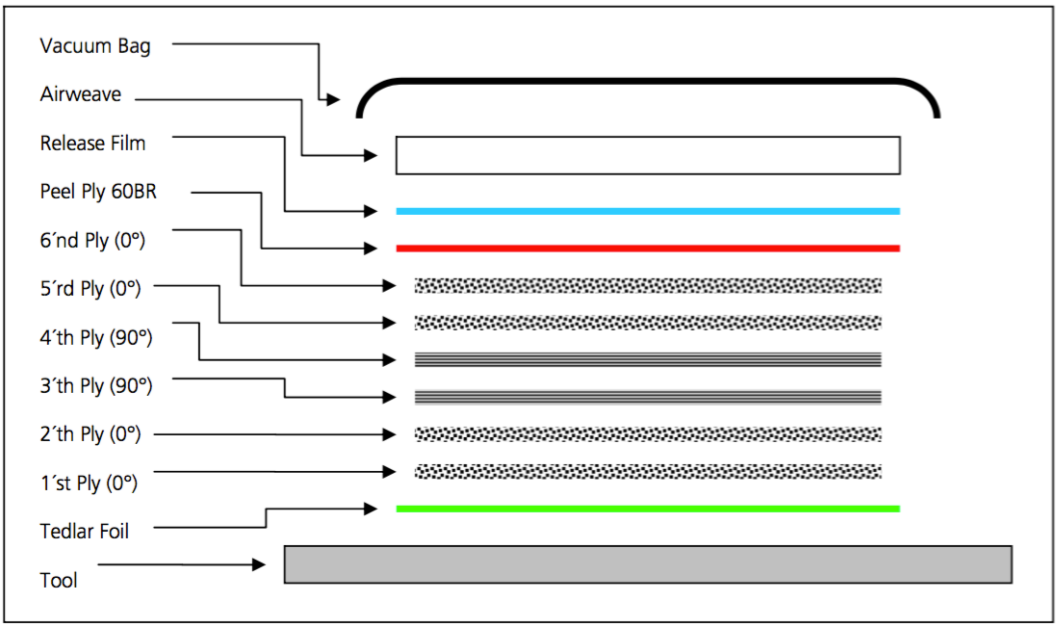

Figure 6.1: Lay up of an unbodied CFRP specimen. The same procedure and manufacturing method, vacuum bagging, was followed for all the four samples.

degree of surface contamination by Frekote 700 NC. For each specimen, the Critical Fracture Toughness G_{Ic} was determined according to ISO 15024 specification for unidirectionally fibre reinforced plastic composites using a double cantilever beam (DCB) specimen, for example $23\,^{\circ}\text{C} \pm 2\,^{\circ}\text{C}$ and $50 \pm 5\%$ relative humidity. The results of the this test procedure are shown if Table 6.2.

Table 6.1: Elemental composition with XPS analysis of CFRP samples. RE stands for Release Agent, the silicon based contamination on the surfaces, Frekote NC700.

Sample	O	N	C	S	Si
CFRP with 1% RE	23.2	2.9	70.4	1.0	2.5
CFRP with 5% RE	25.2	2.9	65.4	0.7	5.8
CFRP with 10% RE	25.5	1.9	64.6	0.7	7.3
CFRP with 20% RE	26.9	1.9	60.5	0.7	10.1

Table 6.2: Critical Fracture Toughness (G_{IC}) of the CRFP samples measured according to ISO 15024 specification for unidirectionally fibre reinforced plastic composites. RE stands for Release Agent (Frekote NC700), the solution which was used to produce different bonding properties.

Sample	G_{IC}
1% RE	1072.72 J/m^2
2% RE	493.24 J/m^2
3% RE	60.83 J/m^2
4% RE	40.37 J/m^2

6.3 Experimental arrangements

All non-collinear mixing tests applied to the carbon fibre reinforced plastics were performed using the immersion method. This is a different set-up compared to the one described in Chapter 3. The arrangement involved the usage of a water tank and a motor / rig which was used to mount the probes and the specimens. The motor also had the ability to control and change the separation of the two input transducers. The reason why the contact set-up described n Chapter 3 was inappropriate and a water tank approach was chosen lied in two main reasons:

- Initially, the area of interaction was chosen to be in the middle of the specimens. Given the fact that the dimension of the specimens were 100 mm$\times$50 mm$\times$4 mm, a contact non-collinear measurement would require a large wedge separation which would exceed the length of the specimen itself.

- Additionally, possible reflections and interaction from the layers of the specimen would decrease the signal to noise ration and would possibly result in problematic measurements.

The motor / rig is shown in Figure 6.2. The input transducers were supported by two rings and were each controlled by two rotation shafts. The rings were mounted on a rail which was responsible for the horizontal movement of the probes. The rings were also connected to an actuator which controlled the linear position by connecting to a motor. This way the separation as well as the angle of the transducers with respect to the specimen could be altered (blue arrows) resulting in a different refraction angles in the material and thus different interaction angles in the middle of

the specimen. In the water tank care was taken so that the level of the water was enough to cover the transmitting area of the transmitting probes for all the sets of different angles that were inspected.

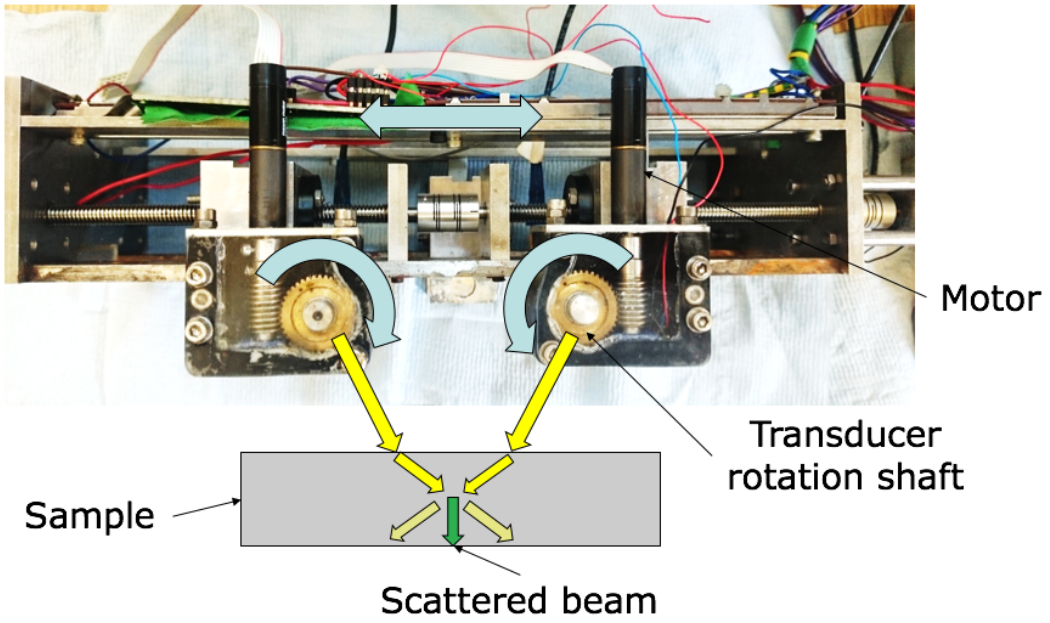

Figure 6.2: Plan view of the test rig and motor used for the immersion tests. The blue arrows show the possible relative movement of the transducer holding rings. The yellow arrows indicate the direction of the incident waves and the green arrow the direction of the scattered wave in the carbon fibre specimen.

It is known from literature Halmshaw (1991)(pp. 105) that in infinite homogenous isotropic elastic solids, the propagation velocity of ultrasound depend on the properties of the material; Youngs Modulus E, Poisson ratio ν and density ρ. Thus the propagation velocities are described by

$$C_l = \sqrt{\frac{E(1-\nu)}{\rho(1+\nu)(1-2\nu)}} \tag{6.1}$$

and

$$C_s = \sqrt{\frac{E}{\rho(1+\nu)}}. \tag{6.2}$$

In the case of fluids, the propagation velocity may be subjected to change depending the temperature of it. Again, Halmshaw (1991)(pp. 105) shows the sound propagation velocity in water is 1490 m/s at 20° Celcius. When the temperature of the water increases, the sound velocity also increases with a temperature coefficient of about +2.5 m/s ° Celcius. In order to control and maintain a constant temperature at 20° Celsius a thermometer was placed and in case of increased temperature extra water was added and in the tank.

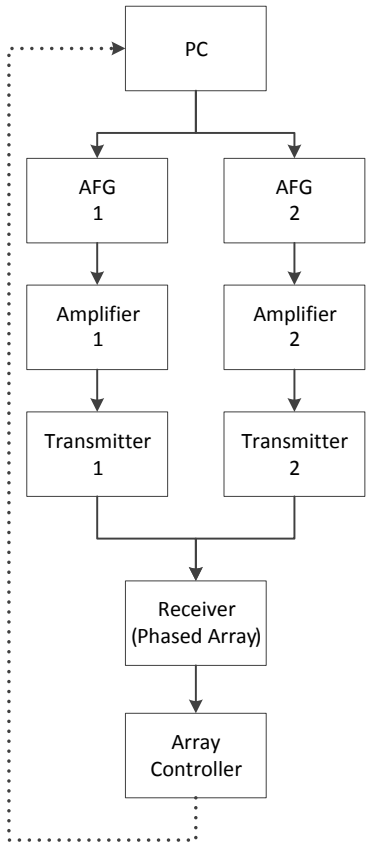

Figure 6.3: Schematic diagram of the experimental procedure for testing the carbon fibre reinforced plastic specimens.

Figure 6.3, shows the schematic diagram of the set-up. The set-up consisted of two single element Olympus accusan A551S-S transducers with a nominal element diameter 10mm and with 5 MHz centre frequency. The holding element from the rig, as seen in Figure 6.2, kept the probes in the

right position and in the desired angle with regards to the plane of interaction for each test. The 20 cycle signals were created by two arbitrary function generators and were amplified by two Amplifier Research 75A250 power amplifiers before being transmitting by the Olympus transducers. After the non-linear interaction, the combined signal was detected and received by a 10 MHz Immasonic phased array with 126 active elements. The array was connected to a Micropulse FMC array controller with output gain 65db which digitised the received signal and stored it in a PC for further processing.

Before starting the experimental procedure it was essential to calibrate the test equipment in terms of the angle between the probes and the plane perpendicular to the surface of water. Small changes in the angles could affect the amplitude of the input waves and also could affect the area of interaction giving misleading results. For this reason, several tests were performed prior to the beginning of the main set of experiments. These tests involved the measurement of the amplitude of non-linear signal in a set of different rig angles, varying from -2 to 2 degrees. The angles were measured with a digital compass which was placed on the rig. Additionally, it was equally important to perform all tests with the same parameters, in order to avoid the generation of further non-linearities in the system and have comparable results. For this reason, the rig remained untouched for all four test cycles with the four different specimens. Finally, the rig itself was placed on top of a metallic bar which held the carbon fibre test specimens in the right place for the whole experimental procedure.

Up until now, during the experimental procedures all the non-linear measurements in aluminium alloys were carried out in frequency ratio equal to one where both input frequencies were same and equal to 5 MHz. This followed the resonance conditions that were investigated for the case of in-

teraction waves in isotropic materials, Jones and Kobett (1963). Carbon fibre composites are anisotropic materials which means that the elastic properties are different in different directions in the material and thus the equations produced by Jones and Kobett do not hold.

In the current set of experiments, the idea was to further investigate the potential of the method by trying a wider range of critical parameters, such as the interaction angles and the frequency ratios. The scope of the experiments was to create a more detailed map of the non-collinear amplitudes with respect to the interaction angles and the frequency ratios so that the potential of the method in carbon fibre composites can be initially assessed and then the most sensitive combination of parameters can be selected for the subsequent tests.

6.4 Processing

The original test rig was designed to have two degrees of freedom, allowing control over the distance between the transducers as well as the angle the input probes with respect to a level perpendicular to the width of the specimen. In all the experiments, the area of interaction was chosen at 2 mm depth from the top of the surface. Since a series of different interaction angles and frequency ratios were selected, care had to be taken to ensure the area of interaction remained the same while the frequency ratio was changing. This was achieved by altering the separation of the input probes. Larger interaction angles were difficult to test due to rig design limitations. The set of the chosen interaction angles was between 40° and 80°, more specifically 40°, 45°, 50°, 55°, 60°, 65°, 70°, 75°, and 80°, and the the frequency ratios that

were chosen for this set of experiments were from 0.6 to 1.1, they can be seen in Table 6.3.

Table 6.3: Sets of frequency ratios and input frequencies applied for each set of interaction angles between 40° and 80°.

Frequency Ratio f_1/f_2	Input Frequency f_1 $[MHz]$	Input Frequency f_2 $[MHz]$
0.60	5	3
0.65	5	3.25
0.70	5	3.5
0.75	5	3.75
0.80	5	4
0.85	5	4.25
0.90	5	4.5
0.95	5	4.75
1.00	5	5
1.05	5	5.25
1.10	5	5.5

In the current setup the maximum and the minimum separation was the closest distance the probes could get and the maximum 110 mm respectively which introduced a limitation over the range of angles that could be tested. In the same sense, the frequency ratio was limited to the transducers' centre frequency; it was impossible to apply frequency higher that 5 MHz due to increase danger of burning the piezoelectric element of the probe. For the test where the frequency ratio was equal to 1.1 (and where the second input frequency had to be equal to 5.5 MHz) it was observed that slight increase in

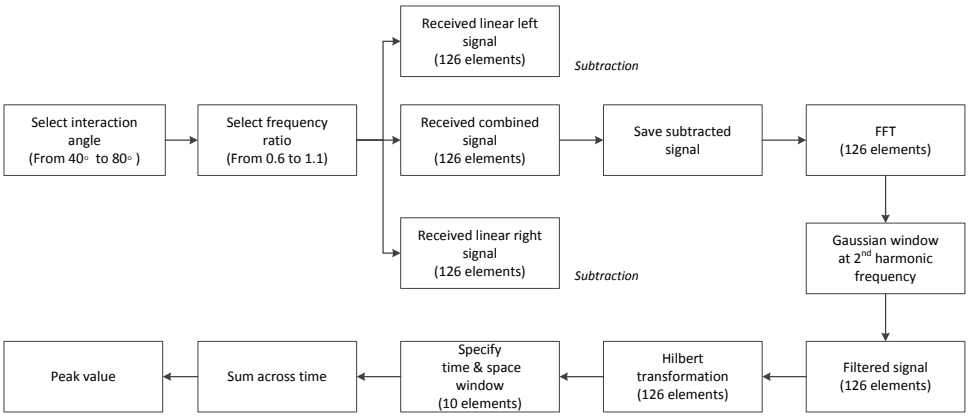

Figure 6.4: Series of steps that were followed to filter the received signal and also to create the surface plots for all the four carbon fibre samples.

the input frequency had no effect in the quality of the generated signal by the piezoelectric element.

For each one of the selected interaction angles, each frequency ratio was applied: 0.60, 0.65, 0.70, 0.75, 0.80, 0.85, 0.90, 0.95, 1.00, 1.05, 1.10. This was easily controlled and changed through the MatLab written script which was responsible for all the test parameters, i.e pulse gain, signal output voltage, number of cycles e.t.c. When the last frequency ratio was applied to a specific interaction angle, that is $f_1/f_2 = 1.10$ at 80°, the distance between the probes was altered resulted in the new interaction angle.

A single experimental procedure was designed and the same steps were applied to all four CFRP specimens. Figure 6.4 shows the steps carried out during the experimental procedure. Similarly to the the experiments carried out in Chapter 3 and Chapter 5, three initial measurements were taken: one measurement with both probes transmitting, one with only the left probe transmitting and finally one with only the right probe transmitting. The

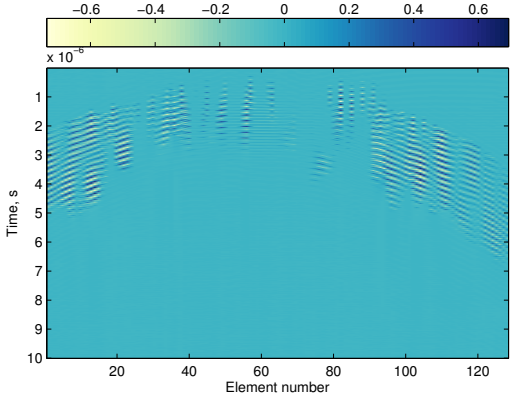

(a) Raw subtracted signal received from the reference sample with 0.95 frequency ratio.

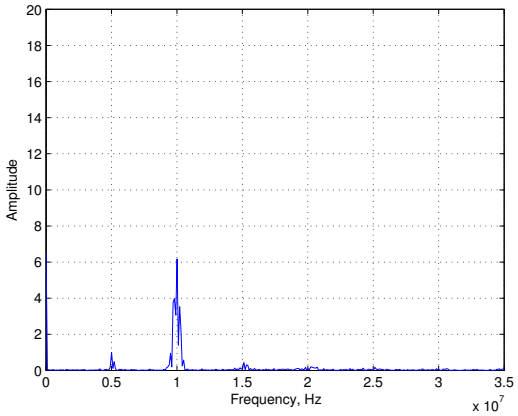

(b) Frequency spectrum received from the 60th element of the raw subtracted signal.

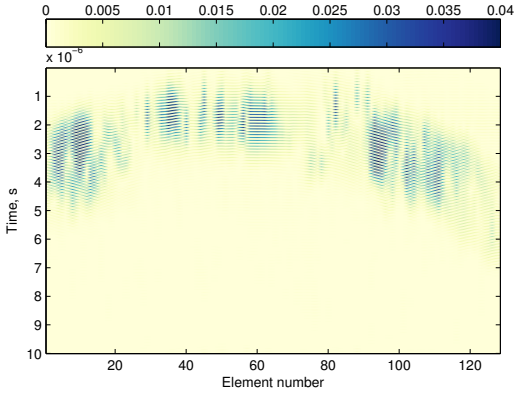

(c) Filtered at the second harmonic frequency signal.

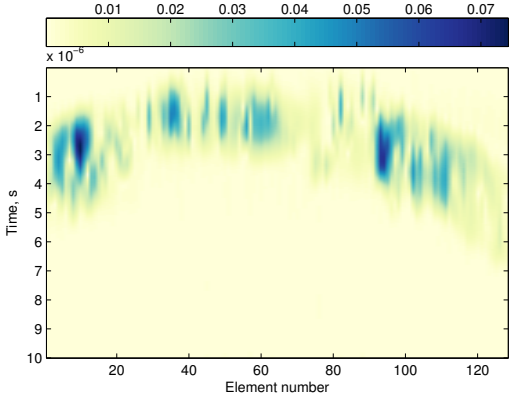

(d) Envelope of the filtered at the second harmonic frequency signal.

Figure 6.5: Images showing step by step the processing method followed to create the surface plots.

reason why these measurements were taken individually was to eliminate system non-linearities as explained in Section 3.3.3.

After the subtraction process, a Fast Fourier Transformation was applied along the length of the subtracted signal to reveal the frequency responses. A Gaussian window was applied at the second harmonic frequency of the spectrum and then an Inverse Fast Fourier Function revealed filtered signal. The same filtering process was performed for all signals received by all 126

elements of the phased array. A space and time window of 10 elements and 10 cycles respectively was applied around the area of the signal where the theoretical time arrival of the non-collinear signal was expected. The remaining signal was summed with respect to space and then the peak value was extracted. This was repeated for all the frequency and interaction angle combinations. These are shown in Figure 6.11c.

The reason why all these processing steps were carried out is the need to present clearly the big amount of data that was collected through the experiments. For example, each measurement for a specific frequency / angle combination resulted in a three dimensional matrix (x, y, z) where x is the number of recording time points, y is the received signal points and z is equal to the number of receiving elements of the array. When this was repeated for all the angles we ended up with $9 \times (x, y, z)$ matrix. That's why it was essential to finally end up with one value for every experiment.

Following the process for all angles and ratios the results were put together creating a surface plot, representative for each one of the four different CFRP samples, Figure 6.6.

6.5 Discussion

As discussed in Chapter 3 the amplitude of the non-linear signals is several orders of magnitude smaller than the amplitude of the input signals. For this reason, for all the non-collinear measurements the output gain was high and set at 65db. This value was the maximum output the array controller could give.

The saturation at the side lobes of the received signal can be identified and seen in Figure 6.5a in the Raw Subtracted received signal. However, it

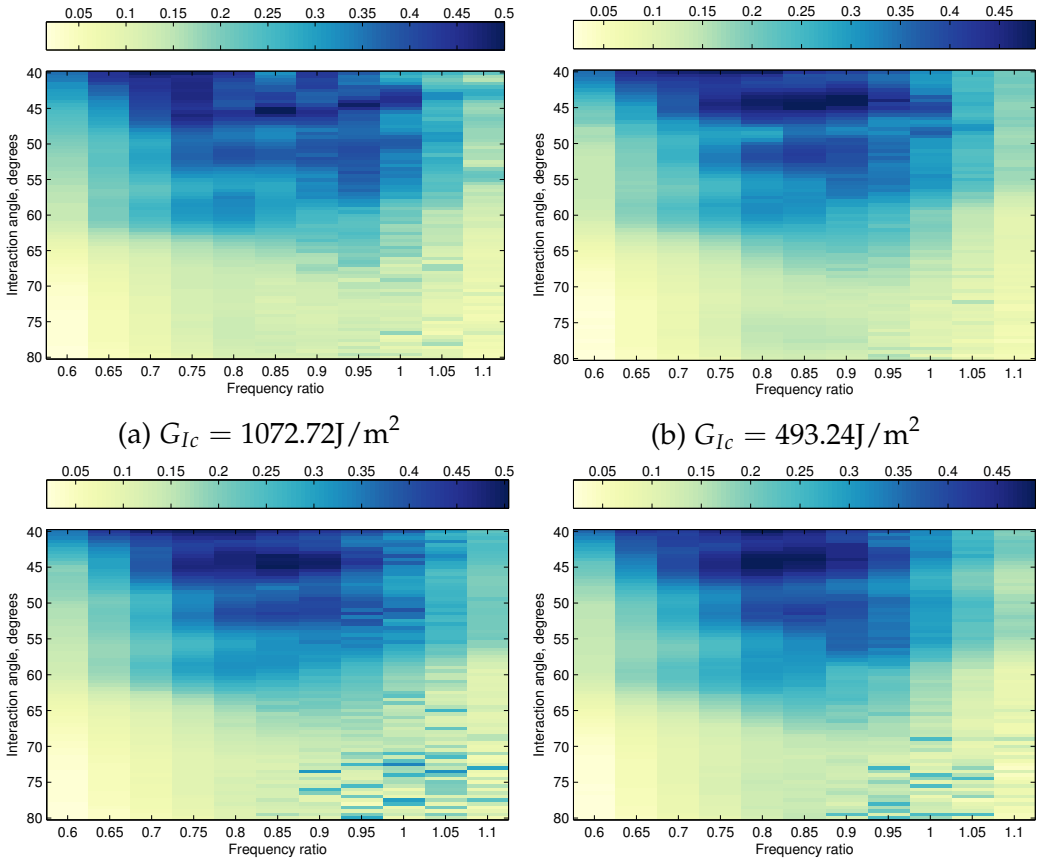

(a) $G_{Ic} = 1072.72\text{J/m}^2$ (b) $G_{Ic} = 493.24\text{J/m}^2$

(c) $G_{Ic} = 60.83\text{J/m}^2$ (d) $G_{Ic} = 40.37\text{J/m}^2$

Figure 6.6: Surface plots of the four samples in a descending fracture toughness order. The plots were created after taking the maximum value over a window around the expected time arrival for all the frequency and angle combinations, for all the four specimens.

was not of concern as the are of interest was restricted in the area close to the 60th element. The high gain was essential in order to increase the amplitude of the non-linear signal and thus be able to identify it. From the Figures 6.11c and especially 6.5d it can be seen that the subtraction process is not very effective in this case as linear signals are still visible in the sides of the lobes. Saturation is again the reason, but it is again of minimal importance because the area of interest is at the centre of the array, since this is the are where the scattering non-linear signal is expected.

Following the signal processing steps described in Section 6.4 all the filtered signals which corresponded to a specific frequency ratio were compiled to surface plots where all possible combinations of interaction angles versus frequency ratio can be seen. For all the aluminium specimens tested in Chapter 3 and 5 the optimum frequency ratio was equal to one, where both input frequencies were 5 MHz, but this is not the case for the Carbon Fibre Reinforced Plastics . From the surface plots in Figure 6.6it can be seen that the optimum frequency ratio lies between 0.7 and 1, the frequency ratios that correspond to the maximum amplitude.

Figure 6.6 shows all the surface plots for all four specimens with different fracture toughness values. All plots exhibit similar amplitude patterns with higher amplitude values corresponding between 40° and 65°. The highest values are in the area around 45° interaction angle. The fact that there is a non-linear response in certain areas in the surface plots in Figure 6.6 is a validation for the effectiveness of the method in the first place. In all Figures 6.6a, 6.6b, 6.6c and **??** the areas corresponding to very low amplitudes (from 0.05 to 0.15 in the z axis) have almost the same border and so do the areas with the high amplitudes (0.2 - 0.5 in the z axis). As a primary result is encouraging that the area of interest is more intense and clearly distinctive from the are of lower amplitudes. In Figures 6.6c and 6.6d an interference of noisy signal can be observed between the frequency ratio of 0.9 and 1.1 and the interaction angles 65° and 80°. These features are incoherent noise and this can be confirmed by looking at the frequency spectra of the respective specimens.

Despite the positive results in the successful non-linear interaction, which was an initial challenge due to the non isotropic nature of the CFRP samples ,there is still work to be done in oder to distinguish the damaged specimens

and the level of effective damage between them. The fact that the results from the surface plots do not differentiate with respect to intensity, interaction angles and frequency ratios make the method relatively ineffective to distinguish difference in the level of damage between the four specimens.

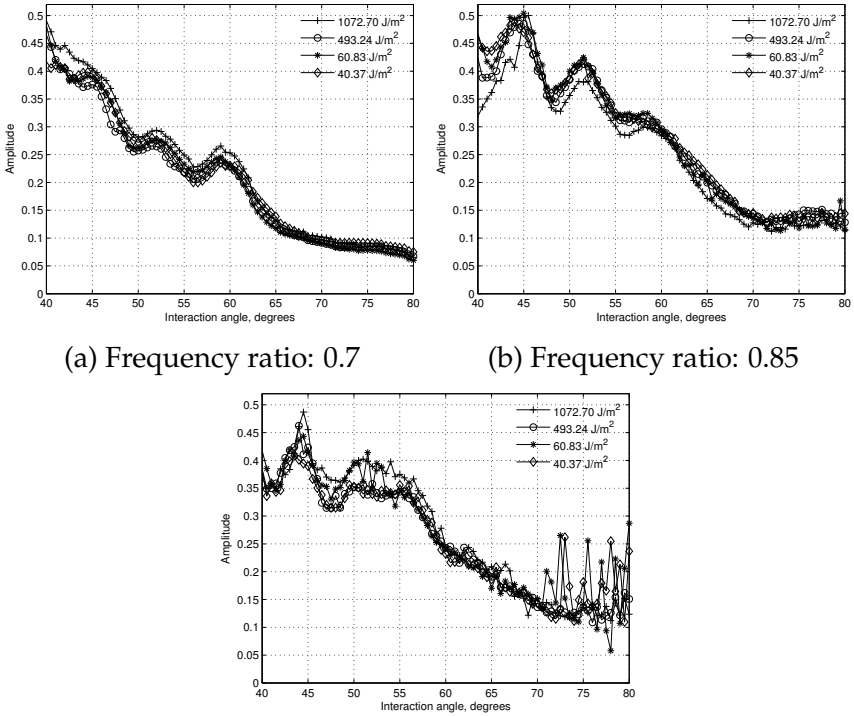

(a) Frequency ratio: 0.7

(b) Frequency ratio: 0.85

(c) Frequency ratio: 0.95

Figure 6.7: Cross section plots of the amplitude of all four CFRP specimens with respect to the interaction angle for three different frequency ratios.

In an attempt to interpret results from the surface plots, it was important to isolate certain features and compare them against the reference specimen with Fracture Toughness $G_{Ic} = 1072.72\text{J/m}^2$. Also, due to the complicated processing algorithm which generated the surface plots, i.e large number of data and summed values, it was essential to narrow down the areas of observation. For this reason three frequency ratios were selected, 0.7, 0.85 and 0.95 and the amplitude response for all the interaction angles was selected.

Thus, three 'slices' of amplitudes were extracted for each surface plot that corresponded to three different frequency ratios and can be seen in Figure 6.7. The selected frequencies were 0.7, 0.85 and 0.95 and they were selected because they exhibited similar trends.

Figures 6.7a, 6.7b and 6.7c show the cross section trends of the amplitudes for all angles. In all Figures the same trend can be observed with the amplitude decreasing with the increase of the interaction angle.

In all four cases the amplitude follows the same descending trend with the alteration of the interaction angle. In Figure 6.7a the reference sample has a consistently higher amplitude, with the peaks being relative higher more distinguished from the trends of the other samples. For the frequency ratios of 0.7 and 0.95 , Figures 6.7a and 6.7c, the highest level of non-linearity is present in the reference specimen with fracture toughness 1072.70 J/m^2. The lowest non-linear amplitude is present at the sample with the lowest fracture toughness at 40.37 J/m^2. The opposite effect with the undamaged specimen showing lowest amplitude and the damages specimen exhibiting higher amplitude was observed if Figure 6.7b. In fact, the four curves corresponding to the samples exhibit a completely different order, with the healthiest specimen showing the lowest non-linear amplitude. The difference in this case was that the healthiest sample was again somewhat easier to differentiate from the other specimens, as in Figure 6.7a. Also, in all cases a series of trough and peaks were present but in different interaction angles in each specimen.

The samples with the higher level of damage, exhibit higher level of noise in larger angles. The high amplitudes are not non-linear features, this can be verified by the frequency spectra of these areas. In order to prove this, a specific interaction angle (75 degrees) and frequency ratio (1) for both

cases can be chosen. 6.7c shows lower level of signal to noise ratio. This is clearly shown in the beginning of the graph where the disturbance is more prominent between 40 and 50 degrees. Things become clearer when the amplitudes are normalised against the amplitude of then noise (Figures 6.8a, 6.8b and 6.8c respectively.

Although from the aforementioned figures it can be seen that with the decrease of interaction angle the trend increases, it is worth investigating smaller angles to to verify the behaviour of the trend. Similarly, it is worth checking bigger angles in order to have a more and more detailed view of the behaviour of the amplitude. Due to the design of the test rig and the motor, there were certain limitations over the ability to inspect certain angles as discussed in Section 6.3.

Since no safe assumptions can be generated so far and it was difficult to distinguish the level of contamination between the specimens and the trend of the curves do not follow a specific pattern and behaviour. The next step is normalise against them against key features and thus try to investigate whether these could potentially be useful to extract safe assumptions. The selected features were the following:

- Level of noise
- Amplitude of first peak
- Amplitude of first trough
- Removed level of noise

Level of noise normalisation: Figures 6.8a, 6.8b and 6.8c are shown the normalised values of the amplitude curves against the average value of the noise, in an attempt to reduce the effect the noise. In Figure 6.8a shows the

curves normalised against the level of noise and it clearly shows that in the lower angles there is a separation of the reference specimen against the three others, with but still it is difficult to specify the it's curve with certainty as it overlaps with the curve of the third sample. Looking at the same graph but in different frequency ratio, Figure 6.8c there is clear differentiation of the reference specimen as well as the second toughest specimen, when the curves are again normalised against the level of noise with their amplitudes having almost twice as the amplitude of the least damaged specimens. In Figure 6.8b with the 0.85 frequency ratio it is difficult to distinguish the samples in order or weakness but the weakest sample exhibits the smallest amplitude.

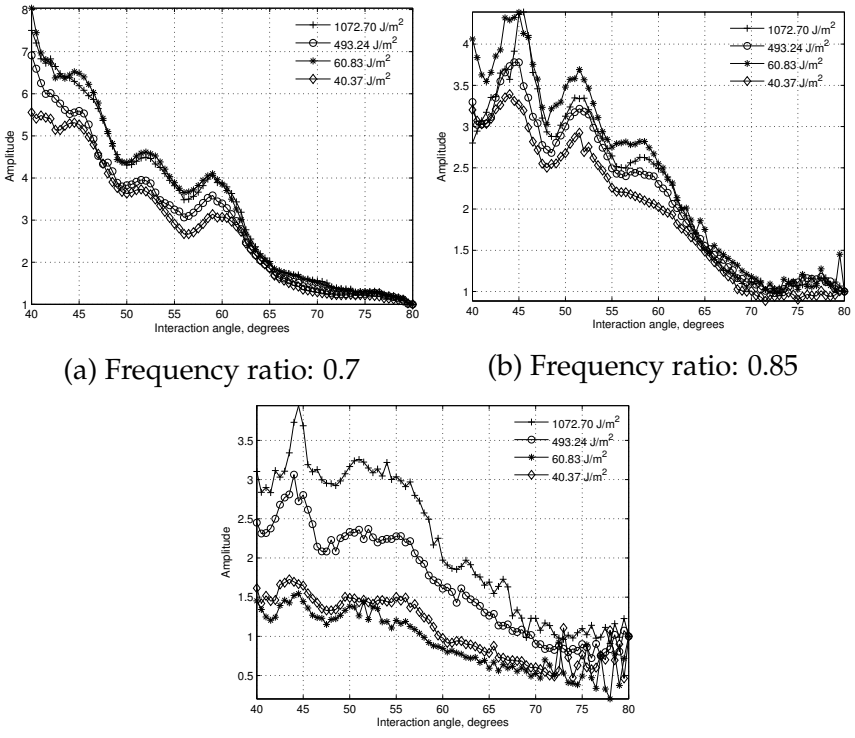

(a) Frequency ratio: 0.7

(b) Frequency ratio: 0.85

(c) Frequency ratio: 0.95

Figure 6.8: Cross section plots of the amplitude of all four CFRP specimens with respect to the interaction angle , normalised against the level of noise, for three different frequency ratios.

Amplitude of the first peak and first trough normalisation: When the 0.7 frequency ratio was tested, in the Figures 6.9a and 6.10a all the curves somewhat overlap apart from the areas that correspond to 55 degrees. It is only there where the weakest specimen shows a smaller amplitude which clearly differentiates over the other three curves. The same can be observed in Figure 6.10b where the weakest specimen shows a clearer trend and minimum amplitude between 55 and 60 degrees. The opposite behaviour is shown in Figure 6.9b. Here there is a more clear difference of the reference specimen along the way of the examined interaction angles. The normalisation process showed no clear results in the case of 0.95 frequency ratio. Here, all samples show similar trend and their curves overlap almost all along the tested angles, apart from the highest angles where high levels of noise is observed.

Removed level of noise normalisation: In the final case of feature investigation, the level of background noise was removed by taking an average value of the noise for each curve and subtracting it from it's amplitude values. In Figure 6.11a the reference specimen as well as the weakest specimen show a similar amplitude level but they are both clearly distinguished over the the other two samples; the reference specimen has the highest amplitude and the weakest has the lowest amplitude respectively. The same behaviour of the reference and weakest specimens is shown in Figure 6.11c. Figure 6.11b is again somewhat different where no clear assumptions can be made.

6.6 Concluding Remarks

- The results show limited sensitivity in the detection of the carbon fibre samples with different fracture toughness values.

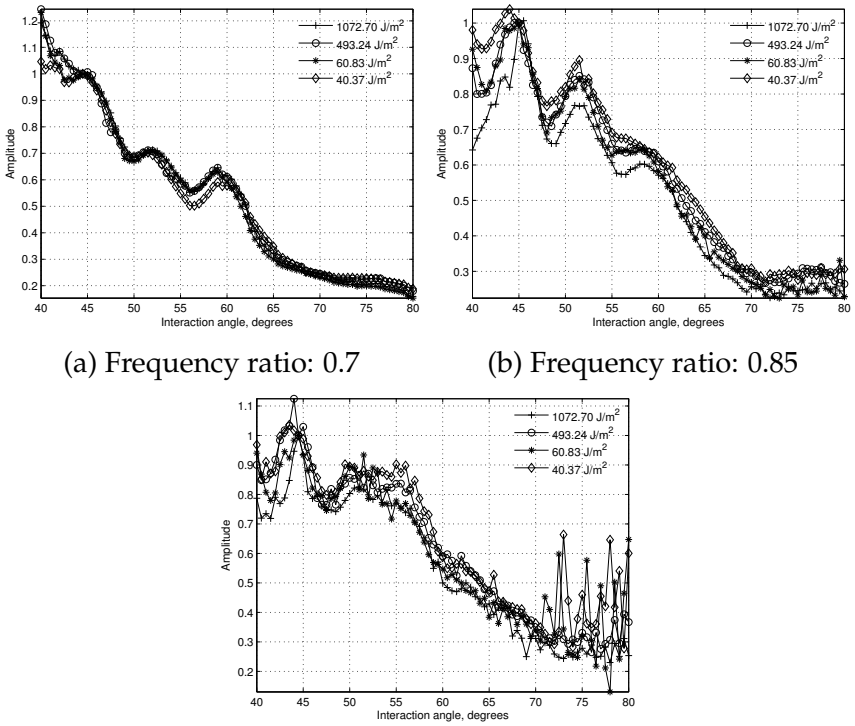

(a) Frequency ratio: 0.7 (b) Frequency ratio: 0.85

(c) Frequency ratio: 0.95

Figure 6.9: Cross section plots of the amplitude of all four CFRP specimens with respect to the interaction angle , normalised against the amplitude of the first peak, for three different frequency ratios.

- The attempt to investigate different frequency ratios shows a trend which is theoretically expected; higher amplitude of received non-collinear signal for the higher interaction angles in all frequency ratios.

- For all four specimens, the frequency ratios which correspond to the highest amplitude are in the range of 0.75-1 frequency ratios.

- The possibility to investigate smaller angles that were difficult to test because of test limitations.

- In the current experimental process, only specific features could be examined, i.e value of first peak of the received signal, value of first

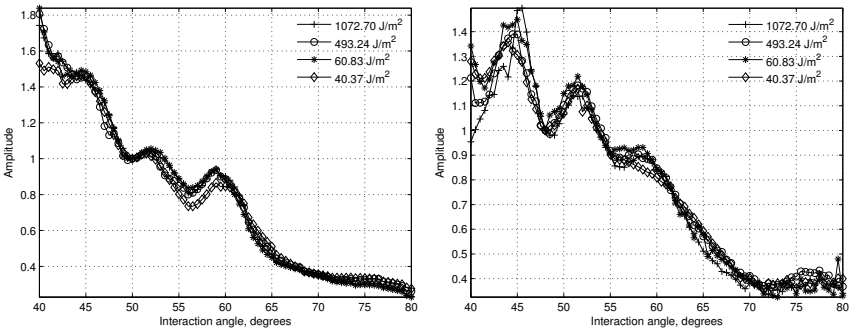

(a) Frequency ratio: 0.7

(b) Frequency ratio: 0.85

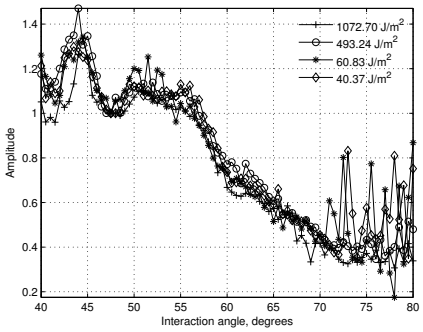

(c) Frequency ratio: 0.95

Figure 6.10: Cross section plots of the amplitude of all four CFRP specimens with respect to the interaction angle, normalised against the amplitude of the first trough, for three different frequency ratios.

trough of the received signal e.t.c, and restricting assumptions could be made.

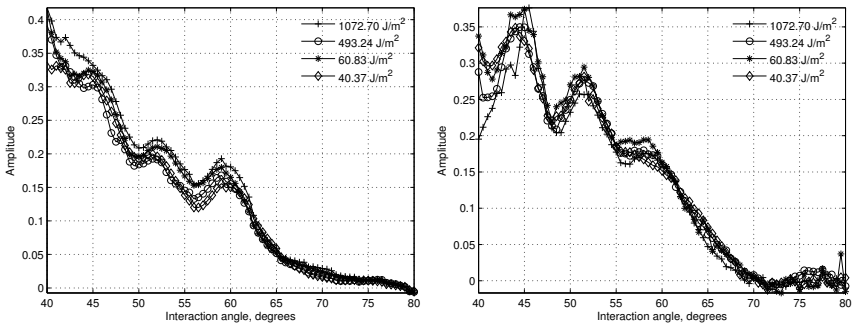

(a) Frequency ratio: 0.7 (b) Frequency ratio: 0.85

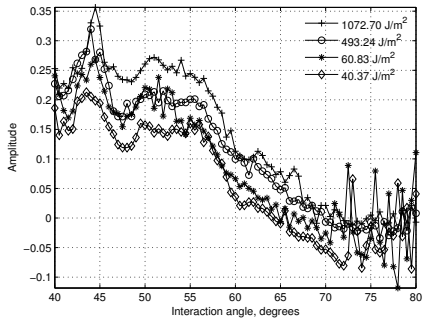

(c) Frequency ratio: 0.95

Figure 6.11: Cross section plots of the amplitude of all four CFRP specimens with respect to the interaction angle, with the noise subtracted, for three different frequency ratios.

Chapter 7

Discussion and Conclusion

In this thesis, the non-linear non-collinear ultrasonic method was used as a non-destructive tool for the assessment of kissing bonds in aircraft materials. Kissing bonds have different definitions in literature but in this thesis a kissing bond is simulated as a partially closed interface subjected to compression loading (Chapter3) as well as a bond subjected to different contaminants (Chapter 6).

Non-linear ultrasonic methods have shown higher sensitivity to early stage defects and show promising capability for the early detection of progressive damage, by detecting the harmonics produced in the material. In non-collinear mixing two intersecting waves propagate within the medium of interest and under certain circumstances interact. This interaction results in the generation of a third wave with different frequency and different scattering direction from the two input waves. This method has more advantages over the non-linear harmonic generation method:

- Spatial selectivity : The source of nonlinearity is limited to the area of interaction

- Modal selectivity: The non-collinear wave is of different modality from the two input waves.
- Frequency selectivity: The non-collinear wave has different frequency from the the two input waves.
- By measuring and subtracting the two input waves when fired separately, the system nonlinearities can be eliminated.

The first chapter describes the motivation of the work emphasising the importance of effective non-destructive methods especially in the aerospace industry.

In the second chapter, a literature review was conducted where research results in the non-destructive detection of kissing bonds were presented. It was shown that there is a gap in the field of non-destructive testing and the reason behind the selection of non-collinear mixing was presented.

In the third chapter, the initial work done in the investigation of kissing bonds is presented. An aluminium-adhesive interface was selected in order to evaluate the sensitivity of the non-collinear wave in the detection of differences in the stiffness the selected bonds. Along with the non-collinear mixing, a non-linear harmonic generation technique was also used as a validation tool. The experimental set-up consisted of two different interfaces: aluminium-adhesive and aluminium-aluminium interface, both subjected to compression loading. This was partially closed interfaces were achieved. The results from the aluminium-adhesive experiments were the following:

- The harmonic generation technique exhibited nonlinearity in accordance to the literature; high levels in low pressure and then normal linear behaviour in higher levels of pressure.

- The non-collinear mixing experiment showed complex nonlinearity with the non collinear wave being unable to detect. That led to inconclusive results.

- It was also observed that the geometry of the experimental set-up was challenging: the time of arrival of reflected waves and mode converted waves matched the time of arrival of the non-collinear wave.

- For this reason, a new set-up was deigned and a less complex interface was selected: an aluminium-aluminium interface with a shorter area of contact which restricted the unwanted reflections.

- New areas of interaction were selected in order to assess the input of the interface, normalised results showed a trend which qualitatively matched the trend the non-linear parameter as seen in literature but the same results were challenging to repeat.

- Experimentation with phased arrays was selected in order to minimise the nonlinearities introduced due to inconsistencies (i.e misalignment, difference in coupling) from the previous experimental set-up.

In the fourth chapter a model was developed to viualise the linear beams from two phased arrays (elements, frequency etc).

- The basic physics of phased arrays and Huygenes principle was described that were used to the model and predict the input beams. The model showed the difference in the interaction area between unfocused and focused interactions.

- Using the geometry of the set-up and the Fermats principle a series of calculations were performed:

  - Delay laws for interaction in certain areas of interest
  - Theoretical interaction angles for different interaction depths
  - Optimum sub aperture of phased array for certain depth and interaction angles.

- The results of the theoretical calculations can determine the limitation of depth scanning with the non collinear mixing. This is useful when it comes to testing complex geometries and separation between the phased arrays has to be introduced.

- Different depths can be tested if separation is introduced between the phased arrays. The main drawback is the interaction of focused beams is a few order of magnitude smaller than that of unfocused beams.

In the fifth chapter the sensitivity of non collinear mixing was tested for kissing bonds in carbon fibre reinforced plastics. A series of different samples with different bods were manufactured. The kissing bonds were simulated with different contaminants in the layers hat affect the fracture toughness.

- Initial experiments showed limited sensitivity in the detection of non-collinear signal. This was somewhat expected due to reflections from multiple layers of the carbon fibre.

- In order to achieve successful detection of the non-collinear signal, different sets of frequency ratios were tested in an attempt to find the optimum resonance conditions. This was challenging due to the anisotropic nature of the material. It was found the best frequency ratios that corresponded to higher amplitudes were between 0.75-1.

- Safe assumptions were difficult to interpret and different normalisation parameters were tested. It was shows that certain features could be

isolated and compared but the classification of the samples in order of damage was proved inconclusive.

References

Achenbach, J. (1992). 'Measurement models for quantitative ultrasonics'. In: *Journal of Sound and Vibration* 159.3, pp. 385–401. DOI: https://doi.org/10.1016/0022-460X(92)90749-N.

Achenbach, J. and O. Parikh (1991). 'Ultrasonic analysis of non-linear response and strength of adhesive bonds'. In: *Journal of Adhesion Science and Technology* 5.8, pp. 601–618. DOI: 10.1163/156856191X00512.

Adams, R. and B. Drinkwater (1997). 'Nondestructive testing of adhesively-bonded joints'. In: *NDT & E International* 30.2. A selection of papers presented at the First Joint Belgian-Hellenic Conference on NDT, pp. 93–98. DOI: 10.1016/S0963-8695(96)00050-3.

Anderson, T. (2005). *Fracture Mechanics: Fundamentals and Applications*. 3rd. CRC Press, p. 640. ISBN: 0849316561.

Anes, V., R. Pedro, E. Henriques, M. Freitas and L. Reis (2016). 'Galvanic corrosion of aircraft bonded joints as a result of adhesive microcracks'. In: *Procedia Structural Integrity* 1, pp. 218–225. DOI: http://dx.doi.org/10.1016/j.prostr.2016.02.030.

Antunes, D., V. Infante and A. Reis (2016). 'Mechanical characterization and experimental performance of an aerospace adhesive'. In: *Engineering Failure Analysis* 69, pp. 43–56. DOI: http://dx.doi.org/10.1016/j.engfailanal.2016.04.010.

Avdelidis, N. P., T.-H. Gan, C. Ibarra-Castanedo and X. P. V. Maldague (2011). 'Infrared thermography as a nondestructive tool for materials characterisation and assessment'. In: vol. 8013, pp. 801313-801313-7. DOI: 10.1117/12.887403.

Baltazar, A., S. I. Rokhlin and C. Pecorari (2002). 'On the relationship between ultrasonic and micromechanical properties of contacting rough surfaces'. In: *Journal of the Mechanics and Physics of Solids* 50.7, pp. 1397–1416. DOI: 10.1016/S0022-5096(01)00119-3.

Beevers, A. (1995). *Forensic Studies of adhesive joints. Part 2-Bonded aircraft structure. Project 3: Environmental durability of adhesive bonds.* Project.

Bhowmik, S., H. Bonin, V. Bui and R. Weir (2006). 'Durability of adhesive bonding of titanium in radiation and aerospace environments'. In: *International Journal of Adhesion and Adhesives* 26.6, pp. 400–405. DOI: http://dx.doi.org/10.1016/j.ijadhadh.2005.05.004.

Brotherhood, C. J., B. W. Drinkwater and R. J. Freemantle (2003). 'An ultrasonic wheel-array sensor and its application to aerospace structures'. In: *Insight - Non-Destructive Testing and Condition Monitoring* 45.11, pp. 729–734. DOI: doi:10.1784/insi.45.11.729.52964.

Brotherhood, C. J., B. W. Drinkwater and F. J. Guild (2002). 'The Effect of Compressive Loading on the Ultrasonic Detectability of Kissing Bonds in Adhesive Joints'. In: *Journal of Nondestructive Evaluation* 21 (3). 10.1023/A:1022584822730, pp. 95–104.

Buck, O., W. L. Morris and J. M. Richardson (1978). 'Acoustic harmonic generation at unbonded interfaces and fatigue cracks'. In: *Applied Physics Letters* 33.5, pp. 371–373. DOI: 10.1063/1.90399.

Buck, O., R. Thompson and D. Rehbein (1984). 'The interaction of ultrasound with contacting asperities: Applications to crack closure and fatigue crack

growth'. In: *Journal of Nondestructive Evaluation* 4 (3-4), pp. 203–212. DOI: 10.1007/BF00566225.

Cantrell, J. H. and W. T. Yost (2001). 'non-linear ultrasonic characterization of fatigue microstructures'. In: *International Journal of Fatigue* 23, Supplement 1.0, pp. 487–490. DOI: 10.1016/S0142-1123(01)00162-1.

Cheng, J., J. Qiu, H. Ji, E. Wang, T. Takagi and T. Uchimoto (2017). 'Application of low frequency ECT method in noncontact detection and visualization of CFRcomposites.' In: *Composites Part B: Engineering* 110, pp. 141–152. DOI: https://doi.org/10.1016/j.compositesb.2016.11.018.

compliant, B. .-.-. P. S. environmentally (1999). *SOL-GEL Surface treatments for metal bonding*. Tech. rep. A&M Environmental Technotes.

Croxford, A. J., P. D. Wilcox, B. W. Drinkwater and P. B. Nagy (2009). 'The use of non-collinear mixing for non-linear ultrasonic detection of plasticity and fatigue'. In: *The Journal of the Acoustical Society of America* 126.5, EL117–EL122. DOI: http://dx.doi.org/10.1121/1.3231451.

Cuevas, E., C. Garca, S. Hernandes, P. Venegas, T. Gomez and M. Canada (2013). 'Non destructive testing for non cured composites: Air coupled Ultrasounds and Thermography'. In: *5th International Symposium on NDT in Aerospace*.

Darmon, M., V. Dorval, A. Kamta Djakou, L. Fradkin and S. Chatillon (Aug. 2015). 'A system model for ultrasonic NDT based on the Physical Theory of Diffraction (PTD)'. In: *Ultrasonics* 64.Supplement C, pp. 115–127. DOI: https://doi.org/10.1016/j.ultras.2015.08.006.

Delsanto, P., S. Hirsekorn, V. Agostini, R. Loparco and A. Koka (2002). 'Modelling the propagation of ultrasonic waves in the interface region between two bonded elements'. In: *Ultrasonics* 40.1-8, pp. 605–610. DOI: 10.1016/S0041-624X(02)00183-X.

Demcenko, A., M. Ravanan, H. A. Visser, R. Loendersloot and R. Akkerman (Oct. 2012). 'Investigation of PVC physical ageing in field test specimens using ultrasonic and dielectric measurements'. In: *2012 IEEE International Ultrasonics Symposium*, pp. 1909–1912.

Demenko, A., V. Koissin and V. Korneev (2014). 'Noncollinear wave mixing for measurement of dynamic processes in polymers: Physical ageing in thermoplastics and epoxy cure'. English. In: *Ultrasonics* 54.2, pp. 684–693. DOI: 10.1016/j.ultras.2013.09.011.

Drinkwater, B. W., R. S. Dwyer-Joyce and P. Cawley (1996). 'A Study of the Interaction between Ultrasound and a Partially Contacting Solid–Solid Interface'. In: *Proceedings of the Royal Society of London. Series A: Mathematical, Physical and Engineering Sciences* 452.1955, pp. 2613–2628. DOI: 10.1098/rspa.1996.0139.

Drinkwater, B., R. Dwyer-Joyce and P. Cawley (31 1994-nov. 3 1994). 'A study of the transmission of ultrasound across real rough solid-solid interfaces'. In: *Ultrasonics Symposium, 1994. Proceedings., 1994 IEEE*. Vol. 2, 1081–1084 vol.2. DOI: 10.1109/ULTSYM.1994.401721.

Driver, D. (1995). *Adhesive bonding for aerospace applications*. Ed. by H. M. Flower. Dordrecht: Springer Netherlands, pp. 318–339. ISBN: 978-94-011-0685-6. DOI: 10.1007/978-94-011-0685-6_11.

'Experimental Adhesive Failure Criteria for Analysis of Aerospace Structures' (2015). In: *Procedia Engineering* 114, pp. 416–421. DOI: http://dx.doi.org/10.1016/j.proeng.2015.08.087.

Felice, M., A. Velichko, P. Wilcox, T. Barden and T. Dunhill (2014). 'Simulation of the ultrasonic array response from real branched cracks using an efficient finite element method'. In: *AIP Conference Proceedings*. Vol. 1581 33, pp. 100–107. DOI: 10.1063/1.4864808.

Fitzer, E. and W. Huttner (1981). 'Structure and strength of carbon/carbon composites'. In: *Journal of Physics D: Applied Physics* 14.3, p. 347.

Fu, S.-Y. and B. Lauke (1996). 'Effects of fiber length and fiber orientation distributions on the tensile strength of short-fiber-reinforced polymers'. In: *Composites Science and Technology* 56.10, pp. 1179–1190. DOI: http://dx.doi.org/10.1016/S0266-3538(96)00072-3.

Gao, L., E. T. Thostenson, Z. Zhang and T.-W. Chou (2009). 'Sensing of Damage Mechanisms in Fiber-Reinforced Composites under Cyclic Loading using Carbon Nanotubes'. In: *Advanced Functional Materials* 19.1, pp. 123–130. DOI: 10.1002/adfm.200800865.

Genovés, V., J. Gosálbez, R. Miralles, M. Bonilla and J. Payá (2015). 'Ultrasonic characterization of GRC with high percentage of fly ash substitution'. In: *Ultrasonics* 60, pp. 88–95. DOI: http://dx.doi.org/10.1016/j.ultras.2015.02.016.

Graham-Jones, J. and J. Summerscales (2015). *Marine Applications of Advanced Fibre-Reinforced Composites*. Woodhead Publishing, pp. 21–22.

Guyott, C. C. H., P. Cawley and R. D. Adams (1986). 'The Non-destructive Testing of Adhesively Bonded Structure: A Review'. In: *The Journal of Adhesion* 20.2, pp. 129–159. DOI: 10.1080/00218468608074943.

Halmshaw, R. (1991). *Non-Destuctive Testing*. 2nd ed. Edward Arnold. Chap. 3.12. ISBN: 0340545216.

Jandejsek, I., J. Jakubek, M. Jakubek, P. Prucha, F. Krejci, P. Soukup, D. Turecek, D. Vavrik and J. Zemlicka (2014). 'X-ray inspection of composite materials for aircraft structures using detectors of Medipix type'. In: *Journal of Instrumentation* 9.05, p. C05062.

Jiao, D. and J. L. Rose (1991). 'An ultrasonic interface layer model for bond evaluation'. In: *Journal of Adhesion Science and Technology* 5.8, pp. 631–646. DOI: 10.1163/156856191X00530.

Jones, G. L. and D. R. Kobett (1963). 'Interaction of Elastic Waves in an Isotropic Solid'. In: *The Journal of the Acoustical Society of America* 35.1, pp. 5–10. DOI: 10.1121/1.1918405.

Karabutov, A. and N. Podymova (2014). 'Quantitative analysis of the influence of voids and delaminations on acoustic attenuation in CFRP composites by the laser-ultrasonic spectroscopy method'. In: *Composites Part B: Engineering* 56, pp. 238–244. DOI: http://dx.doi.org/10.1016/j.compositesb.2013.08.040.

Katsiropoulos, C., A. Chamos, K. Tserpes and S. G. Pantelakis (Mar. 2012). 'Fracture toughness and shear behavior of composite bonded joints based on a novel aerospace adhesive'. In: 43.

Kendall, K. and D. Tabor (1971). 'An Ultrasonic Study of the Area of Contact between Stationary and Sliding Surfaces'. In: *Proceedings of the Royal Society of London. Series A, Mathematical and Physical Sciences* 323.1554, pp. 321-340.

Kim, J.-Y., V. A. Yakovlev and S. I. Rokhlin (2004). 'Surface acoustic wave modulation on a partially closed fatigue crack'. In: *The Journal of the Acoustical Society of America* 115.5, pp. 1961–1972. DOI: 10.1121/1.1695012.

Kim, J.-Y., A. Baltazar and S. Rokhlin (2004). 'Ultrasonic assessment of rough surface contact between solids from elastoplastic loading-unloading hysteresis cycle'. In: *Journal of the Mechanics and Physics of Solids* 52.8, pp. 1911–1934. DOI: 10.1016/j.jmps.2004.01.006.

Kim, J. W., J. J. Lee and D. G. Lee (Aug. 2005). 'Effect of Fiber Orientation on the Tensile Strength in Fiber-Reinforced Polymeric Composite Materials'.

In: *Advances in Fracture and Strength*. Vol. 297. Key Engineering Materials. Trans Tech Publications, pp. 2897–2902. DOI: 10.4028/www.scientific.net/KEM.297-300.2897.

Kim, J., K.-J. Lee and K.-Y. Jhang (2016). 'Comparison of ultrasonic non-linear parameters measured by PZT and $LiNbO_3$ transducers'. In: *AIP Conference Proceedings* 1706, 060008. DOI: http://dx.doi.org/10.1063/1.4940514.

Krolikowski, J. and J. Szczepek (1991). 'Prediction of contact parameters using ultrasonic method'. In: *Wear* 148.1, pp. 181–195. DOI: 10.1016/0043-1648(91)90216-H.

Krolikowski, J., J. Szczepek and Z. Witczak (1986). 'High pressure in ultrasonic study of contact of solids'. In: *Physica B+C* 139-140, pp. 803–805. DOI: 10.1016/0378-4363(86)90706-0.

Li, C., D. Pain, P. D. Wilcox and B. W. Drinkwater (2013). 'Imaging composite material using ultrasonic arrays'. In: *NDT & E International* 53, pp. 8–17. DOI: http://dx.doi.org/10.1016/j.ndteint.2012.07.006.

Lighthill, M. J. (1956). *Viscosity effects in sound waves of finite amplitude*. Collected papers of Sir James Lighthill. Ed. by M.Yousuff. Vol. 1. Oxford Univeristy Press, pp. 250–351.

Littles, J. W., L. J. Jacobs and A.-H. Zureick (1998). 'Single-Sided Ultrasonic Technique to Characterize Thick FRP Composites'. In: 17.4, pp. 223–230. DOI: 10.1023/A:1022628705782.

McGovern, M. E., W. G. Buttlar and H. Reis (2014). 'Characterisation of oxidative ageing in asphalt concrete using a non-collinear ultrasonic wave mixing approach'. In: *Insight - Non-Destructive Testing and Condition Monitoring* 54, 367–374(8). DOI: http://dx.doi.org/10.1784/insi.2014.56.7.367.

Meng-Chou Wu Prosser, W. H. P. (1991). 'Harmonic generation measurements in unidirectional graphite/epoxy composites'. In: *Review of progress in quantitative nondestructive evaluation*. 17th Annual Review of Progress in Quantitative Nondestructive Evaluation; July 15-20, 1990; La Jolla, CA; United States. Vol. 10B (A92-28555 11-38). Plenum Press, pp. 1477–1482.

Nagy, P. B. (1991). 'Ultrasonic detection of kissing bonds at adhesive interfaces'. In: *Journal of Adhesion Science and Technology* 5.8, pp. 619–630. DOI: doi:10.1163/156856191X00521.

Non Destructive Testing - A Survey (1973). Tech. rep. National Aeronautics and Space Administration.

Pain, D. and B. W. Drinkwater (2013). 'Detection of Fibre Waviness Using Ultrasonic Array Scattering Data'. In: *Journal of Nondestructive Evaluation* 32.3, pp. 215–227. DOI: 10.1007/s10921-013-0174-z.

Rollins, F. R., L. H. Taylor and P. H. Todd (Nov. 1964). 'Ultrasonic Study of Three-Phonon Interactions. II. Experimental Results'. In: *Phys. Rev.* 136 (3A), A597–A601. DOI: 10.1103/PhysRev.136.A597.

Rothenfusser, M., M. Mayr and J. Baumann (2000). 'Acoustic non-linearities in adhesive joints'. In: *Ultrasonics* 38.1-8, pp. 322–326.

El-Sabbagh, A., L. Steuernagel and G. Ziegmann (2013). 'Characterisation of flax polypropylene composites using ultrasonic longitudinal sound wave technique'. In: *Composites Part B: Engineering* 45.1, pp. 1164–1172. DOI: http://dx.doi.org/10.1016/j.compositesb.2012.06.010.

Smith, R. A., S. Mukhopadhyay, A. Lawrie and S. R. Hallett (2013). 'Applications of ultrasonic NDT to aerospace composites'. In: *Proc. 5th International Symposium on Aerospace NDT, Singapore*.

Smith, R., L. Nelson, M. Mienczakowski and R. Challis (2009). 'Automated analysis and advanced defect characterisation from ultrasonic scans of

composites.' In: *Insight - Non-Destructive Testing and Condition Monitoring* 51.2, pp. 82–87. DOI: 10.1784/insi.2009.51.2.82.

Solodov, I. Y. (1998). 'Ultrasonics of non-linear contacts: propagation, reflection and NDE-applications'. In: *Ultrasonics* 36.1-5, pp. 383–390. DOI: 10.1016/S0041-624X(97)00041-3.

W. Steinchen, L. Y. and P. Mackel (n.d.). 'Non-destructive testing of aerospace composite materials using digital shearography.' In: ().

Yan, D. (2010). 'The detectability of kissing bonds in adhesive joints using non-linear ultrasonic techniques'. PhD thesis. University of Bristol.

Yan, D., B. W. Drinkwater and S. A. Neild (2009). 'Measurement of the ultrasonic non-linearity of kissing bonds in adhesive joints'. In: *NDT & E International* 42.5, pp. 459–466. DOI: 10.1016/j.ndteint.2009.02.002.

Yan, D., S. A. Neild and B. W. Drinkwater (2012). 'Modelling and measurement of the non-linear behaviour of kissing bonds in adhesive joints'. In: *NDT & E International* 47, pp. 18–25. DOI: 10.1016/j.ndteint.2011.12.003.

Yost, W. and J. Cantrell (Oct. 1992). 'The effects of fatigue on acoustic nonlinearity in aluminum alloys'. In: *Ultrasonics Symposium, 1992. Proceedings., IEEE 1992*. Vol. 2, pp. 947–955. DOI: 10.1109/ULTSYM.1992.275820.

Zalameda, J. N., E. R. Burke, F. R. Parker, J. P. Seebo, C. W. Wright and J. B. Bly (2012). 'Thermography inspection for early detection of composite damage in structures during fatigue loading'. In: vol. 8354, pp. 835403-835403-9. DOI: 10.1117/12.918126.

Zarembo, L. K. and V. A. Krasil'nikov (1971). 'Non-linear phenomena in the propagation of elastic waves in solids'. In: *Soviet Physics Uspekhi* 13.6, p. 778. DOI: 10.1070/PU1971v013n06ABEH004281.